EVANESCENT FIELD COUPLING BETWEEN A SINGLE-MODE OPTICAL FIBRE AND A THIN FILM WAVEGUIDE.

A Thesis
submitted to the faculty of engineering
of the university of Glasgow
for the degree of

Doctor of Philosophy

by

Laurence Daniel Bradley.

October 1986.

ProQuest LLC.
789 East Eisenhower Parkway
P.O. Box 1346
Ann Arbor, MI 48106 – 1346

Of me thou hast become a part:-
Some kindred with my human heart;
For we have been together more
Than galley slave and weary oar.

Alexander Smith, 'Glasgow' 1857.

Acknowledgements.

I wish to thank Professor J.Lamb for the provision of the excellent research facilities in the Department of Electronics and Electrical Engineering. I also wish to thank Dr.C.J.Todd, Head of the Optical Project Division R.17, in British Telecom Research Laboratories for access to specialist equipment and facilities.

I am indebted to my academic supervisors Dr.J.Arnold and Professor P.Laybourn and my industrial supervisor Dr.C.A.Millar, for their advice and their many useful suggestions during the course of this work.

I would also like to express my gratitude to M.Brierley of BTRL for his very considerable encouragement and practical advice. Also at BTRL I am grateful to A.Gotts for the skilled and patient fabrication of coupler blocks, to N.Vankoningsfelt for the accurate manufacture of experimental jigs, to J.Wright for BPM calculations and to J.Ainslie for the provision of planar waveguide samples.

Within the department of Electrical Engineering I would like to thank the technical staff for manufacturing jigs and for help in materials processing, in particular K.Piechowiak, W.Irvine, J.Clark, K.Melvin and L.Hobbs.

The financial support of the Science and Engineering Research Council and of BTRL is gratefully acknowledged.

The friendship and assistance of my fellow research students is acknowledged with gratitude, in particular Messrs. J.Clink, J.F.Duffy, W.C.Michie, D.M.Halliday, V.M.Airaksinen, I.S.McIntyre and M.A.Grant.

Finally it is a great pleasure to thank my family, my fiancée and my friends for their love and patient support.

TABLE OF CONTENTS

SUMMARY

The work of this thesis is concerned with a new method of coupling light from an optical fibre to a thin film waveguide using the interaction of the evanescent fields of the two guides. In particular the fibre used was standard single mode fibre, in widespread use in telecommunications networks. The fibre and film characteristics are discussed in chapter 2. In this type of fibre light is guided by a central core region which is typically 8-10μm in diameter and is surrounded by a cladding which is typically 125μm in diameter. The evanescent field of the guided light decays very rapidly away from the core region. The main difficulties in exploiting the fibre evanescent field are its limited extent, its isolation by the cladding layer and the physical dimensions involved, typically microns.

It was necessary to employ a device geometry which allowed micron and sub-micron tolerances to be achieved using mechanical tools. This geometry known as the tapered v-groove coupler (TVC) allowed access to the fibre evanescent field by removing a portion of the cladding and it is described in chapter 4. It also incorporated a planar surface which was suitable for planar film deposition. This allowed thin-film waveguides to be formed directly onto the TVC where they were in rigid and intimate contact with the polished fibre.

Evanescent field coupling requires (for significant power transfer) that the two waveguides have almost identical propagation constants. The TVC incorporated a tapered region which reduced the fabrication tolerances involved in achieving synchronism between the two guides. Using the TVC, coupling from fibre to film to fibre was demonstrated with an insertion loss of 2dB. The wavelength dependence of the coupler was investigated and is discussed in chapter 5. Coupling to rib and channel guides is discussed in chapter 6. It was found that although planar films could be straightforwardly aligned with the fibre core using this geometry, alignment of rib guides involved meeting tolerances of microns.

This work has important applications in the field of coupling between standard fibres and integrated optical waveguides since it complements, rather than competes with the existing technique of butt-coupling. It is particularly suitable for coupling to very thin films (<1μm thick) which can be deposited on a silica substrate.

Chapter 1 Introduction

1.1 Extending the applicability of integrated optics

This thesis is concerned with the improvement of an interface; that between integrated and fibre optics.

The transmission loss of optical fibres was improved from 20dB/km in 1970[1] to 0.2dB/km in 1979[2]. Laser diodes have also improved remarkably since the realisation of the AlGaAs/GaAs heterojunction in 1969[3] as have the range and sensitivity of the available detectors[4,6]. These three components (laser-fibre-detector) form the basis of the optical communications links in widespread use today[7]. Perhaps the maturity of this technology is best represented by the demonstration of coherent detection systems performing close to the theoretical detection limit[8,9].

There have been many advances during this period in the field of integrated optics, which has been reviewed extensively[10,11]. Integrated optical circuits are close in concept to microwave stripline waveguide circuits rather than being dielectric analogues of integrated electronic circuits. Their fabrication involves the use of thin transparent dielectric layers on planar substrates as optical waveguides. Rib and channel guides as well as planar guides have been used to produce e.g. switches modulators and beam deflectors[12]. Much of this work has been carried out on $LiNbO_3$, GaAs and related materials but a significant amount of research is now directed at passive low index materials[13] and non-linear organic materials[14].

There are many areas in which optical-fibre systems are superior to 'electronic' systems such as coaxial-cable, microwave and twisted-wire, particularly because of their large bandwidth. If integrated optical circuits are to be incorporated in such systems then they must also have superior performance to their electronic counterparts. One example is the high speed waveguide intensity modulator. Direct current modulation of semiconductor lasers is limited, for reasonable drive power, to about 1-2GHz[15]. Furthermore, in most semiconductor lasers fast current modulation also results in an undesirable wavelength modulation which would be detrimental for wavelength multiplexing[16]. A directional coupler modulator has been demonstrated to work at almost 10GHz[17] and by employing this device the available fibre bandwidth can be more efficiently utilised.

It is necessary to couple light into and out of the modulator with

reasonable efficiency and at reasonable cost. Reducing the insertion loss of fibre to integrated optics couplers without undue sophistication will extend the applicability of integrated optics in fibre-based systems. It is precisely this problem which this thesis addresses.

1.2 The coupling problem

The dimensions of optical waveguides are small, of the order of a few wavelengths. The core of a standard single-mode telecommunication fibre[18] is approximately 8μm in diameter. It is surrounded by a silica cladding of diameter 125μm which shields the core. The electromagnetic field of the guided light is concentrated in the core and decays rapidly away from it. This decaying field is also known as the evanescent field. This will be discussed in more detail in chapter 2. A single-mode channel waveguide in $LiNbO_3$ can be fabricated with similar transverse-field dimensions[19]. However, in general, a wide range of transverse field dimensions can exist in rib and channel waveguides. A planar guide is essentially unbounded in one transverse dimension, with a large range of thicknesses possible in the other. The transverse field extent depends critically on the index difference between the core and cladding regions of the guide. For locally doped materials (fibres, channel guides) this index difference is normally very small (typically 4×10^{-3}) and the field extent is relatively large. For planar waveguides formed by deposition onto a substrate a large index difference is possible resulting in a relatively well confined field. Each guide is normally invariant in the direction of propagation. The guided light is characterised by a transverse field pattern (mode shape) and a characteristic wavenumber (or propagation constant) in the direction of propagation.

1.2.1 Complementary techniques; butt and transverse coupling

The two principal methods for coupling light efficiently from cylindrical fibres to integrated optics waveguides are the 'end-fire' (or butt) and 'evanescent' (or transverse) field techniques. In the end-fire method the two guides are precisely aligned so that light leaving the end-face of the first guide is radiated directly into the end face of the second. The two end-faces are normally cleaved or polished. Efficient coupling requires very accurate alignment of the

guides (submicron) and a number of techniques have been devised to achieve this. Notable are the use of 'preferentially etched' alignment grooves in an external silicon substrate[20] and alignment grooves etched directly into the planar substrate[21]. The butt coupling method has a number of inherent loss mechanisms:-

Fresnel loss; due to reflection at the fibre/air and air/waveguide boundaries

Alignment loss; due to positional and angular misalignments.

Field mismatch; for maximum power to be transferred between two optical fields they must be made as similar as is possible[22].

Butt coupling has been most widely applied to Lithium Niobate devices and the best reported loss to date, from fibre to waveguide to fibre was 0.5dB[23]. This excellent result was achieved by a complex double diffusion technique which buried the channel waveguide to optimise mode matching. A similar optimisation program would be necessary to achieve this performance for each waveguide material of interest.

In the second technique the two waveguides are placed side by side in close proximity. If they are sufficiently close that their evanescent fields overlap then power can be coupled from one to the other. However in order to achieve 100% power transfer the propagation constants of the two waveguide modes must be equal, i.e. it must be a resonant structure. The fabrication tolerances required to achieve resonance or synchronism are in practice exacting. The technique of tapered velocity coupling has been used to provide the necessary degree of synchronism with reduced fabrication tolerances[24,25].

Externally mounted fibres[26] have been used but these require in addition an end-fire connection to standard telecommunications fibre. There may however be renewed interest in this work with the development of D-fibres made from standard fibre preforms[27]. The appeal of evanescent coupling despite its technical difficulties is that it offers virtually 100% power transfer and that it may be applied to guides supporting modes of widely differing field shape. This thesis describes the fabrication and characterisation of an evanescent field coupler using standard single mode fibre. Coupling to substrates having a wide range of refractive indices has been demonstrated. A fibre-film-fibre loss of 2dB has been reported[28] at the wavelengths

1.36 and 1.54 microns. These are of particular interest for telecommunications because they correspond to the regions of minimum loss and dispersion in optical fibres.

1.2.2 The tapered V-groove coupler (TVC)

This thesis is concerned with the TVC. A detailed description of the fabrication of the TVC is given in chapter 4. The coupler consists of a silica block with a groove cut at a shallow angle, θ_b, into which the fibre is bonded before being polished, (figure 1.1). The fibre is polished through completely and its cross-section at the block surface is an ellipse. Thin film waveguides are then formed directly onto the polished silica substrate. This approach gives rigid and intimate alignment of the two guides, essential for efficient directional coupling. Optical power is coupled initially, in the region adjacent to the exposed core where the cladding is only a few microns thick. Power was also found to couple from the tapered core region (see chapter 3 and 5). The experimental and theoretical evidence shows that tapered velocity coupling occurs, easing the synchronisation tolerances for efficient coupling. Prism coupling experiments and a BPM analysis indicated that the majority of power was transferred in the tapered core region. It was not however possible to quantify analytically the asymptotic efficiency[29] of the taper coupling. The coupler efficiency was found to be a strong function of wavelength and its behaviour is described further in section 1.4.

1.3 Applications of the TVC

As described in 1.4 the TVC has potential uses as a sensor or (using an active film) as a tunable wavelength filter. Provided that the synchronism conditions can be met (chapter 3) it is useful for coupling to guides supporting modes of markedly different field shapes from that of the fibre. One example of its use- coupling to non-linear films- is discussed below.

1.3.1 Coupling to non-linear films

Dielectric materials show non-linear effects when subjected to very high intensity optical fields. It is cheaper to produce these fields by concentrating light from a low power (e.g. diode) laser than

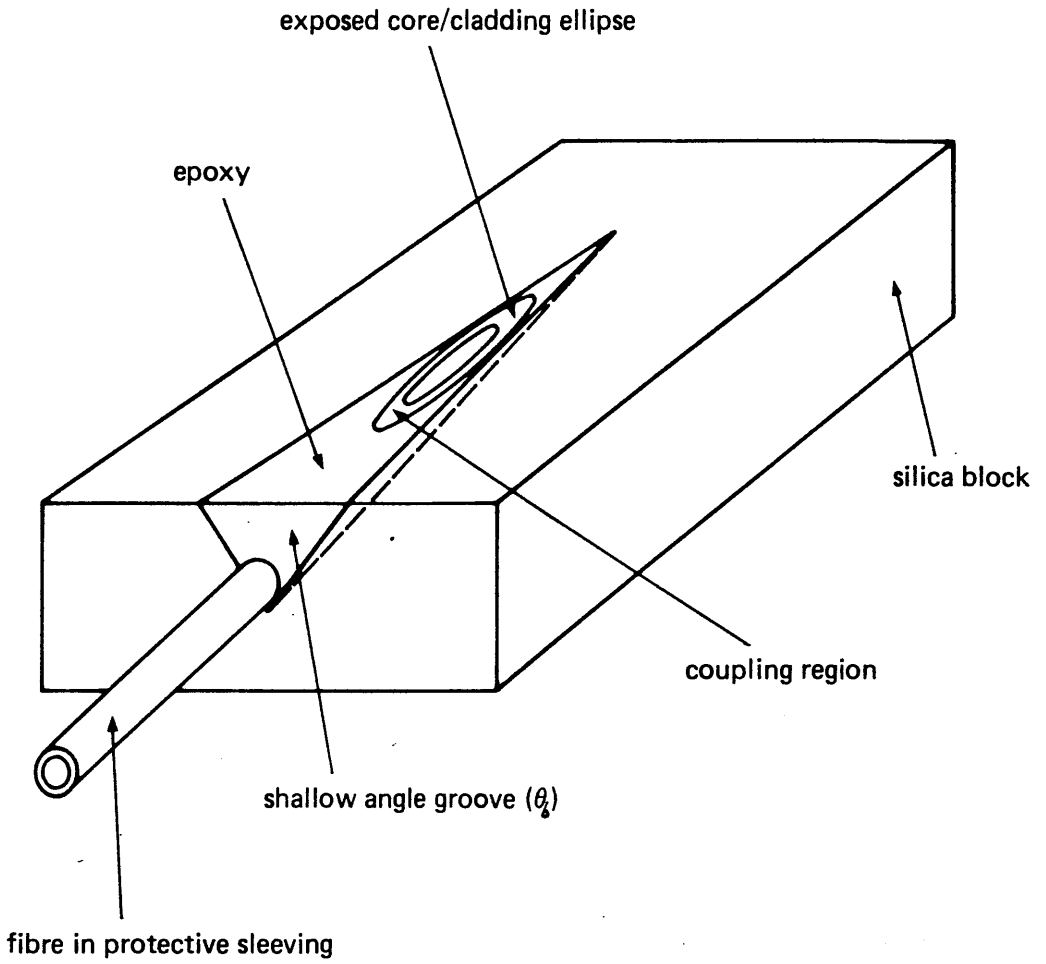

Figure 1.1 Schematic diagram of coupler block before film fabrication.

by simply using a high power laser. By confining the light in a waveguide suitably high intensities can be obtained[30]. The power requirements will clearly be eased further by coupling the light efficiently into the waveguide. By using the TVC light can be coupled efficiently and in addition the device is then 'packaged', ready for insertion into an optical system. Another advantage of the TVC in this context arises from the tapered velocity nature of the coupling proces. The efficiency of transverse (prism) coupling into a material with an intensity dependent refractive index has been shown to be a strong function of intensity[31]. This is because the propagation constant of the prism field and the waveguide field must be precisely matched for optimum power transfer. The propagation constant of the non-linear waveguide changes with intensity and matching cannot be maintained without manually adjusting the prism[31]. The maximum efficiency obtained by this technique was an insertion loss of -20dB. The intensity dependent mismatch could be minimised by using tapered velocity coupling from a TVC.

Another related example of a non-linear optics application is that of second harmonic generation or frequency doubling.

Frequency doubling has been observed using a thin (4.8-6.5μm) single crystal organic waveguide grown between two silica substrates[32]. If such a crystal were grown between two TVC couplers it would constitute a packaged low-insertion loss frequency doubler.

1.3.2 Further applications.

Other applications for devices such as the TVC are in the areas of local area networks[33] and of optical interconnects[34]. Both areas require a low-cost, efficient, fibre-waveguide connection before integrated optics can be competitive with electronics for information processing. In both areas, light from a single laser is often split between a number of channels, this number being determined by the launch power, the system losses and the detector sensitivity. By reducing system losses (e.g. insertion loss) higher splitting levels can be achieved, reducing costs.

1.4 Theoretical and experimental results

1.4.1 Coupling to planar films; theory

Evanescent field coupling between a cylindrical fibre and a planar film is an interesting theoretical problem. The modes of the film form a continuum (or 'mode-sink') and it is necessary to consider coupling from the fibre mode to each film mode. Coupling problems are normally treated by coupled mode theory (CMT) which was developed to describe coupling between two single-mode guides[35], and is discussed together with mode-sinking in chapter 3. In chapters 3 and 5 the published work on this subject is discussed . Based on CMT it has inherent limitations for describing this problem and these are also discussed. An improved model of the coupled guide behaviour is proposed in chapter 5 for 'weakly coupled'[36] guides. The results of numerical calculations, for 'strongly coupled'[36] guides, based on the beam propagation method[37,38] are also given. The theoretical wavelength dependence of the coupler is predicted and compared with experimental results.

1.4.2 Coupling to planar films: experiment

In chapter 5 the experimental arrangement used to investigate fibre-film-fibre coupling is described. TVC's were used with planar oil films of known index. The dispersion diagram of the two guides, fibre and film is calculated in terms of propagation constant against wavelength. From this it is seen that synchronisation and hence efficient power transfer can only be achieved at particular wavelengths (for a given film thickness) and particular film thickness (at a given wavelength). Synchronisation was achieved by using a multiwavelength source and an optical spectrum analyser. Loss was measured by a cut-back technique giving a direct measurement of total insertion loss. Experimental results of mode sinking are given, both multiwavelength using oil films and single wavelength using a flip-chip[39]. A flip-chip is a substrate block on which integrated optical componentry has been formed and which is connected to a second optical circuit by physically clamping the two together. The dimensions of the two optical circuits are normally tailored to each other and coupling between them may be end-fire, evanescent or both.

The comb-filter characteristic of the coupler (in wavelength terms) was found to have two regimes. For thin films of low mode order the pass bands were relatively broad (in terms of FWHM), typically 100nm. These were suitable for environmentally insensitive coupling to a film where processing occurs in the film. For thick films of high mode

order the passbands were relatively narrow, typically 10nm. These were suitable for environmentally sensitive coupling where processing occurs at the interface i.e. where wavelength selection is performed, by the coupler e.g. in sensor applications. A sharp cut filter was also made using the same experimental arrangement. The transmission of the coupler changed by 17dB over a 1nm range at 1.32μm, with an insertion loss of only 2dB.

1.4.3 Coupling to rib-waveguides

The fabrication of rib waveguides directly onto the TVC and on flip chips is described in chapter 6. A dip-coating technique[40] was used to form polymer films directly onto TVC block. These were patterned and etched to form rib-waveguides. Rib-waveguides were also etched on flip-chips and flip-chip coupling was investigated. Coupling to channel waveguides such as those fabricated on polymer films by Bennion and co-workers[41] is similar in principle and was not investigated.

Chapter 7 contains a brief summary of this work and the conclusions drawn from it. A novel method of performing wavelength division multiplexing is described.

References

1. Kapron, F.P., Keck, D.B., Maurer, R.D., 'Radiation losses in glass optical waveguides', Appl. Phys. Letts. Vol. 17, No. 10, 15 Nov (1970) pp.423-425.

2. Miya, T., Terunuma, Y., Hosaka, T., Miyashita, T., 'Ultimate low loss single mode fibre at 1.55μm', Electron. Letts., Vol. 15, pp.106-108, Feb 15 (1979).

3. Kressel, H., Butler, J.K., 'Semiconductor Lasers and Heterojunctions, LEDs', New York; Academic Press, 1978.

4. Washington, M.A., Hahory, R.E. Pollack, M.A., Beebe, E.D., 'High efficiency $In_{1-x}Ga_xAs_yP_{1-y}$/InP photodetectors with selective wavelength response between 0.9 and 1.7μm', Appl. Phys. Lett., Vol. 33, No. 10, Nov (1978) pp.854-856.

5. Smith, D.R., Hooper, R.C., Garret, I., 'Receivers for optical communications: A comparison of avalanche photodiodes with PIN-FET hybrids', Opt. Quantum Electron., Vol. 10, 1978, pp.292-300.

6. Ogawa, K., 'Optical repeater gain achievable with light-activated p-n p-n LEDs', in Tech. Dig. Topical Meet. Optical Fibre Communication (Washington D.C.) Paper ThB.5, pp.94-95 Mar 1979.

7. Henry, P.S., 'Introduction to Lightwave Transmission', IEEE Communications, Vol. 23, No. 5, pp.12-16.

8. Linke, R.A., Kasper, B.L., Olsson, N.A., Alferness, R.C., Bunhl, L.L., McCormick, A.R., 'Coherent Lightwave Transmission over 150km fibre lengths at 400Mb/s and 1Gb/s Data Rates Using DPSK Modulation', IOOC-ECOC 1985 (Venice) pp.35-38.

9. Malyon, D.J., Smith, D.W., Wyatt, R., 'Semiconductor Laser Homodyne Optical Phase Locked Loop', Electron. Letts. Vol. 22, No. 8, 10th Apr 1986, pp.421-422.

10. Botez, D., Herskowitz, G.J., 'Components for Optical Communications Systems: A Review', Proc. IEEE Vol. 68, No. 6, June 1980, pp.689-731.

11. Alferness, R.C., 'Guided wave devices for Optical Communication', IEEE J. Quant. Electron., Vol. QE-17, No. 6, June 1981, pp.946-959.

12. Laybourn, P.J.R., Lamb, J., 'Integrated Optica: A tutorial Review', The Radio and Electron. Eng., Vol. 51, No. 7/8, pp.397-431 July/Aug 1981.

13. Shimizu, N., Imoto, N., Jkeda, M., 'Fusion splicing between optical circuits and optical fibres', Electron. Letts., Vol. 19, No. 3, 3rd Feb (1983), pp.96-97.

14. Goodwin, M.J., Glenn, R., Bennion, I., 'Organic Nonlinear Optical Waveguides Formed by Solvent Assisted Indiffusion', Submitted to Electron. Letts.

15. Nakamura, M., 'Single mode operation of semiconductor injection lasers', IEEE Trans. Circuits., Syst. Vol. CAS-26, pp.1055-1065 (1979).

16. Kimura, T., 'Single mode systems and components for longer wavelengths', IEEE Trans. Circuits., Syst. Vol. CAS-26, pp.978-1010 (1979).

17. Alferness, R.C., Economou, N.P., Buhl, L.L., 'Fast, Compact optical directional coupler switch/modulator', Appl. Phys. Lett. Vol. 38, pp.214-216 (1981).

18. Ainslie, B.J., Beales, K.J., Day, C.R., Rush, J.D., 'The Design and Fabrication of Monomode Optical Fibre', IEEE J. Quant. Electron. Vol. QE-18, No. 4, April (1982). pp.514-523.

19. Alferness, R.C., Ramaswamy, V.R., Korotky, S.K., Divino, M.D., Buhl, L.L., 'Efficient single mode fibre to Titanium Diffused Lithium Niobate Waveguide Coupling for λ=1.32μm', J. Quant. Electron. Vol. 18, No. 10, Oct (1982) pp.1807-1812.

20. Murphy, E.J., Rice, T.C., 'Low loss coupling of Multiple Fibre Arrays to single mode waveguides', J. Lightwave Tech. Vol. LT-1, No. 3, pp.479-482, Sept (1983).

21. Nutt, A.C.G., Bristow, J.P.G., McDonach, A., Laybourn, P.J.R., 'Fibre to waveguide coupling using Ion Milled alignment grooves in Lithium Niobate at 1.3 m wavelength', Opt. Lett., Vol. 9, No. 10, October (1984) pp.463-465.

22. McCaughan, L., Bergmann, E.E., 'Index Distribution of Optical Waveguides from their mode profile', J. Lightwave Tech., Vol. LT-1, No. 1, pp.241-244, March (1983).

23. Komatsu, K., Kondo, M., Ohta, Y., 'Titanium/Magnesium Double Diffusion Method for Efficient Fibre-Lithium Nibate Waveguide Coupling', IGWO, Feb (1986) PDP-2, Atlanta, pp.11-13.

24. Stewart, G., Hutchins, R.H., Laybourn, P.J.R., 'Hybrid Integration of Active and Passive Devices', 3rd Int. Conf. on Int. Opt. and Opt. Fibre Commun., San Francisco U.S.A. April (1981).

25. Stewart, G., Hutchins, R.H., Laybourn, P.J.R., 'Controlled growth of Arsenic Trisulphide Films for coupling to integrated optical devices', J. Phys. D. Appl. Phys., Vol. 14 (1981), pp.323-331.

26. Dalgoutte, D.G., Smith, R.B., Achutaramayya, G., Harris, J., 'Externally mounted fibres for integrated optics interconnections', Appl. Opt., Vol. 14, No. 8, Aug (1975), pp. 1860-1865.

27. Millar, C.A., Ainslie, B.J., Brierley, M.C., Craig, S.P., 'Fabrication and characterisation of D-fibres with a range of accurately controlled core/flat distances', Electron. Lett. Vol. 22, No. 6, 13th Mar (1986), pp.322-324.

28. Bradley, L., Millar, C.A., 'A new method of fibre film coupling', Conf. on Lasers and Electro. Opt. Paper MF5, San

Francisco U.S.A. June (1986).
Bradley,L.,Millar,C.A.,'Evanescent FieldCoupling between a single mode fibre and a thin film waveguide'Submitted to Optics Letters.

29. Burns, W.K., Milton, A.F., 'Tapered Velocity Couplers for Integrated Optics: Design', Appl. Opt., Vol. 14, No. 5, May (1975), pp.1207-1212.

30. Stegeman G.I.,Seaton C.T.,'Non-linear integrated optics'J.Appl. Phys. Vol.58, No.12 Dec (1985) pp57-78

31. De Valera, J.D., Stevensson, R.B., Seaton, C., Stegeman, G., Mai, X., 'Non-linear prism coupling and propagation in non-linear waveguides', Electromagnetic Surface Excitations, Springer-Verlag (1986) New York, pp.302-303.

32. Itoh, H., Takara, H., Hotta, K., Sasaki, K., 'Phase matched frequency doubling in a very thin 2-methyl-4-nitroaniline single crystal waveguide, with a Nd:YAG Laser', Conf. on Lasers and Electro. Opt. Paper WR4, San Francisco, U.S.A., June (1986).

33. Payne, D.B., Stern, J.R., 'Transparent Single-mode Fibre Optical Networks', J. Lightwave Tech. Vol. LT-4 No. 7 July (1986). pp.864-869.

34. Bergman, L., Johnston, A., Nixon, R., 'Applications and design considerations for optical interconnects in VLSI' SPIE Los Angeles U.S.A. Jan 24 (1986), pp.1-10.

35. Miller, S.E., 'Coupled wave theory and waveguide applications', B.S.T.J., May (1954), pp.661-719.

36. Marcuse, D., 'The coupling of degenerate modes in two parallel dielectric waveguides', B.S.T.J., Vol. 50, No. 6, July (1971), pp.1791-1816.

37. Van der Donk, J., 'The beam propagation method in integrated optics', Ph.D. Thesis, University of Ghent (1982).

38. Feit, M., Fleck, J.A., 'Comparison of calculated and measured performance of Diffused Channel-waveguide couplers', J. Opt. Soc. Am., Vol. 73, pp.1296-1302 (1983).

39. Hsu, H.P., Milton, A.F., 'Flip-chip approach to end fire coupling between single-mode optical fibres and channel waveguides', Electron. Lett. Vol. 12, No. 16, Aug (1976), pp.404-405.

40. Fibson, M., Frejlich, J., 'Dipcoating method for fabricating thin photoresist films', Thin Solid Films Vol. 128, (1985), pp.11-170.

41. Bennion, I., Hallan, A.G., Stewart, W.J., 'Optical waveguide components in organic photochromic materials', Radio and Electron. Eng. Vol. 53, pp.313-317 (1983).

Chapter2.The Slab and Fibre Guides in Isolation

2.1 Introduction

In order to understand coupling from a thin-film waveguide to a single mode fibre it is necessary to examine the behaviour of the waveguides in isolation. The dielectric thin film or slab waveguide (figure 2.1a) is the simplest form of optical waveguide. It consists of a high index guiding region of thickness t and index n_g, of infinite extent in the x and z directions. It is bounded by two cladding regions of lower refractive index known as the superstrate and substrate which are in general different. Light is confined by the cladding/guiding layer boundary and the slab therefore provides guidance in one dimension.

The simplest form of fibre guide consists of a dielectric rod surrounded by a cladding region of lower refractive index. Light is confined by the core/cladding boundary and the fibre therefore provides guidance in two dimensions. For both guides the cladding is in theory of infinite extent but in practice a thickness of a few tens of microns is normally sufficient to isolate the high index region.

In this chapter the theory of the slab guide is discussed in terms of the mode effective index. The fibre theory is treated in more detail beginning with the weakly guiding approximation and leading to the concept of an equivalent step index fibre. The technique is described by which the parameters of the fibre used in experiments were obtained. An approximate expression for the effective index of the fibre at any wavelength in the experimental range is given. Finally the Gaussian approximation to the fibre mode is discussed.

2.2 Slab waveguide

The slab waveguide has been extensively analysed [1-4] and its behaviour is well understood. The modes of the slab guide can be found by solving Maxwell's equations using the appropriate boundary conditions. There is a finite set of guided wave solutions (guided modes) and a continuum of radiation solutions (radiation modes). The modes are further subdivided by polarization into transverse electric (TE) with $E_z = 0$ and transverse magnetic (TM) with $H_z = 0$. E, H represent the electric and magnetic fields respectively, with propagation in the z-direction. The m^{th} TE (TM) guided wave solution,

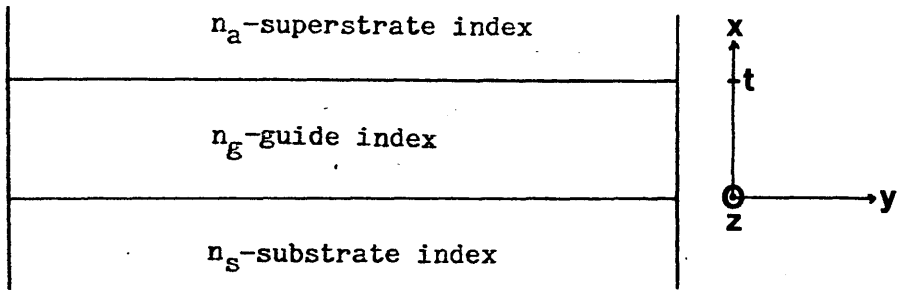

$$n_s < n_g > n_a$$

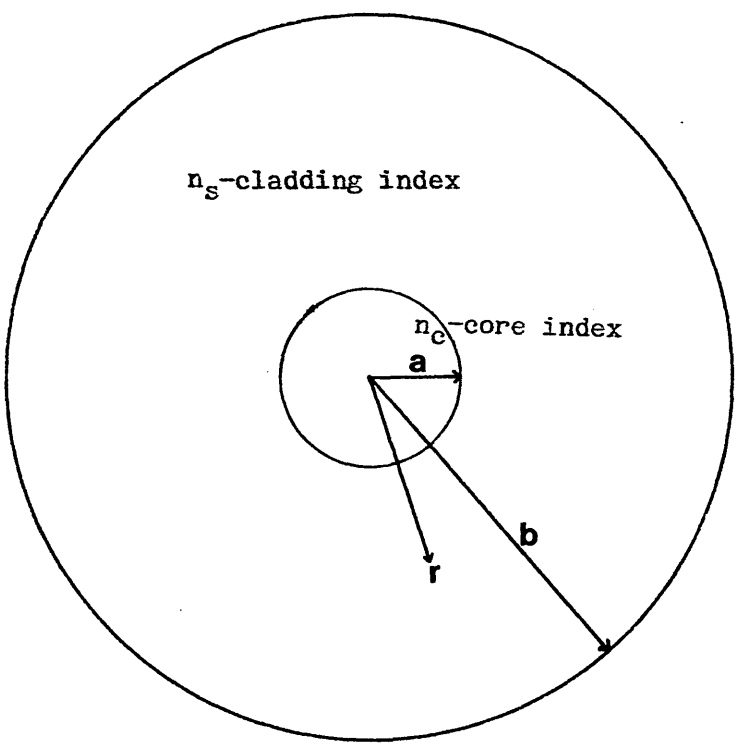

Figure 2.1a) Geometry of step-index, slab waveguide.

b) Geometry of step-index, fibre waveguide.

(i.e. the m^{th} TE (TM) mode) designated TE_m (TM_m) has propagation constant k_s^{mTE} (k_s^{mTM}). For a particular polarisation the normalised propagation constant is given by;

$$n_e = k_s^m/k_o \qquad 2.1$$

where $k_o = 2\pi/\lambda_o$ = the wave number 2.2

λ_o = the free space wavelength

and n_e = the effective index.

For a slab guide with $n_g > n_s \geq n_a$ the guided modes are constrained to have an effective index in the range $n_g > n_e > n_s$. Working in terms of the effective index leads to an intuitive understanding of how strongly a mode is guided. An effective index close to n_g indicates that most of the guided power travels in the high index region. An effective index $n_e=n_s$ indicates that the optical power is entirely in the cladding and the mode is said to be "cut-off". A continuum of radiation modes exists in the cladding with a range of effective indices between 0 and n_s.

In figure 2.2 the fundamental TE and TM modes of a film of index 1.59, substrate index 1.4575 with an air superstrate are shown for a range of film thicknesses. As the thickness increases the effective index tends towards the bulk film index and as thickness is decreased the mode tends towards the substrate index where it is cut-off.

2.2.1 Characteristic equation of film modes.

If the substrate and superstrate indices are dissimilar the guide is said to be asymmetric while if they are identical it is said to be symmetric. The characteristic equation for an asymmetric slab is;

$$k_o t(n_g^2-n_e^2)^{1/2} = \tan^{-1}\left[F\left[\frac{n_e^2-n_s^2}{n_g^2-n_e^2}\right]\right]^{1/2} + \tan^{-1}\left[G\left[\frac{n_e^2-n_a^2}{n_g^2-n_e^2}\right]\right]^{1/2} + m\pi \qquad 2.3$$

where $F = (n_g/n_s)^4$ and $G = (n_g/n_a)^4$ for TM modes

$F = 1$ and $G = 1$ for TE modes.

In the majority of experiments symmetrical, silica-clad waveguides were used for which 2.3 may be slightly simplified, becoming;

$$k_o t(n_g^2-n_e^2)^{1/2} = 2\tan^{-1}(F(n_e^2-n_s^2)/(n_g^2-n_e^2))^{1/2} + m\pi \qquad 2.4$$

and

$$(n_e^2-n_s^2)/(n_g^2-n_e^2) = H \qquad 2.5$$

is a measure of the strength of guidance.

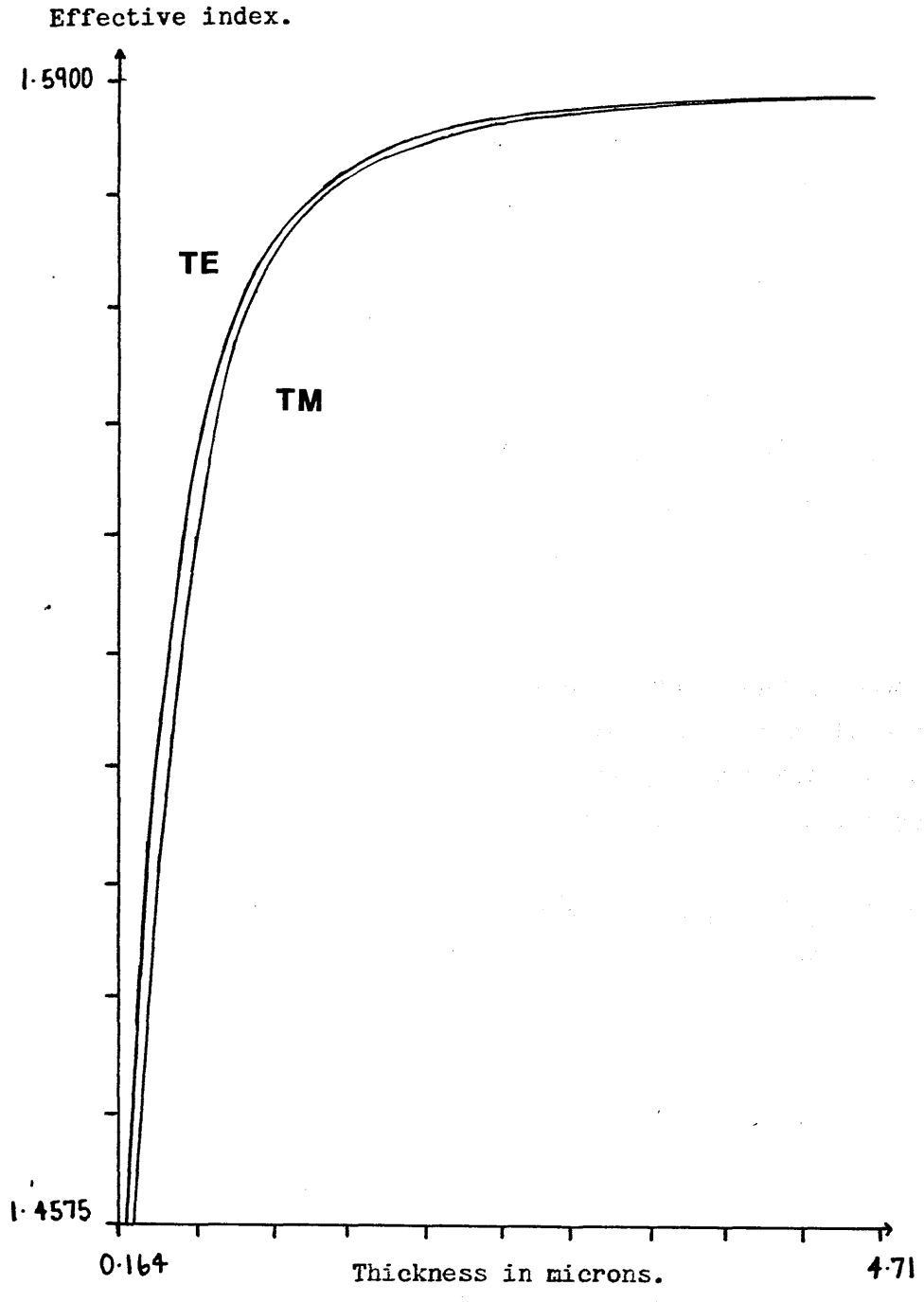

Figure 2.2 Effective index of the TE_0 and TM_0 modes of a film of index 1.590 on a silica substrate (index 1.4575) at a wavelength of 633nm for a range of film thicknesses.

2.2.2 Slab modes near cut-off

If H is small i.e. if $(n_g^2-n_e^2) >> (n_e^2-n_s^2)$ the mode is near cut-off and for a sufficiently high order mode ($m \neq 0$);

$$m\pi >> 2\tan^{-1}(FH)^{1/2} \qquad 2.6$$

In this case the characteristic equation may be greatly simplified and written as;

$$m=2t/\lambda_o(n_g^2-n_e^2)^{1/2} \qquad 2.7$$

Analytically it is convenient to work in this regime since 2.7 is an algebraic equation while 2.4 is a transcendental equation.

2.2.3 Mode field shape

In the slab guide of figure 2.1a, a mode propagating in the z-direction has no variation in the y-direction, i.e. $\partial/\partial y = 0$. The phase fronts of the mode lie in the x-y plane and extend to infinity in the y-direction. The electric field (of a TE mode) in the y-direction is given by

$$E_y = E_c\exp[-k_o(n_e^2-n_s^2)^{1/2}\ (x-t)] \quad x>t \qquad 2.8$$

$$E_y = E_g\cos[k_o(n_g^2-n_e^2)^{1/2}\ x-\tan^{-1}(H^{1/2})] \quad 0<x<t \qquad 2.9$$

$$E_y = E_c\exp[k_o(n_e^2-n_s^2)^{1/2}\ x] \quad x<0 \qquad 2.10$$

E_c is the field at the film-cladding interface and E_g is the peak field in the guide. Higher order modes have more field turning points which affects coupling to other fields in terms of the field overlap, discussed in section 3.4.2. The field in the regions $x>t$ and $x<0$ decays with distance from the guiding region and is said to be evanescent. The extent of the evanescent field is greater as n_e becomes closer to n_s and as wavelength increases. This result also applies to fibre guides.

2.2.4 Mode sinking

As the thickness of a film guide increases the number of TE or TM modes, N, it can support (each with a different effective index value) increases according to the following relation;

$$N=(n_g^2-n_e^2)^{1/2}\ 2t/\lambda_o \quad \text{(from 2.7)} \qquad 2.11$$

At a single wavelength the mode effective indices lie in the range;

$$n_s<n_e<n_g$$

As the optical thickness of the film is increased (i.e. thickness is increased or wavelength is decreased) the mode density within this range is proportionately increased. In an extremely thick film (i.e. 1000's of wavelengths thick) the mode density is so high that it is effectively continuous. This mode-continuum is known as a mode sink.

2.3 Fibre waveguide

2.3.1 Weakly guiding step index fibres

The clad dielectric rod (figure 2.1b) or step-index fibre has an exact analytical solution[5]. This solution is mathematically more involved than the slab waveguide analysis since it is stated in terms of circular functions and the modes are solutions of the vector wave equation. However ultra low-loss[6] single mode fibres for telecommunications have a graded index profile and have a very small index difference Δ, between the peak index in the central core region and the silica cladding region. Such fibres are said to be "weakly guiding" and their analysis is considerably simplified by the "weakly guiding approximation" of Gloge[7]. This shows that the longitudinal field components E_z, H_z of a step index fibre with a small index difference Δ are small compared with the transverse components and may be neglected. The modes then satisfy the scalar wave equation and are linearly polarised. The fundamental mode LP_{01} (or HE_{11}) can be described with an error of <2% by[7];

$$u(V) = (1+\sqrt{2})V/(1+(4+V^4)^{1/4}\ ] \qquad 2.11$$

where

$$u = a_s k_o (n_c^2-n_e^2)^{1/2} \qquad 2.12$$

$$w = a_s k_o (n_c^2-n_e^2)^{1/2} \qquad 2.13$$

$$V = u^2+w^2 = a_s k_o (n_c^2-n_s^2)^{1/2} \qquad 2.14$$

The fibre supports only the LP_{01} mode provided that $V<2.405$.

Very few graded index profiles[8] are amenable to exact analysis and a smoothly varying profile is almost impossible to manufacture due to evaporation and compositionally dependent layering effects in the fabrication process[9]. Monomode graded fibres are therefore treated by approximate and numerical methods. Very accurate solutions have been obtained by variational techniques[10] the beam propagation method[11] and others[12,13]. For the analysis of fibre-film coupling presented

here it has been sufficient to use an approximate technique known as the 'equivalent step index' method.

2.3.2 The equivalent step index fibre

This model is based on the observation that the fields of an HE_{11} mode of a graded fibre are very similar to the fields of an HE_{11} mode on <u>some</u> step profile[14]. Similarity can be expected only for a core profile monotonically decreasing with radius, which is circularly symmetric. Related approaches have been used to analyse non-monotonic functions such as depressed cladding fibres[15]. The accuracy of the method is highest for profiles which closely approximate the step index profile, so called quasi-step index profiles. A schematic diagram of the actual and ESI profiles of the fibre used in the majority of these experiments is shown in figure 2.3. The fibre, BTRL Type B 9419 is designed to have an ESI core radius a_s=4μm and an equivalent index difference Δ_s = 0.004.

The actual profile has a central dip formed as the fibre preform is collapsed. The central dip affects the fibre dispersion and is important in the study of picosecond pulse broadening for which very accurate dispersion data are required and for which the ESI method is insufficient. There is an error in using the ESI approximation for fibre-film coupling calculations but it is acceptable since the calculated dispersion is in sufficient agreement to explain the experimental results (in chapter 5).

Only two parameters are required to specify a step-index fibre. Suitable parameters include λ_{co}, w_o. Where λ_{co} is the wavelength above which the LP_{11} mode does not propagate (i.e. is cut off) and the fibre is single moded, and w_o is the mode spot size[16]. An alternative is to measure the actual profile by a near[17] or far[18] field technique and calculate the ESI profile. A number of techniques aimed at different parameters have been developed including one which is wavelength insensitive[19] and another for prediction of waveguide dispersion[20].

2.3.3 ESI measurement of experimental fibre

In the analysis of fibre-film coupling it was found that the technique described in ref. 16 gave an ESI profile of sufficient accuracy. It is shown that the width a_s, and index difference Δ_s of the ESI profile can be found by measuring the variation of the mode

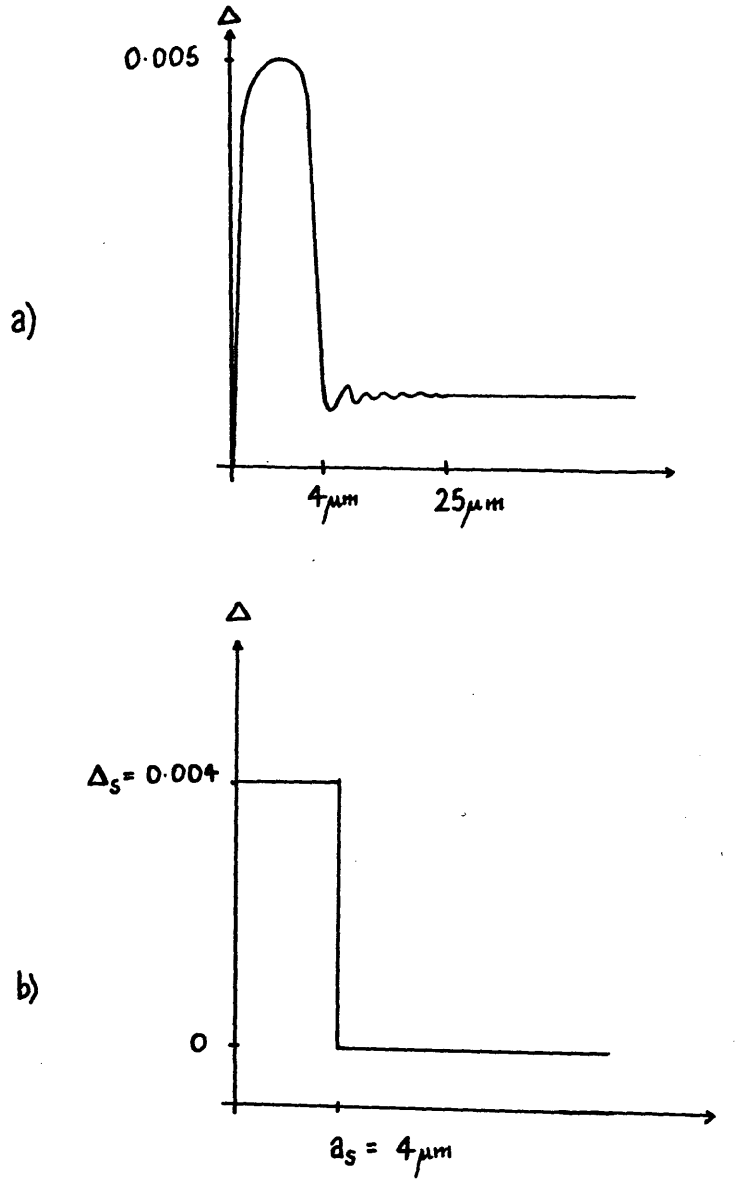

Figure 2.3 Schematic diagram of actual and ESI profiles of type B, single mode fibre. The central index depression occurs in the MCVD process due to GeO_2 evaporation as the preform is collapsed.

spot size w_s (at 1/e intensity) around the cut-off wavelength. From equation 2.14 we have, at cut-off,

$$V = V_{co} = 2.405, \quad \lambda=\lambda_{co}$$

$$(n_c^2-n_s^2)^{1/2}=\lambda_{co}V_{co}/(a_s 2\pi) = 0.38277\ \lambda_{co}/a_s \qquad 2.15$$

$$(n_c^2-n_s^2)^{1/2}= \text{Numerical Aperture, } NA_s. \qquad 2.16$$

From the variation of the mode spot size w_s around λ_{co} it is shown that;

$$a_s = 1.0737(2.1757\ w_{sco}-1.45047\lambda_{co}\ dw_s/d\lambda\Big|_{\lambda=\lambda_{co}}) \qquad 2.17$$

where w_{sco} is the mode spot size at the cut off wavelength. The experimental fibre was measured and the field width against wavelength is shown in figure 2.4. I am grateful to G.C. Warnes of BTRL for performing the measurement. The point of measurement is the intersection of the two asymptotes. The data points were processed after manual estimation of the asymptote directions giving calculated parameters of;

$$a_s = 4.06\mu m \qquad 2.18$$

$$\Delta_s = 0.0044 \qquad 2.19$$

$$NA_s = 0.1131 \qquad 2.20$$

2.3.4 Use of the ESI parameters

The ESI parameters are convenient because the effective index of the HE_{11} mode can be obtained at any wavelength within the experimental range. It is assumed that the numerical aperture of the fibre remains constant over this range. It was shown by Wood and Fleming[21] who measured the dispersion of bulk samples of pure and Ge-doped silica glass that the index difference between them remained constant.

$$\text{Writing } NA_s = (n_c^2-n_s^2)^{1/2}=((n_s+\Delta)^2-n_s^2)^{1/2} \qquad 2.21$$

$$NA_s \simeq (2\Delta)^{1/2}(n_s)^{1/2} \qquad 2.22$$

The variation of $(n_s)^{1/2}$ over the wavelength range 1.1 to 1.6μm is approximately 0.2% leading to the assumption of constant numerical aperture.

Returning to 2.14 we can say;

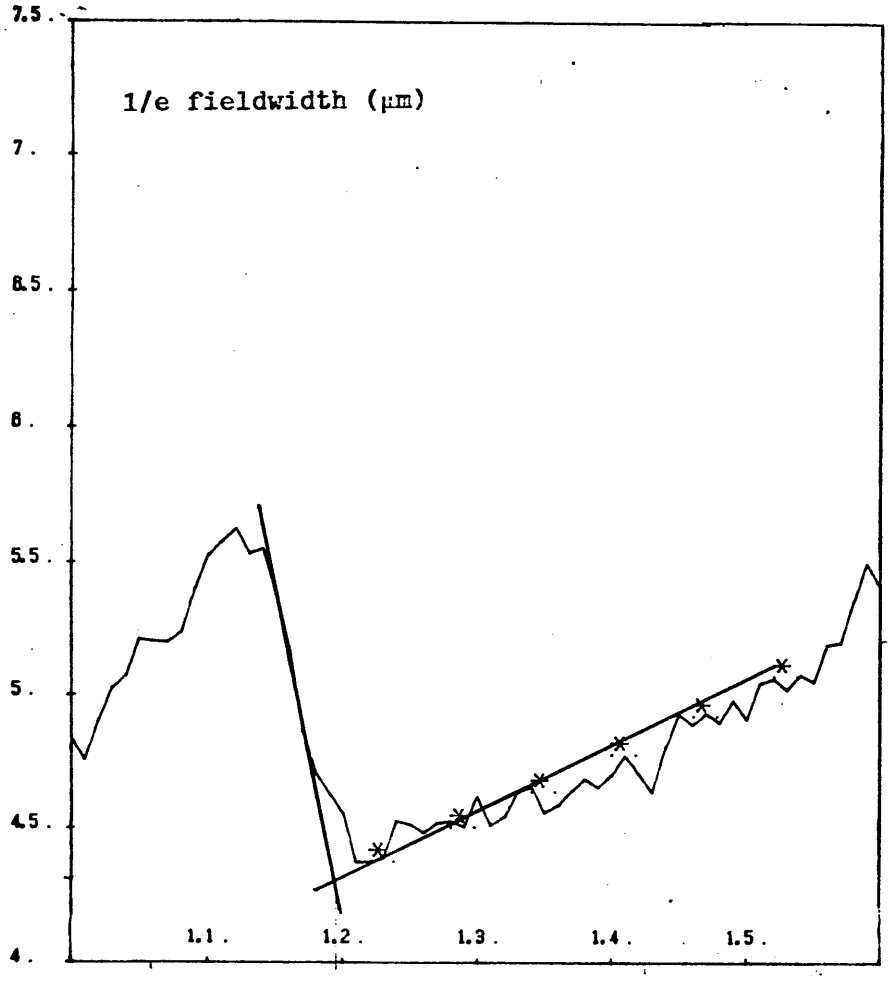

Fibre BTRL 9419-B

λ_{co}=1.2μm

w_{sco}=4.32μm

Figure 2.4 Plot of 1/e fieldwidth against wavelength of single mode fibre to determine ESI parameters.

$$V = k_o a_s NA_s \quad \text{or} \quad V\lambda_o = 2\pi a_s NA_s \qquad 2.24$$

Therefore knowing V_{co}, λ_{co} we can specify V at a particular wavelength. Also knowing the dispersion of silica[21] and the index difference Δ, we can specify n_c, n_s at each wavelength. We determine $n_e(\lambda)$ the fibre effective index as follows.

$$n_e^2(\lambda) = n_c^2(\lambda) - (u\lambda/a_s 2\pi)^2 \quad \text{Rearranging} \quad 2.12$$

$$n_e^2(\lambda) = n_c^2(\lambda) - ((1+\sqrt{2})V\lambda/(1+(4+V^4)^{1/4})/2\pi a_s)^2 \quad \text{Using 2.11}$$

$$n_e^2(\lambda) = n_c^2(\lambda) - \frac{(1+\sqrt{2})V_{co}\lambda_{co}/(2\pi a_s)}{(1+(4+(V_{co}\lambda_{co}/\lambda)^4)^{1/4})} \qquad 2.25$$

Equation 2.25 is the characteristic equation of the fibre.

Thus we are able to specify the effective index of the fibre using an ESI technique and a knowledge of the glass dispersion. This technique is sufficiently accurate to explain the fibre-film coupling behaviour. It also has the advantage of being relatively simple to compute.

2.3.5 The Gaussian approximation

The field of the HE_{11} mode of a step index fibre is described by the Bessel[22] function $J_o(ur/a)$ in the core and decays as the modified Hankel function $K_o(wr/a)$ in the cladding. For large values of the argument (wr/a) i.e. for large r the evanescent field in the cladding decays as exp(-wr/a).

An alternative to the ESI approximation is the gaussian approximation. It has been shown, both experimentally[23] and theoretically[24] that the field of a single-mode, weakly guiding, quasi-step index fibre is very nearly gaussian in shape. The overlap between a gaussian beam and the HE_{11} is greater than 94% over the single mode region considered in this work. It is possible to approximate the mode field by a Gaussian; although this model is unsuitable for calculations such as evanescent field coupling[25] it gives a good conceptual understanding of fibre propagation. The mode can be thought of as a gaussian beam at the beam waist, with a plane phase front with a divergence equal to the confining power of the fibre waveguide. the nett divergence is zero and the mode propagates with the shape of the

beam waist[26].

References

1. Tien, P.K., Ulrich, R., Martin, R.J., "Modes of propagating light waves in thin deposited semiconductor films". Appl. Phys. Letters, Vol. 14, pp.291-294, May 1969.

2. Kogelnik, H., "Theory of dielectric waveguides", In "Integrated Optics" Edited by T. Tamir, Topics in Applied Physics, Volume 7. Published by Springer Verlag, New York.

3. Yariv, A., "Introduction to optical electronics", (Holt Rinehart and Winston, London 1976.

4. Marcuse, E., "Theory of dielectric optical waveguides", (Academic Press, New York, 1974).

5. Snitzer, E., "Cylindrical dielectric waveguide modes", J. Opt. Soc. Amer. 51, (1961) p.491.

6. Miya, T., Terunuma, Y., Hosaka, T., Miyashita, T., "Ultimate low loss single-mode fibre at 1.55μm", Electron. Lett. Vol. 15, pp.106-108, 1979.

7. Gloge, D., "Weakly guiding fibres", Applied Optics, Vol. 10, No. 10, October 1971, pp.2252-2258.

8. Marcuse, D., "The impulse response of an optical fibre with parabolic index profile", B.S.T.J. Vol. 52, No. 7, (1973) pp.1169-1174.

9. Ainslie, B.J., Beales, K.J., Day, C.R., Rush, J.D., "The design and manufacture of monomode optical fibre", IEEE J. Quant. Electron. Vol. QE-18, No. 4 (1982) pp.514-523.

10. Okoshi, T., Okamoto, K., "Analysis of wave propagation in inhomogeneous optical fibres using a variational method", IEEE Trans. Microwave Theory and Techniques, Vol. MTT-22, No. 11, (1974) pp.938-945.

11. Feit, M.D., Fleck, J.A., "Mode properties and dispersion for two optical fibre index profiles by the propagating beam method,' Appl. Optics, Vol. 19, No. 18, 15th September 1980, pp.3140-3150.

12. Yeh, C., Manshadi, F., "On weakly guiding single mode optical waveguides", IEEE J. Lightwave Tech., Vol. LT-3 No. 1, February (1985) pp.199-205.

13. Feit, M.D., Fleck, J.A., "Light propagation in graded index optical fibre", Appl. Optics, Vol. 17, No. 24, 15th December 1978, pp.3990-3998.

14. Snyder, A.W., Sammut, R.A., "Fundamental (HE_{11}) modes of graded optical fibres", J. Opt. Soc. Am., Vol. 69, No. 12, (1979) pp.1663-1671.

15. Hussey, C.D., De Fornel, F., "Effective refractive index and range of monomode operation for W-Fibres", Electron. Letts. Vol. 20, No. 8, pp.346-347, April 1984.

16. Millar, C.A., "Direct method of determining equivalent step index profiles for monomode fibres", Electron. Letts., Vol. 17, No. 13, June (1981) pp.458-460.

17. Sharma, .K., Tewari, R., "Accurate estimation of single mode fibre characteristics from near field measurements", Electron. Letts., Vol. 20, No. 20, Sep. (1984) pp.805-806.

18. Srivistava, R., Roversi, J.A., Campos, A.C., "Equivalent step index fibre determination from wavelength dependence of far field", Electron. Letts. Vol. 20, No. 4, Feb. (1984) pp.161-162.

19. Black, R.J., Pask, C., "Developments in the theory of equivalent step index fibres", J. Opt. Soc. Am., Vol. 1, No. 11, (1984) pp.1129-1131.

20. Martinez, F., Hussey, C.D., "Enhanced ESI for prediction of waveguide dispersion in single mode optical fibres", Electron.

Letts., Vol. 20, No. 24, No. (1984) pp.1019-1021.

21. Wood, D.L., Fleming, J.W., "Computerized refractive index measurements for bulk materials at UV, visible and IR wavelengths", Rev. Sci. Instrum. 53(1). Jan. (1982) pp.43-47.

22. Abramovitz, M., Stegun, I.A., "Handbook of mathematical functions", U.S. Government Printing Office, Washington D.C., (1964) Chapter 9.

23. Stern, J.R., Peace, M., Dyott, R.B., "Launching into optical fibre waveguide", Electron. Letts. Vol. 6, No. 6, March 1970, pp160-162.

24. Marcuse, D., "Loss analysis of single-mode fibre splices", B.S.T.J., Vol. 56, No. 5, May-June 1977, pp.703-718.

25. Nelson, B.P., Wright, J.V., "Problems in the use of ESI parameters in specifying monomode fibres", Br. Telecom. Technol. J., Vol. 2, No. 1, Jan. 1984, pp.81-85.

26. Snyder, A.W., Love, J., "Optical waveguide theory", Chapman and Hall, London.

3. Coupled waveguides and coupled mode theory

3.1 Introduction.

In chapter two it was shown that a fibre provides confinement in two dimensions while a planar film provides confinement in only one dimension. This simple observation is central to an understanding of evanescent field coupling between these structures. A rib guide[1,2] also provides two dimensional confinement while a prism or a similar very thick region has zero-dimensional confinement, acting as a mode sink.

Two parallel waveguides are coupled when the evanescent field decaying from the core boundary of one guide has a finite (and non-negligible) amplitude at the core boundary of the second guide. Since the evanescent field decays rapidly over a few wavelengths the guides must be in close proximity and the coupling strength increases as the guide spacing decreases. The different geometries in which this coupling occurs are classed according to the degree of guide confinement, in Table 3a.

3.2 Degree of confinement in coupled waveguides

Table 3a

Classification of transverse coupling according to the degree of confinement inherent in each waveguiding or mode sinking structure.

Category	Coupling Description	Degree of confinement	Reference
A	Slab - Mode Sink	1 - 0	3
B	Fibre - Mode Sink	2 - 0	4
C	Slab - Slab	1 - 1	5
D	Fibre - Slab	2 - 1	6
E	Fibre - Fibre	2 - 2	7

The prism film coupler (category A) was analysed using a method of plane wave expansion[3]. Coupling between guides of equal confinement (categories C and E) has been treated by coupled mode theory (CMT)[5,7]. Both Arnaud[6] and Marcatili[9] treated the problem of fibre-film coupling

(category D). Although their analyses are approximate and based on highly multimode fibres they explain some of the basic phenomena observed in this work. Both analyses employ as their starting point the concepts of CMT applicable to coupled guides of equal confinement and these are discussed below. The analysis of Arnaud was further refined and applied to single mode fibres recently[4]. Lasers can be thought of as providing three dimensional confinement and have been successfully coupled in large arrays (category F). Reference 8 explains the principles of this subject, also based on CMT. We derive at this point some of the basic results of CMT for parallel dielectric waveguides.

3.3 Coupled waveguides of equal confinement

3.3.1 Weak coupling of parallel guides

CMT can be usefully applied to analyse structures such as that shown in figure 3.1. The modes of the structure cannot be found analytically because the boundary conditions are too complicated but from perturbation theory they must be related to the modes of the individual waveguides (weak coupling).

For a lossless guide with finite transverse dimensions which is z-invariant the guided mode fields can be written

$$\underline{E}(x,y,z) = \underline{E}(x,y)\ \exp(j\beta z) \qquad 3.1a$$

$$\underline{H}(x,y,z) = \underline{H}(x,y)\ \exp(j\beta z) \qquad 3.1b$$

Where $E(x,y)=E_t$ and $H(x,y)=H_t$ are the transverse field distributions. The phase of the electric field changes according to;

$$d\underline{E}(x,y,z)/dz = j\beta\underline{E}(x,y,z) \qquad 3.2$$

with a similar expression for the magnetic field.

It has been shown by Arnaud[10] that; if the single mode of guide a (figure 3.1) has field E_a, H_a and propagation constant $\beta_a=k_o n_{ea}$ and that of guide b has field E_b, H_b; propagating as $\exp(-j\beta_b z)$ then the modes of the composite structure are given by;

$$(j\Gamma - j\beta_a)(j\Gamma - j\beta_b) = C_{ab}^2/P_aP_b \qquad 3.3$$

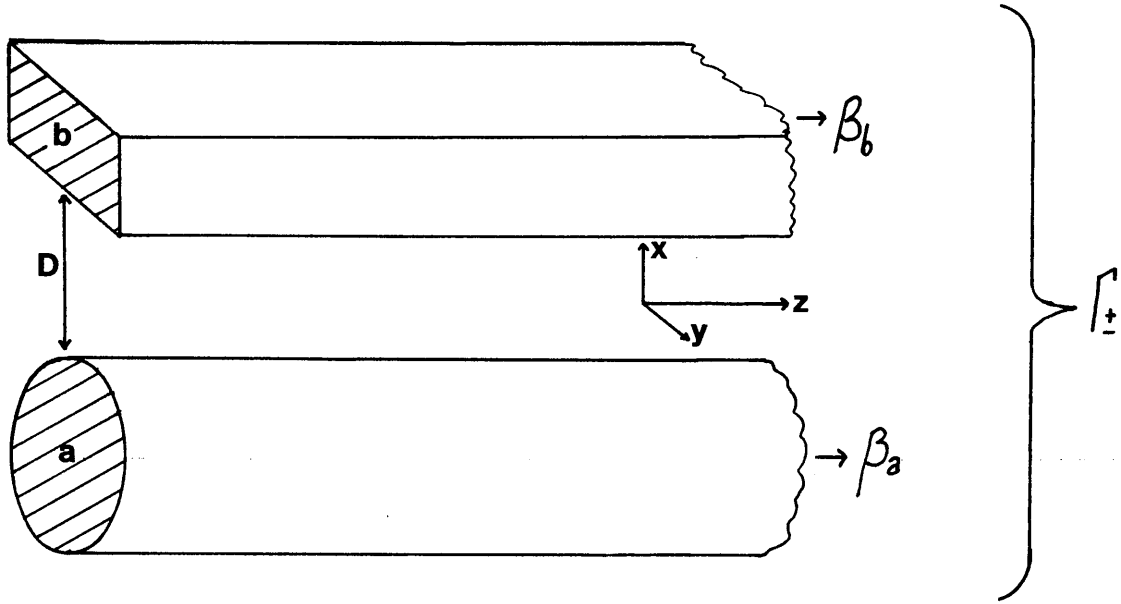

Figure 3.1. Two guide structure with common cladding. The individual guides are coupled and each guide in isolation has two dimensional confinement.

where $C_{ab} = 1/2 \int (\underline{E}_{ax}\underline{H}_{bx} + \underline{E}_{az}\underline{H}_{bx} - \underline{E}_{bx}\underline{H}_{az} - \underline{E}_{bz}\underline{H}_{ax})dx$ 3.4

$$P_a = \iint (\underline{E}_a \times \underline{H}_a) \cdot \hat{z}\, dydx \qquad 3.5a$$

$$P_b = \iint (\underline{E}_b \times \underline{H}_b) \cdot \hat{z}\, dydx \qquad 3.5b$$

and Γ is the propagation constant of a mode of the composite guide (i.e. a composite or coupled mode), $\hat{z}$ is a unit vector in the z direction. The assumptions here are that the guides are z-invariant, lossless, nearly synchronous and that to a first approximation the field E,H in the composite guide is given by;

$$\underline{H} = \underline{H}_a + \underline{H}_b \qquad 3.6a$$

$$\underline{E} = \underline{E}_a + \underline{E}_b \qquad 3.6b$$

Equation 3.5 is based on perturbation analysis and is valid for weakly coupled guides. In the case when the two guides a,b are synchronous, i.e. when;

$$\beta_a = \beta_b = \beta = k_o n_e \qquad 3.7$$

then equation 3.1 becomes;

$$j(\Gamma - \beta) = (C_{ab}^2/P_aP_b)^{1/2} \qquad 3.8$$

or $$\Gamma_{\pm} = \beta \pm K_{ab} \qquad 3.9$$

where $$jK_{ab} = C_{ab}/(P_aP_b)^{1/2} \qquad 3.10$$

K_{ab} is the coupling coefficient between guides a,b and Γ_+, Γ_- are the propagation constants of the coupled modes. The result (3.7) shows that the degeneracy (modes having equal propagation constants are said to be degenerate) of the modes of the isolated waveguides is removed by coupling. The amount of "mode splitting" is dependent on the coupling strength. If the guide separation were increased then C_{ab} would decrease since the field intensity of each guide in the vicinity of the other would fall and Γ_+, Γ_- would converge towards the original

value β. This allows us to define weak coupling as a small perturbation such that [11];

$$\beta \gg K_{ab} \qquad 3.11$$

3.3.2 Coupled line equations

The two coupled modes Γ_+, Γ_- beat as they propagate in the z-direction and some optical power is transferred between the waveguides. This can be described for synchronous guides according to the coupled line equations [12];

$$dE_a(x,y,z)/dz = j\beta E_a + jK_{ba}E_b \qquad 3.12a$$

$$dE_b(x,y,z)/dz = j\beta E_b + jK_{ab}E_a \qquad 3.12b$$

In addition to the phase change with propagation, of the guide in isolation predicted by 3.2, there is an additional contribution from the second guide. In equation 3.12a,b K_{ba} represents coupling from guide b to guide a while K_{ab} represents coupling from guide a to guide b. From the analysis leading to equation 3.9 it is clear that these two coupling coefficients are equal. This follows from the weak coupling assumption in equation 3.6. If the initial field amplitudes in guides a and b are A_o, B_o then it can be shown (Appendix 1) that the field amplitude in guides a,b are given by [5];

$$A(z)=(A_o \cos[K_{ab}K_{ba})^{1/2}z] + jB_o(K_{ba}/K_{ab})^{1/2}\sin[(K_{ab}K_{ba})^{1/2}z])e^{j\beta} \qquad 3.13a$$

$$B(z)=(B_o \cos[K_{ab}K_{ba})^{1/2}z] - jA_o(K_{ab}/K_{ba})^{1/2}\sin[(K_{ab}K_{ba})^{1/2}z])e^{j\beta} \qquad 3.13b$$

If the initial conditions are $A_o = 1$, $B_o = 0$ then the amplitude in guide b at a distance z, such that;

$$(K_{ab}K_{ba})^{1/2}\, z = \pi/2 \qquad 3.14$$

is clearly $(K_{ba}/K_{ab})^{1/2}.A_o$. This is only valid (under power conservation relations) if $K_{ab} = K_{ba}$. Equation 3.13 can therefore be written;

$$A(z) = (A_o \cos K_{ab}z + jB_o \sin K_{ab}z)e^{j\beta} \qquad 3.15a$$

with $A(o) = A_o$, $B(o) = 0$, is;

$$A(z) = A_o \exp[-j\int_o^z \beta(z)dz] \cos[\int_o^z K(z)dz] \qquad 3.18a$$

$$B(z) = jA_o \exp[-j\int_o^z \beta(z)dz] \sin[\int_o^z K(z)dz] \qquad 3.18b$$

The first integral contributes only phase if β is real and since we are interested only in power transfer it is neglected. The power transferred between the guides is therefore;

$$P(z) = \sin^2 T(z) \quad \text{with } T(z) = \int_o^z K(z)dz \qquad 3.19a$$

As the waveguide separation increases this tends asymptotically to

$$P(\infty) = \sin^2[T(\infty)] \text{ with } T(\infty) = \int_o^\infty K(z)dz \qquad 3.19b$$

It is not possible in this case to define a coupling length, L_c over which complete power transfer occurs. It is important to understand however, the length over which significant power transfer occurs. We define significant as the length L_s, at which

$$T(L_s)/T(\infty) = 0.95 \qquad 3.20$$

This is of most value when $T(\infty) = \pi/2$ since it is then effectively the length over which complete power transfer occurs.

3.3.5 Coupling strength in the TVC

The TVC is a branching coupler in the sense described by Findakly[14] with branching angle $=\theta_b$ (Figure 3.2). It can be coupled to a planar overlaid film [category D Table 3a] or to an overlaid rib waveguide [category E]. In both cases the local coupling strength depends on the guide spacing. Initially they are weakly coupled, becoming strongly coupled with decreasing spacing and are very strongly coupled prior to merging.

Matsuhara[15] has defined the local cross-section of non parallel guides for the general case of coupled, smoothly curved transmission lines. For branching guides the local cross section is normal to a line bisecting the branching angle (θ_b). This line is therefore the propagation axis of the coupled modes [figure 3.2]. In the experiments

Accurate analysis using:-

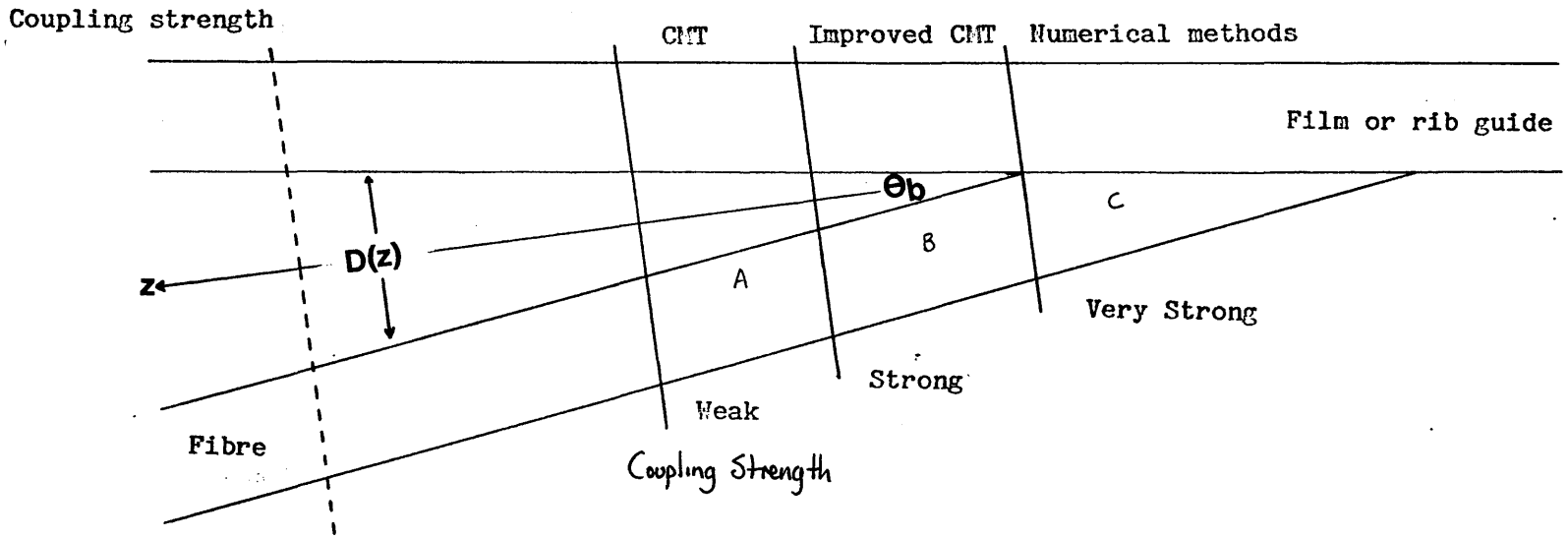

Figure 3.2 Strength of directional coupling between fibre and film or fibre and rib in a TVC. The guides are shown in cross section and the z-axis is at an angle $\theta_b/2$ to each guide according to reference 3.15.

reported here θ_b is typically 1^o and the multiplying factor $\cos(1^o/2)$ would appear in a strict calculation. Neglecting this results in an (acceptable) error of 4 parts in 10^5 but it is shown in the diagram for completeness.

3.3.6 Accurate analysis of strongly coupled branching guides

It can be seen from figure 3.2 that an analytical solution of fibre-film coupling using the TVC would be of limited accuracy. It does however give a good conceptual understanding of the coupling process. Experimental results for strongly coupled fibre and film guides show the behaviour predicted by the analysis of Marcatili, based on the concepts of CMT, (Chapter 5). Strongly coupled parallel guides have been shown to couple in the manner predicted by CMT[16] although the weak coupling approximation has been shown to be of limited accuracy in predicting the values of coupling coefficients and lengths[12]. The very strong coupling region cannot accurately be analysed by CMT and requires a computational technique such as the beam propagation method (BPM)[17,18]. A BPM program of 3-dimensional capacity is required, this is discussed with results, in ch5.4.

3.4 Consequences of non-synchronism

3.4.1 Power transfer efficiency

The directional coupler is a fundamental component of integrated optics. In practice it is very difficult to achieve synchronism i.e. $\beta_a=\beta_b$ and it is important to understand the effect of a mismatch $\Delta\beta=\beta a-\beta b$. Mismatch results in incomplete power transfer and therefore loss or crosstalk[19]. For two parallel guides of equal confinement the maximum power transfer efficiency falls with mismatch according to;

$$P_{mt} = (1 + (\Delta\beta/2K)^2)^{-1} \qquad 3.21$$

This result is derived in the Appendix. Strong coupling (large K) allows a relatively large mismatch $\Delta\beta$ for a given efficiency i.e. strong coupling is equivalent to low finesse. High finesse requires weak coupling and in a multipass device, a low cavity loss[20].

β is typically 10^7 and K is typically 10^3 so that a small mismatch $\Delta\beta/\beta= 10^{-4}$ is typically sufficient to halve power transfer.

Significant power transfer therefore only occurs between modes of nearly identical effective index.

3.4.2 Coupling between multimode guides

A strict analysis of coupling between multimode guides must include every guided mode. This results in a large set of equations (nxn) describing coupling between the p^{th} mode of guide a and the q^{th} mode of guide b. (where $1<p<n$, $1<q<n$) It has been shown[11] that this set of equations can often be reduced to two.

Provided that $\beta_a^p \simeq \beta_b^q$ and the coupling coefficient between the modes is much smaller than the propagation constants, coupling to a third mode is negligible unless $\beta_3 \simeq \beta_a^p, \beta_b^q$. Whenever this condition;

$$\beta_3 \neq \beta_a^p, \beta_b^q \qquad 3.22$$

is satisfied, coupling between two modes may be treated in isolation using 3.12.

It has been shown[5,24] and experimentally verified[25] that the coupling coefficient of two weakly coupled synchronous guides can be written simply in terms of the spatial field overlap;

$$K = w/(\varepsilon_o 4 P_o) \iint_A (n^2(x,y) - n_s^2) E_a^* \cdot E_b \, dxdy \qquad 3.23$$

w is the angular frequency, P_o is the total power carried by the waveguides, ε_o is the permittivity of free space and n(x,y) is the refractive index distribution of the composite waveguide.

If the guides are non-identical then this may occur for $p \neq q$. The transverse fields of the modes will have reduced overlap by comparison with modes of the same order, since positive and negative field contributions will cancel, figure 3.3. The coupling coefficient is reduced in comparison and the required coupling length increased.

Since the integral is only non-zero in the guiding (i.e. perturbation) regions, the limits of integration are set by the guide geometry. The coupling coefficient as a function of wavelength depends strongly on the extent and amplitude of the evanescent field (increasing with wavelength) multiplied by the amplitude of the core field (decreasing with wavelength). For fibre-fibre coupling[26] $K(\lambda)$ was found to peak at a particular wavelength, which varied with the fibre separation. $K(\lambda)$ is discussed for fibre film coupling in chapter

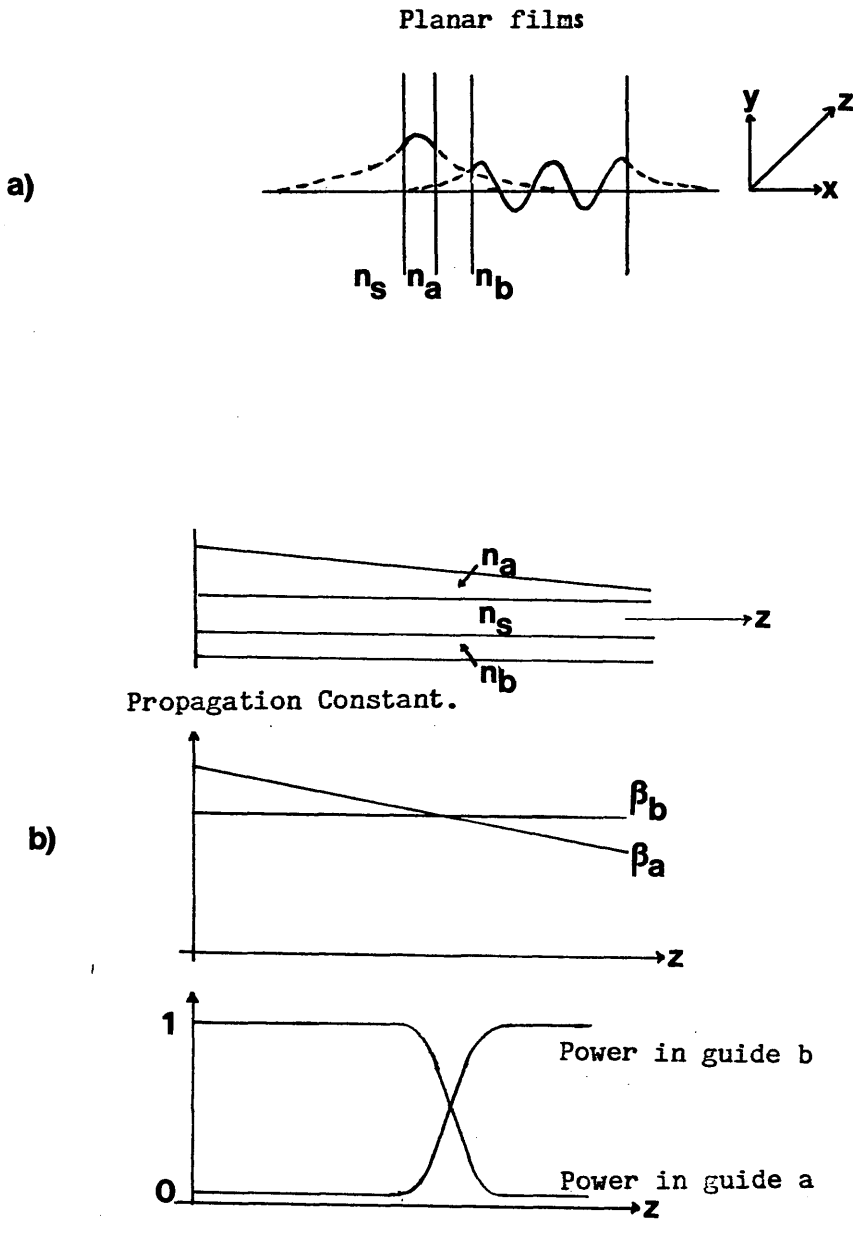

Figure 3.3 a) The field overlap is reduced for modes having differing amplitude profiles, by partial cancellation of positive and negative contributions.

b) As the thickness and mode effective index of guide a decreases, it becomes synchronous with guide b at one point and power is transferred in this region.

5.

3.4.3 Tapered velocity coupling

Since the fabrication requirements for synchronism are exacting, alternative phase matching methods have been investigated e.g. Electro-optic tuning of β_a and/or β_b[21] and taper coupling[22,23]. The principle of taper coupling is shown in figure 3.4 for two parallel slab waveguides. The effective index of one guide changes with distance and at one point the two guides are synchronous. Around this point significant power transfer occurs after which the guides are again isolated by their phase mismatch. This principle is employed in Chapter 5 to explain wavelength dependent coupling. Since modes having a range of effective indices can couple from guide a to b it is a broad band device.

A mode sink supports a continuum of modes over a specified effective index range. A guide supporting a mode in this range and coupled to the mode sink, will be phase matched to some point in the continuum and can transfer its total power into the mode sink. This power is normally lost as radiation and does not return to the guide[3,6].

3.4.4 Mismatch in non-parallel guides

An analytical solution cannot be obtained for non-parallel, non-synchronous guides. The fall-off in power transfer efficiency must be calculated numerically. it has been shown however that the efficiency decreases sharply with mismatch for branching waveguides[14].

3.5 Transverse fibre-film coupling

The concepts of CMT remain intuitive in the study of fibre-film coupling, that is;

a) Total power transfer requires synchronism
b)for parallel or non parallel guides coupling falls rapidly with mismatch
c) some power can couple from fibre-to-film-to-fibre.

These concepts are verified in chapter 5.

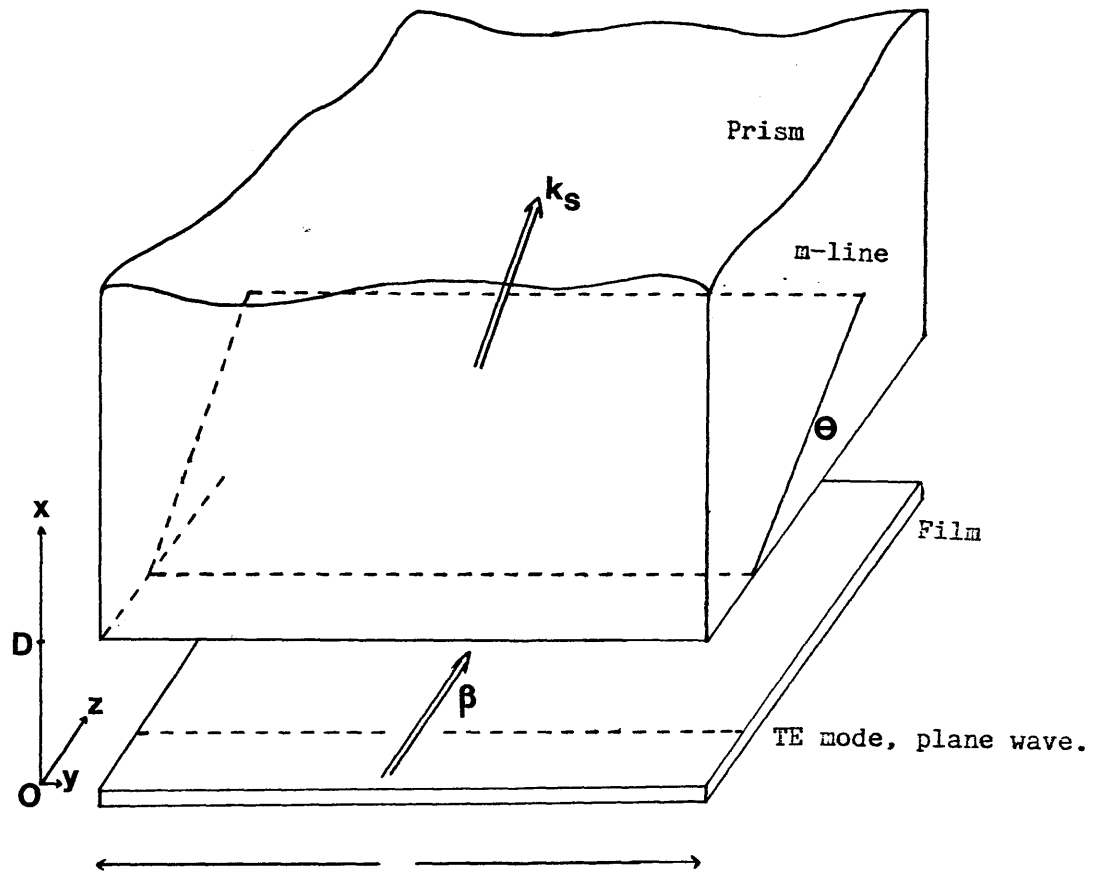

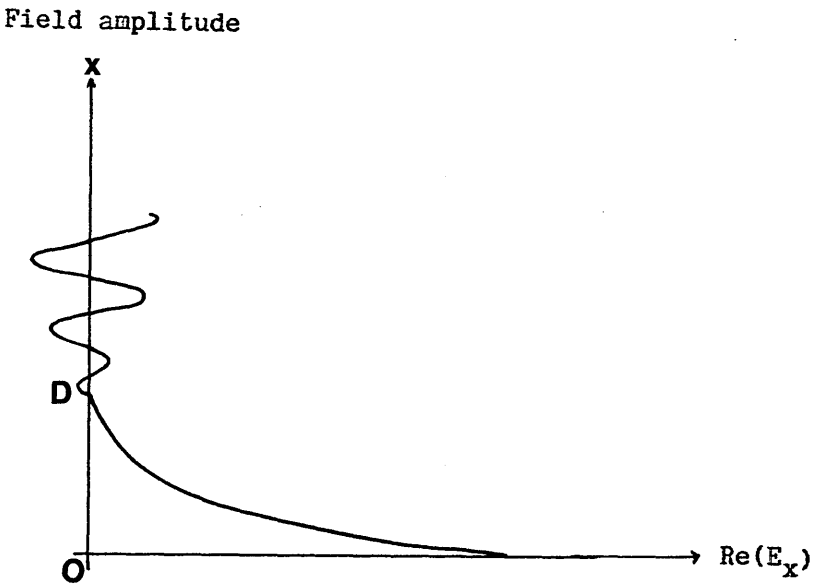

Figure 3.4a) Film prism coupling, n_p,n_a are the prism and gap indices ,D is the film-prism spacing.

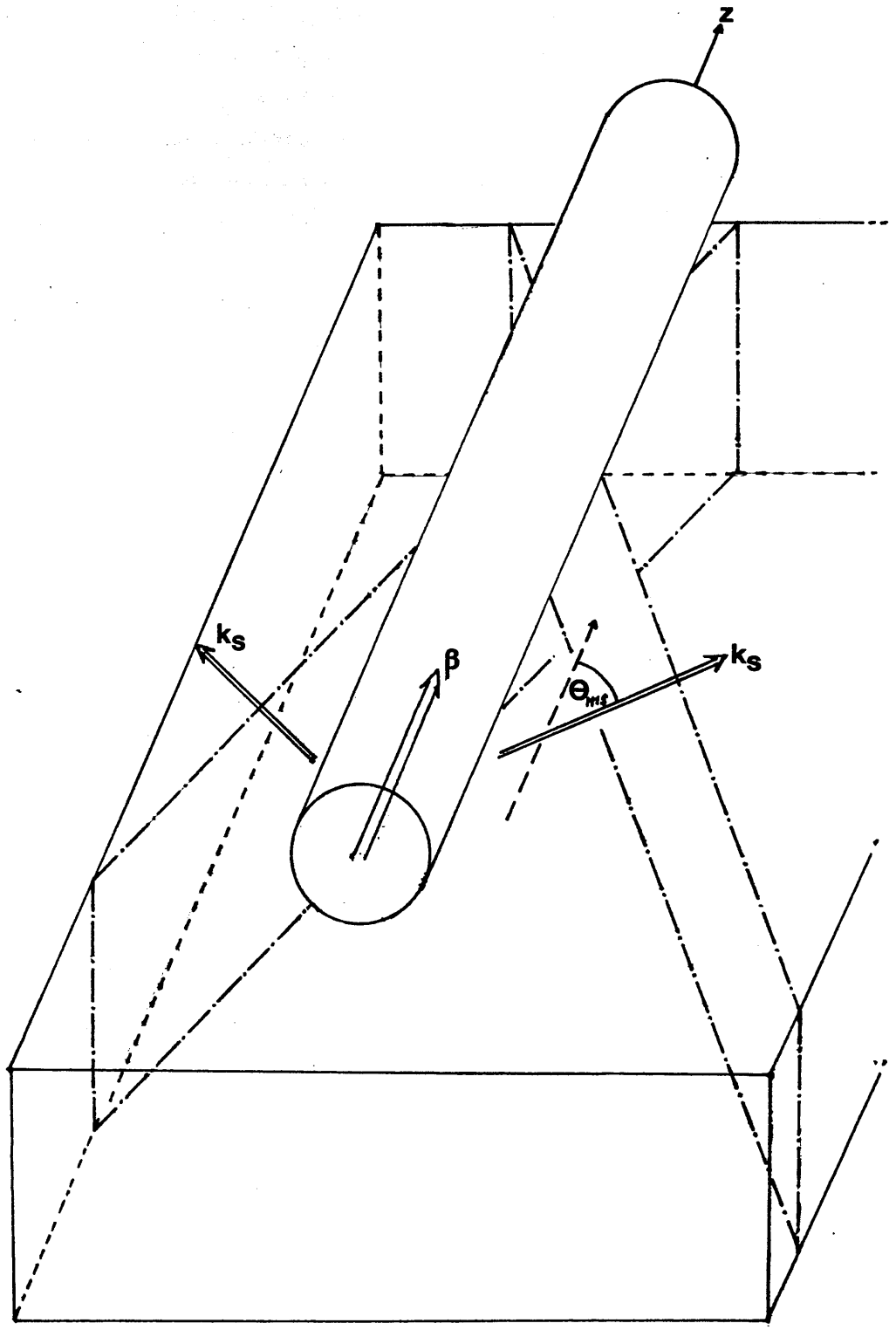

Figure 3.4b) Fibre film coupling, the plane waves in the film have propagation constant k_s, with a component along the z-axis equal to β.

In this section, the general principles of coupling between guides of different confinement are outlined. Fibre-film coupling is shown to be more complex than coupling between guides of equal confinement.

In general, the modes of a composite structure which is invariant in the z-direction propagate as $\exp(-j\beta z)$. During mode sinking, the loss of one degree of confinement results in the modes having a transverse propagation constant corresponding to divergence. Figures 3.4a,b show the result for film-prism coupling and fibre-film coupling respectively. (The fibre-film result shown,is a special case for $k_s > \beta$. This and other cases are discussed in more detail below.) Light coupled from a film to a prism has propagation constant $k_o n_p$ with a component β in the z-direction. Similarly for fibre-film coupling, the film mode has a propagation constant k_s with a component β along z. In each case the mode sinking occurs at an angle;

$$|\theta_{ms}| = \cos^{-1}\beta/k_s \qquad 3.24$$

β can be found by prism coupling from a film or fibre by measuring the angle θ_{ms} and knowing the prism index n_p.

Until 1985, only two analyses of evanescent fibre film coupling had been published; those of Arnaud[6] and Marcatili[9] in 1974. Growing interest in this field was indicated by a recent paper by Lamouroux and co-workers[27]. This paper was largely based on numerical analysis and offered little advancement on the existing analytical work. Arnaud's analysis was based on CMT in order to obtain a figure for the rate of fibre film leakage during mode sinking. Developed from expressions for 'feebly coupled' guides of equal confinement it had as a result, inherent limitations when applied to this problem. It is described below, together with the complementary analysis of Marcatili. This was published at the same time and makes use of Arnauds results. It gives a good conceptual understanding of the mode-sinking phenomenon and is the basis for understanding rib guides which are shown to be equivalent to a tightly coupled fibre/film structure.

3.5.1 Mode sinking from film to prism.

Arnaud begins by considering mode-sinking from the discrete (forward) mode spectrum of a thin film guide into the continuous spectrum of a high index half space (i.e. a prism). This is then developed to explain mode sinking from a fibre to a thin film which itself acts as a mode sink. This analysis proceeds as follows.

Consider a film supporting a TE mode, coupled to a prism as shown

in figure 3.4. The prism region is initially considered to be of finite thickness and both regions to be of finite width X. If β and k_s are the propagation constants of the film mode and a mode of the mode sink respectively then 3.3 can be solved for;

$$(j\Gamma - j\beta)(j\Gamma - jk_s) = +K^2 \qquad 3.24$$

$$\Gamma^2 - \Gamma(\beta + k_s) + (\beta k_s + K^2) = 0 \qquad 3.25$$

$$\text{Roots } \Gamma_{\pm} = 1/2(\beta + k_s) \pm 1/2((\beta + k_s)^2 - 4(\beta k_s + K^2))^{1/2} \qquad 3.26$$

$$\Gamma_{\pm} = 1/2(\beta + k_s) \pm (1/4(\beta - k_s)^2 - K^2)^{1/2} \qquad 3.27$$

We are interested in the mode whose field originates in the film guide i.e. Γ_-. That is when $K = 0$, $\Gamma_- = \beta$. It is necessary to artificially introduce material loss in the film such that;

$$k_s = k_{sr} + jk_{si} \qquad 3.28$$

$$\text{and} \qquad k_{si} \gg K^2 \qquad 3.29$$

This allows the second term of 3.27 to be expanded using the binomial expansion since the imaginary term dominates when $\beta = k_{sr}$. The imaginary part of Γ which we call Γ_i is therefore the loss suffered by the coupled mode

$$\Gamma_i = \text{Im}(1/2\ jk_{si} - (1/2(k_{sr} + jk_{si} - \beta) + K^2/(k_s - \beta))) \qquad 3.30$$

$$= \text{Im}(K^2/(k_{sr} - \beta + jk_{si}))$$

$$= K^2 k_{si}((k_{sr} - \beta)^2 + k_{si}^2)^{-1} \qquad 3.31$$

It is then necessary to assume that the imaginary part of K is negligible. The total loss W, from the film into the m prism modes is then given by the sum;

$$W = \sum_{m'} K^2_{m'} k_{si}((ksr_{m'} - \beta)^2 + k_{si}^2)^{-1} \qquad 3.32$$

and $m' \equiv mnp$ where m refers to modes in the x-direction, n modes in the y direction and p, the polarization.

The cross section of the prism XY and the width of the film Y, are then allowed to tend to infinity. At a fixed power density in the film guide the power density in the prism tends to zero. The field overlap therefore becomes infinitesimal i.e. the coupling coefficient becomes small. The summation W becomes an integral as XY tends to infinity i.e.;

$$W = \lim_{XY\to\infty} \sum K^2_{m'} k_{si}((k_{srm'} - \beta)^2 + k_{si}^2)^{-1} \qquad 3.33$$

Defining the coupling density; $\lim_{XY\to\infty} K^2_{m'} = C(k_{sr})dk_{sr}$ 3.34

$$\text{where } k_{sr} < k_{srm'} < k_{sr} + dk_{sr} \qquad 3.35$$

Leads to the integral;

$$W = \int C(k_{sr}) k_{si}((k_{sr} - \beta)^2 + k_{si}^2)^{-1}\, dk_{sr} \qquad 3.36$$

It is now possible to allow the loss k_{si} to tend to zero while maintaining the condition 3.29. The factor $(k_{sr} - \beta)$ acts as a delta function in equation 3.36, in the limit as $k_{si}\to 0$. The loss is therefore simply given by

$$W = \pi C(\beta) = \pi N K_m^2 \qquad 3.37$$

where N is the mode density.

The light radiated into the prism propagates away from the film-gap-prism interface. In the bulk prism light propagates as $k_o n_p$ but in the z-direction the radiated light must have a component equal to β according to 3.36, 3.37. it is clear from figure 3.4 therefore that $k_o n_p \cos\theta_{ms} = \beta$ or;

$$\text{Mode sinking angle } \theta_{ms} = \cos^{-1}(\beta / k_o n_p) \qquad 3.38$$

This shows that for a single plane wave mode in the film, light is radiated at a single angle θ_{ms}. This result is used in Chapter 4 in discussing prism coupling from a fibre. Although this derivation is based on a film guide it has been shown[4] that it gives excellent agreement with experimental fibre / prism experiments in the case of

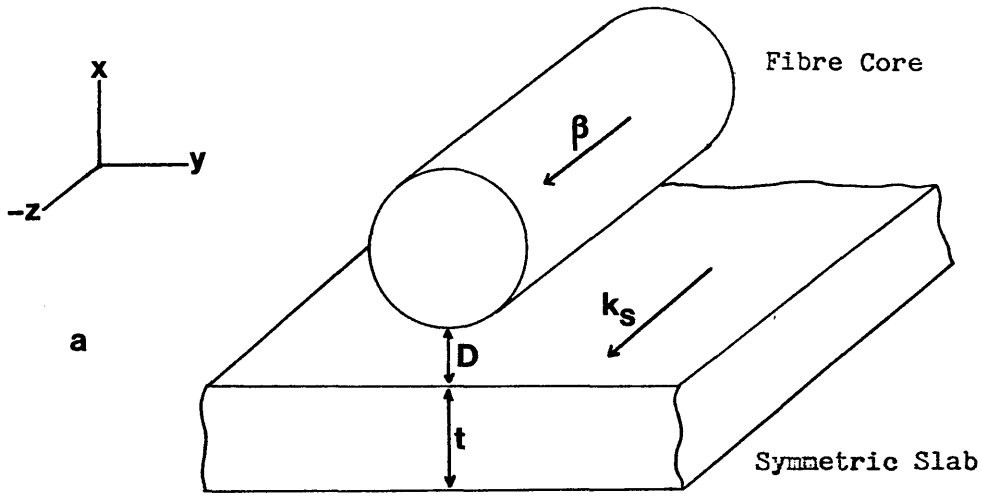

For one mode at one wavelength

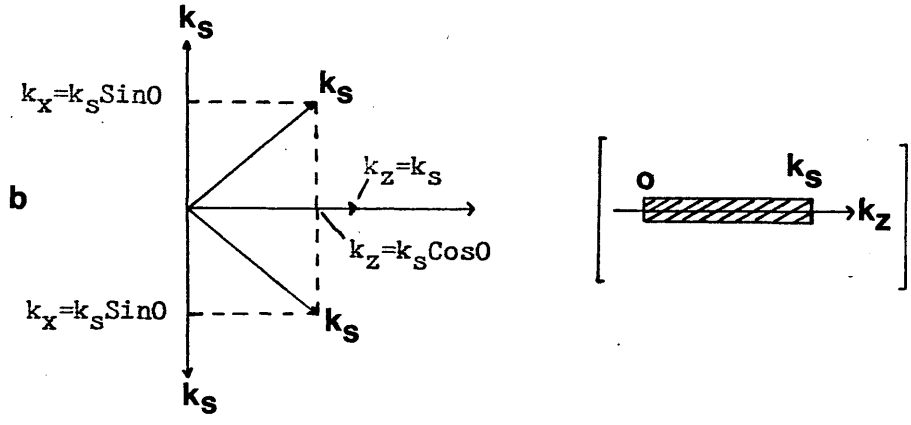

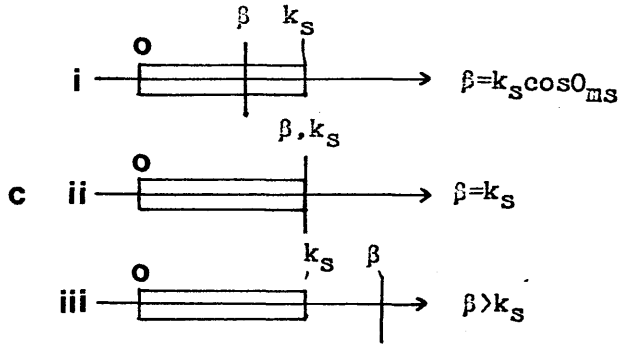

Figure 3.5 a) Geometry of fibre film coupling

b) Film mode components resolved along the forward fibre axis.

c) Conditions for guiding in and mode-sinking from the fibre.

feeble coupling.

3.5.2 Mode sinking from fibre to planar film

The geometry of the coupled fibre and film guide is shown in figure 3.5. Arnaud's analysis applied to the case of large D while that of Marcatili, followed here, applied for all D. Marcatili used the result (3.36) that the factor $(k_{sr}-\beta)$ acted as a delta function so that modes with a finite mismatch (in the z-direction) were effectively decoupled as described below.

The modes of the slab in isolation are guided plane waves at arbitrary directions θ, to the z-axis, in the y-z plane. For simplicity it is convenient to assume that the slab field is well confined with wave vectors k_x, $k_y = m\pi/t$, k_z, related by;

$$k_z = (k_o^2 n_g^2 - k_x^2 - (m\pi/t)^2)^{1/2} \qquad 3.39$$

This follows from equation 2.25 when H is small.
The propagation constant k_s^m of the m^{th} slab mode is given by;

$$k_s^m = (k_z^2 + k_x^2)^{1/2} = k_o n_{es} \qquad 3.40$$

where n_{es} is the effective index of the slab mode. If a fibre is weakly coupled to the film a direction is imposed on the slab. The slab modes have a component k_z along the fibre axis. Neglecting backward modes, the values of k_z present for modes with m turning points are given by;

$$k_z = k_o n_{es}\cos\theta = (k_o^2 n_g^2 - k_o^2 n_{es}^2 \sin^2\theta - (m\pi/t)^2)^{1/2} \qquad 3.41$$

The range of k_z for forward modes lies between;

$$0 < k_z < k_s^m \qquad 3.42$$

where $k_s^m = (k_o^2 n_g^2 - (m\pi/t)^2)^{1/2}$
Corresponding to;

$$0 < \theta < \pi/2 \qquad 3.43$$

This is shown in figure 3.5b.

For each mode m, the values of k_z form a continuum from 0 to k_s^m.

Effective power transfer only occurs between transversely coupled guides when the propagation constants k_z are **almost** equal. Marcatili considers that for weak coupling power transfer is effective only when the propagation constants k_z **are** equal. If the fibre has propagation constant β then the behaviour of the coupled guides may be described as follows;

(i) If $\beta > k_s^o$ then no power is lost from the fibre. $k_z = k_s^o$ is less than β so the guides are mismatched along z.
(ii) If $\beta \leq k_s^o$ then at some angle $\pm\theta ms$ the propagation constants along z are matched according to;

$$\beta = k_z = k_s^o \cos\theta ms \qquad \text{where} \qquad \theta ms = \cos^{-1} \beta/k_s \qquad 3.44$$

Since the fibre is matched to the mode continuum power is lost from the fibre into film modes propagating at angles $\pm\theta ms$ to the fibre axis. The conditions above are shown to hold for modes of a rib-waveguide, (i.e. when D = 0). Modes of the fibre will suffer loss unless the condition $\beta > k_s^o$ is satisfied. Similarly the effective indices of the guided modes of a rib waveguide must be higher than that of the fundamental slab mode k_s^o, or must suffer leakage. Arnaud derives an approximate analytical expression for the rate of leakage from a fibre into a planar film in the weakly coupled case of large D. This follows from the analysis of film-prism mode sinking thus;

If the width of the slab is L_x and the film mode components are related by;

$$k_z = f(k_x); \quad k_x = f^{-1}(k_z) \qquad 3.45$$

then it is shown that the loss to the fibre mode is given by;

$$W = 1/2[\beta/f^{-1}(k_z)] K_m^2 L_x \Big|_{k_z=\beta} \qquad 3.46$$

Obtained from 3.37 by using $N = (k_z/k_x)\, L_x/(2\pi)$ 3.47

In the case of film-prism coupling, it was shown that the product $K_m^2 Lx$ tends to zero as the substrate dimensions tend to infinity. However for fibre-film coupling this product remains finite. Therefore when $\beta = k_s$ (and $k_x = 0$) the loss predicted by 3.46 is infinite. In practice this would not happen since the perturbation method (Equation 3.6a,b)

on which 3.46 was based is then invalid. For a finite mismatch (k_x finite) equation 3.46 was used to calculate the leakage from a highly multimode fibre to a multimode film. These losses were typically 10's of dB's per km. The matching condition for leakage was found to be that of 3.44 above. However the use of the symbolic δ-function (in 3.36) results in coupling from the fibre into a single plane wave propagating at each angle $\pm\theta_{ms}$ to the fibre axis. A plane wave is of infinite extent transversely and if it is excited with a finite amplitude it carries infinite power. Both analyses are therefore only an approximation in this respect. It is not possible to obtain a figure, either for the coupling loss from a fibre with $\beta < k_s^o$ or for a tightly coupled structure. Both analyses are restricted to coupling to single plane waves which is physically unrealisable but is a useful basis for understanding the coupling process. The amplitude and shape of the beams excited in the film are discussed further in chapter 5.

Appendix A.

Derivation of coupled mode propagation from coupled line equations

The fields on the coupled guides a and b, can be written;

$$A = A_o\, e(x,y)\exp j\beta_a z \qquad \text{A.1a}$$

$$B = B_o\, e(x,y)\exp j\beta_b z \qquad \text{A.1b}$$

The coupled line equations are;

$$dA/dz = A' = j\beta_a A + jK_{ba}B \qquad \text{A.2a}$$

$$dB/dz = B' = j\beta_b B + jK_{ab}A \qquad \text{A.2b}$$

Let $j\beta a = C_1$, $j\beta_b = C_2$, $jK_{ba} = C_3$, $jK_{ab} = C_4$, then

$$A' = C_1A + C_3B \qquad B' = C_2B + C_4A \qquad \text{A.3a,b}$$

$$B = A'/C_3 - AC_1/C_3 \qquad A = B'/C_4 - BC_2/C_4 \qquad \text{A.4a,b}$$

The second derivative of A.2a gives

$$\begin{aligned} A'' &= C_1A' + C_3B' \\ &= C_1^2A + C_1C_3B + C_2C_3B + C_3C_4A \\ A'' &= A(C_1^2 + C_3C_4) + B(C_1C_3 + C_2C_3) \end{aligned} \qquad \text{A.5}$$

Substitution of A.4a into A.5 gives;

$$A'' = A'(C_1 + C_2) + A(C_3C_4 - C_1C_2) = -A'C_5 - AC_6$$

where $-C_5 = (C_1 + C_2)$; $-C_6 = (C_3C_4 - C_1C_2)$.

A similar result is obtained for B''giving a pair of second order homogeneous equations;

$$A'' + C_5A' + C_6A = 0 \qquad B'' + C_5B' + C_6B = 0 \qquad \text{A.6}$$

The roots Γ_+, Γ_- of these equations are given by;

$$\Gamma^2 + C_5\Gamma + C_6 = 0 \qquad \text{A.7}$$

The roots are (j times) the propagation constants of the coupled modes and are given by;

$$\Gamma_{\pm} = (-C_5 \pm (C_5^2 - 4C_6)^{1/2})/2$$

$$\Gamma_{\pm} = (C_1+C_2)/2 \pm ((C_1 - C_2)^2/4 + C_3C_4)^{1/2} \qquad \text{A.8}$$

Let $(C_1 + C_2)/2 = C_7$, $(C_1-C_2)=\delta = j\Delta\beta$, then;
$\Gamma_{\pm} = C_7 \pm (\delta^2/4 + C_3C_4)^{1/2} = C_7 \pm C_8$ where $C_8 = (\delta^2/4 + C_3C_4)^{1/2}$ A.9

General Solution

The general solution for two second order homogeneous equations with identical coefficients is;

$$A(z) = k_1 \exp \Gamma_+ Z + k_2 \exp \Gamma_- Z, \quad B(z) = k_3 \exp \Gamma_+ Z + k_4 \exp \Gamma_- Z \qquad \text{A.10a,b}$$

The coefficients $k_1 - k_4$ are determined by the initial conditions.

$$A(0) = A_o = k_1 + k_2 \quad B(0) = B_o = k_3 + k_4$$
$$k_2 = A_o - k_1 \qquad k_4 = B_o - k_3 \qquad \text{A.11a,b}$$

$$A'(0) = \Gamma_+ k_1 + \Gamma_- k_2 = C_1A_o + C_3B_o$$
$$k_1(\Gamma_+ - \Gamma_-) = A_o(C_1 - \Gamma_-) + B_oC_3 \qquad \text{A.12a}$$

With a similar result for B'(0) giving

$$k_3(\Gamma_+ - \Gamma_-) = B_o(C_2 - \Gamma_-) + C_4A_o \qquad \text{A.12b}$$

giving the coefficients k_1 to k_4 after some algebra as;

$$k_1 = A_o/2[1 + \delta/2C_8] + B_o/2 \cdot C_3/C_8 \qquad \text{A.13a}$$
$$k_2 = A_o/2[1 - \delta/2C_8] - B_o/2 \cdot C_3/C_8 \qquad \text{A.13b}$$
$$k_3 = B_o/2[1 - \delta/2C_8] + A_o/2 \cdot C_4/C_8 \qquad \text{A.13c}$$
$$k_4 = B_o/2[1 + \delta/2C_8] - A_o/2 \cdot C_4/C_8 \qquad \text{A.13d}$$

We are interested in the power transferred between the guides. Let

$A_o = 1$ and $B_o = 0$ then $k_3 = -k_4$ and;
$B(z) = k_3 \exp \Gamma_+ z - k_3 \exp \Gamma_- z$
$= k_3 \exp C_7 z \; 2j(\exp C_8 z - \exp -C_8 z)/2j$

$$B(z) = 2jk_3 \exp(C_7 \sin C_8 z/j)$$
$$B(z)^2 = C_4^2/C_8^2 \sin^2 C_8 z/j \qquad \text{A.14}$$

Maximum power is transferred when $z = (2n-1)\pi/(2C_8 j)$ n-integer and is given by

$$P_{mt} = C_4/(\delta^2/4 + C_3C_4)^{1/2}$$
$$= 1/((\delta/2C_4)^2 + (C_3/C_4)^2) \qquad \text{A.15}$$

A.15 must hold for $\delta=0$ so power conservation dictates that $C_3 \geq C_4$. But a similar expression exists for $B_o = 1$, $A_o = 0$ dictating that $C_4 \geq C_3$. Thus we have

$$C_3 = C_4 = jK \qquad \text{A.16}$$

Maximum power transfer is given by;

$$P_{mt} = (1 + (\Delta\beta/2K)^2)^{-1} \qquad \text{A.17}$$

The coupling length L is given by;

$$L = \pi/2/(K^2 + \Delta\beta^2/4)^{1/2} \qquad \text{A.18}$$

For synchronous guides $\Delta\beta = 0$ and 100% power transfer occurs over a length L given by;

$$L_c = \pi/2K \qquad \text{A.19}$$

With coupled mode propagation constants given by

$$\Gamma_{\pm} = \beta \pm K \qquad \text{A.20}$$

References

1. Ohtaka, M., Matsuhara, M., Kumagai, N., "Analysis of the guided modes in slab-coupled waveguides using a variational method", IEEE J. Quant. Electron. Vol. QE-12, No. 7, July (1976) pp.378-382.

2. Butler, J.K., Wang, C.S., "Modal characteristics of optical stripline waveguides", J. Appl. Phys. Vol. 47, No. 9, September (1976) pp.4033-4043.

3. Ulrich, R., "Theory of the prism-film coupler by plane wave analysis", J. Opt. Soc. Am. Vol. 60, No. 10, October (1970) pp.1337-1350.

4. Leminger, O.G., Zengerle, R., "Determination of single-mode fibre coupler design parameters from loss measurements", J. Lightwave. Tech. Vol. LT-3, No. 4, August (1985) pp.864-867.

5. Marcuse, D., "The coupling of degenerate modes in two parallel dielectric waveguides", B.S.T.J. Vol. 50, No. 6 (1971) pp.1791-1816.

6. Arnaud, J., "Transverse coupling in fibre optics, Part II: coupling to mode sinks", B.S.T.J. Vol. 53, No. 4, April (1974) pp.675-696.

7. Vanclooster, R., Phariseau, P., "The coupling of two parallel dielectric fibres, Part II Characteristics of the coupling in two fibres", Physica, Vol. 47, (1970) pp.501-514.

8. Harnagel, G., Scifres, D., Kung, H., Welch, D., Cross, P., Burnham, R., "Five Watt continuous wave AlGaAs Laser Diodes", Electron. Letts. Vol. 22, No. 11, May 1986, pp.605-606.

9. Marcatili, E.A.J., "Slab coupled waveguides", B.S.T.J., Vol. 53, No. 4, April 1974, pp.645-674.

10. Arnaud, J., "Transverse coupling in fibre optics: Part 1: Coupling between trapped modes", B.S.T.J. Vol. 53, No. 2, February

1974, pp.217-224

11. McIntyre, P.D., Snyder, A.W., "Power transfer between optical fibres", J. Opt. Soc. Am. Vol. 63, No. 12, Dec. (1973) pp.1518-1527.

12. Hardy, A., Streifer, W., "Coupled mode theory of parallel waveguides", J. Lightwave Tech., Vol. LT.3, No. 5, October 1985 pp.1135-1146.

13. Miller S.E.,"Coupled wave theory and waveguide applications," B.S.T.J. Vol. 33, No. 3, May (1954) pp.661-719.

Louisell, W.H., "Analysis of the single tapered mode coupler", B.S.T.J. Vol.34, No.6, (1955) pp.853-866.

14. Findakly, T., "Optical directional couplers with variable spacing", Appl. Opt. 1 Mar. (1979), Vol. 17, No. 5, pp.769.

15. Matsuhara, M., Watanabe, A., "Coupling of curved transmission lines and application to optical directional couplers", JJ. Opt. Soc. Am., Vol. 65, No. 2, February 1975, pp.163-168.

16. Millar, C.A., Hutchins, R.H., "Measurement of the coupling coefficient for two coupled optical waveguides by detuning", Z. Naturforsch., Vol. 31 (1978) pp.140-141.

17. Van der Donk, J., "The beam propagation method in integrated optics", Ph.D. Thesis, University of Ghent (1982).

18. Feit, M., Fleck, J.A., "Comparison of calculated and measured performance of Diffused Channel-waveguide couplers", J. Opt. Soc. Am., Vol. 73, pp.1296-1302 (1983).

19. Kobayashi, M., Terui, H., Kawachi, M., Noda, J., "2x2 optical waveguide matrix switch using nematic liquid crystal", IEEE J. Quant. Electron., Vol. QE-18 No. 10, October 1982, pp.1603-1609.

20. Urquart, W.P., Brierley, M.C., Millar, C.A., Mallinson, S.R., "Transversely coupled fibre resonators", IOOC Conference on Lasers

and Electro Optics, (CLEO) June 1986, Paper FN2.

21. Kogelnik, H., Schmidt, R., "Switched directional couplers with alternating Δβ", IEEE J. Quant. Electron. Vol. QE-12, No. 7, July (1976) pp.396-401.

22. Wilson, M., Teh, G., "Improved tolerance in optical directional couplers", Electron. Letts. 20th September (1973) Vol. 9, No. 19, pp.453-455.

23. Stewart, G., Hutchins, R.H., Laybourn, P.J.R., "Controlled growth of arsenic trisulphide films for coupling integrated optical devices", J. Phys. D: Appl. Phys. Vol. 14 (1981) pp.323-331.

24. Yariv, A., "Introduction to optical electronics", Holt Rinehart and Winston, London 1976.

25. Digonnet, M., Shaw, H., "Analysis of a tunable single mode optical fibre coupler", IEEE J. Quant. Electron. Vol. QE-18, No. 4, April (1982) pp.746-754.

26. Digonnet, M., Shaw, H., "Wavelength multiplexing in single mode fibre couplers", Appl. Opt. Vol. 22, No. 3, Feb. (1983) pp.484-491.

27. Lamouroux B., Morel P., Prade B., Vinet J.Y., 'Evanescent field coupling between a monomode fibre and a high index medium of limited thickness,' J.Opt.Soc.Am. Vol.2, No.5, May (1985) pp759-764.

Chapter 4 Coupler construction and mode-sinking

4.1 Introduction

It was established in chapters 2 and 3 that transverse coupling requires access to the evanescent field of the guided modes and that these fields are localized around the guiding regions. In a fibre, a cladding of effectively infinite extent [typical O.D. 125μm] surrounds the core giving two possible options for transverse coupling. The mode field may be expanded as demonstrated in sandwich ribbon fibres[1] or the cladding may be (partially) removed[2-9]. Mode field expansion is unsuitable for silica based fibres since they are difficult to dope and field expansion of an order of magnitude is required for single mode. The method of cladding removal has been used successfully to perturb the evanescent field of silica fibres to build couplers and other devices.

In this chapter the fabrication of the TVC is described and compared with other reduced-cladding couplers. The problems and advantages of this geometry are explained. The use of the TVC in fibre-parameter analysis is described and the results obtained are analysed using Fraunhofer diffraction derived from the paraxial approximation and the plane wave decomposition of an optical beam. Plane wave decomposition is later used in chapter 5 in the analysis of fibre-film coupling.

4.2 Evanescent field access

Prism coupling from a single-mode fibre was demonstrated by Hsu in 1976[2]. The fibre was placed in a preferentially etched silicon v-groove[10] and polished to within a few microns of the core. A high index prism was then used to remove the HE_{11} mode power. Also in 1976 a coupler was constructed by pulling 2 heated fibres, forming biconical tapers and placing them in close proximity[3]. This was a forerunner of the fused biconical tapered coupler[4] in which two or more fibres are pulled and fused together simultaneously, forming an efficient, passive, all-fibre coupler. In a similar technique fibres twisted together were etched until the cladding thickness was sufficiently low to allow coupling[5]. Once made the power splitting ratio of these fibre-couplers remained fixed.

A tunable fibre-fibre coupler was developed by Bergh et al giving

any desired coupling ratio with very low insertion loss and cross talk[6,7]. This coupler, known as the 'Stanford coupler' or 'polished directional coupler' (PDC) was constructed by polishing away the fibre cladding. The fibre (for each half of the coupler) was bonded into a groove in a silica substrate block. The groove had a radius of curvature of typically 25cm and was formed using a wire saw. Extreme care was necessary to maintain an accurate radius of curvature. The polished fibre surface was in the same plane as the substrate block, figure 4.1a and in shape is the cross-section of a torus.

This allowed the polished fibres to be accurately and stably superimposed figure 4.1b. The coupling ratio was tuned by translating the fibres in the x-direction. A similar technique which also gave a 0-100% tuning range was developed by Parriaux et al[2]. In this experiment an accurate curvature was provided by bonding the fibre to a plano-convex lens of known focal length. The solution employed by Nayar[9] to the problem of accurate curvature was to polish an entire block to a known curvature in one direction. The block was then sliced into thin strips having consistent parameters. These strips were in turn, cemented between rectangular blocks figure 4.1c and coupler fabrication proceeded as in ref. 6. In each polished fibre technique the epoxy was chosen because of polishing hardness rather than optical index. Similarly the silica substrate blocks were not chosen for index matching as neither the epoxy or substrate blocks are in close proximity to the mode field.

4.3 The tapered V-groove coupler

The TVC was originally suggested by Millar, as a method of reducing the alignment tolerances in fibre-fibre coupling[11]. The work described here, relating to fibre-film coupling is that of the author. A schematic diagram of the fibre-film coupler construction is shown in figure 4.2. A tapered groove was cut in a silica substrate block, figure 4.2a. A single mode fibre was then bonded into the groove (figure 4.2a) and the block was subsequently polished giving an optically smooth surface (figure 4.2c). The fibre forms an ellipse at this surface and was polished through completely. The polished block was suitable for thin film deposition (figure 4.2d). The end of the groove was further recessed to incorporate a protective fibre sleeving which reduced fibre breakage almost to nil. By measuring the length L, of the surface ellipse with a travelling microscope and knowing the

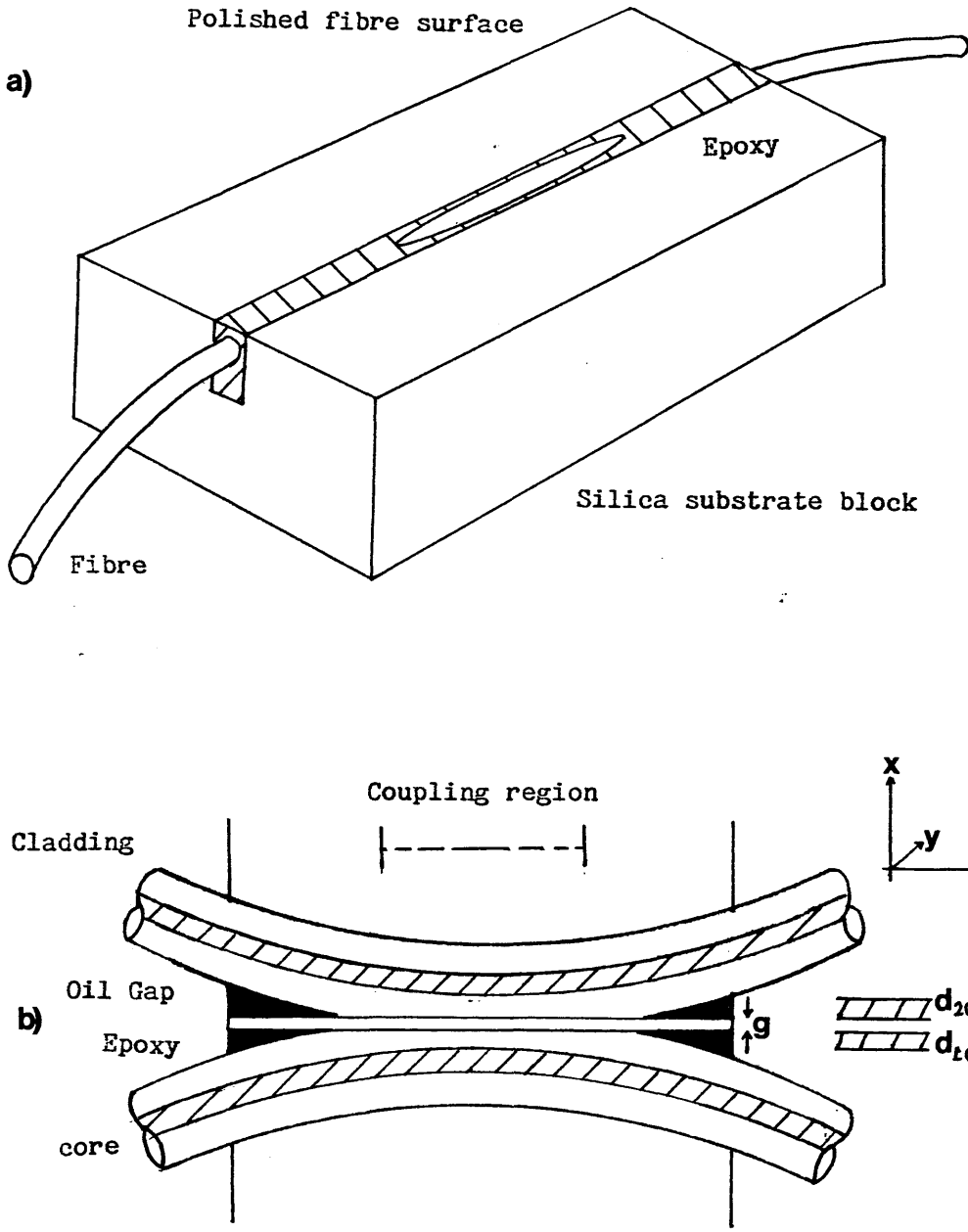

Figure 4.1a Half of Stanford coupler showing fibre set in silica block.

b Coupler assembly, tunable by movement in the $\pm x$ direction. The core to surface distances d_{io} plus the matching oil film thickness equals the core separation.

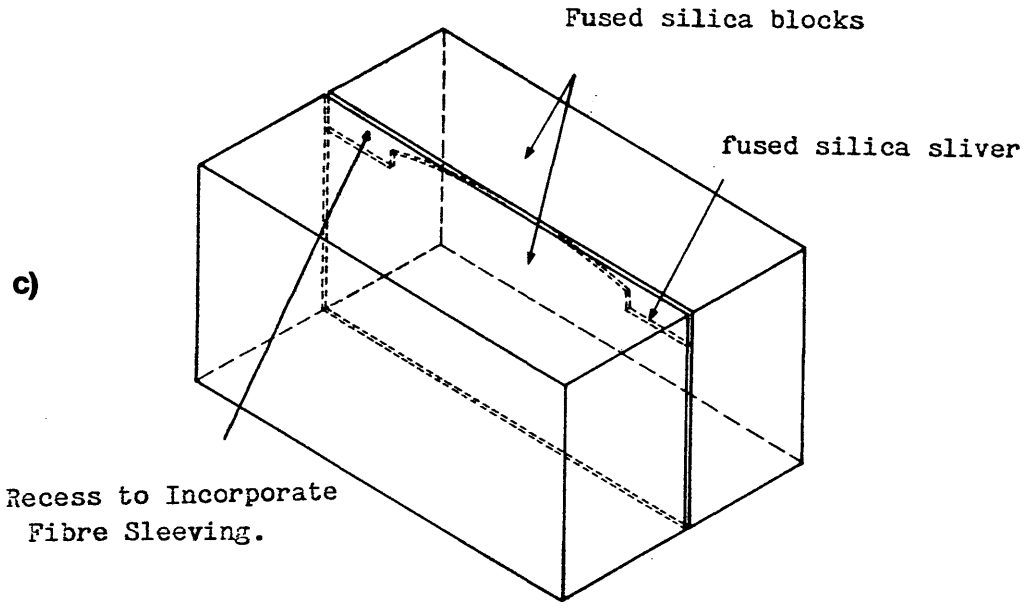

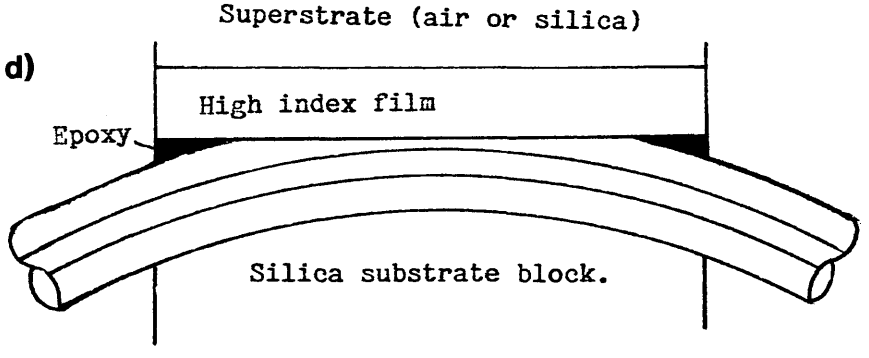

Figure 4.1c Coupler construction facilitating controlled fibre curvature.

d Geometry of fibre-film coupling using PDC (cross-section)

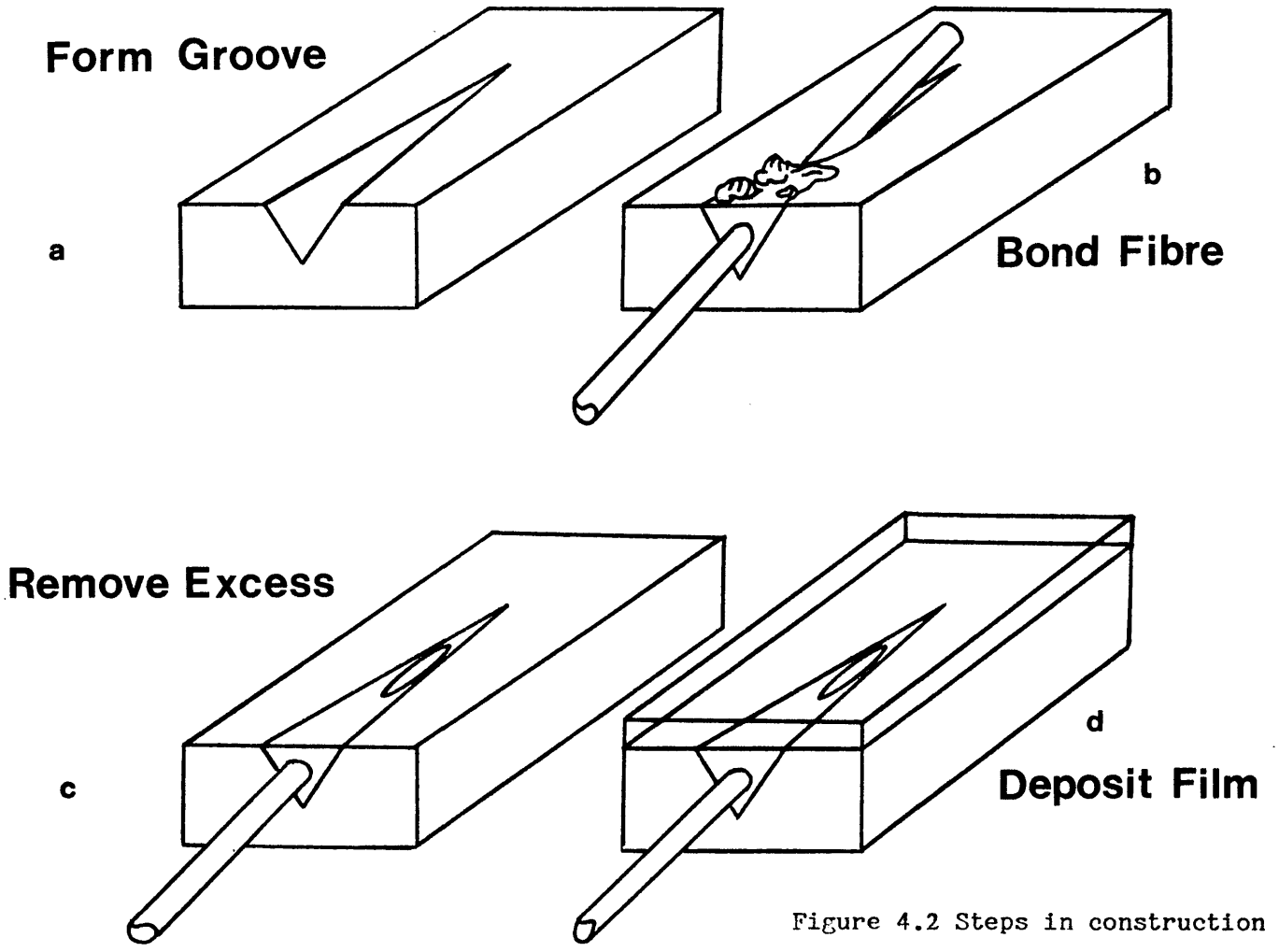

Figure 4.2 Steps in construction of TVC.

fibre outside diameter OD, the groove angle, θ_b was obtained as;

$$\tan\theta_b = OD/L \qquad 4.1$$

Optical power was initially coupled between the fibre and film, in the region adjacent to the exposed core (figure 4.3) where the cladding was only a few microns thick. The fibre and film were non-parallel and their coupling behaviour was analagous to the branching guide structures treated by Findakly[15] with branching angle θ_b. (This was discussed in chapter 3.3.5.) The planar thin film was formed directly onto the polished surface and was therefore intimately and rigidly aligned with the fibre. This is essential to stable directional coupling. Additional processing steps such as the formation of a rib or channel guide were performed after the fibre and film were aligned in this way. (See Chapter 6.) The advantages and disadvantages of this approach to fibre-film coupling are discussed below.

4.3.1 Advantages of the TVC for fibre-film coupling

There were four main advantages to this geometry. Firstly the groove was straight, i.e. there were no problems associated with curvature control. Secondly the core/surface gap d_{10} for a PDC (figure 4.1b) is a difficult parameter to estimate[12]. One group[13] has abandoned the accurate control of d_{10} and has polished each half-coupler block until the core was bisected, forming a zero-gap directional coupler. The gap d_{10} controls the coupling strength and is difficult to define since the fibre is not exactly step index. Thirdly the total coupling strength (equation 3.19)(fibre to film) was controllable by varying the angle θ_b at which the groove was cut. Fourthly, the coupler geometry was suitable for multi input-output devices (figure 4.4) and devices requiring a long interaction length in the film region, e.g. non-linear devices[14]. The importance of transverse coupling in general is that it offers low insertion loss, i.e. the efficiency of power transfer is theoretically very high.

4.3.2 Problems of the TVC for fibre-film coupling

The principle disadvantage of the TVC compared to the PDC (figure 4.1d) is that (ignoring coupling to backward modes) the former is a two port device while the latter is a three port device. In the PDC any

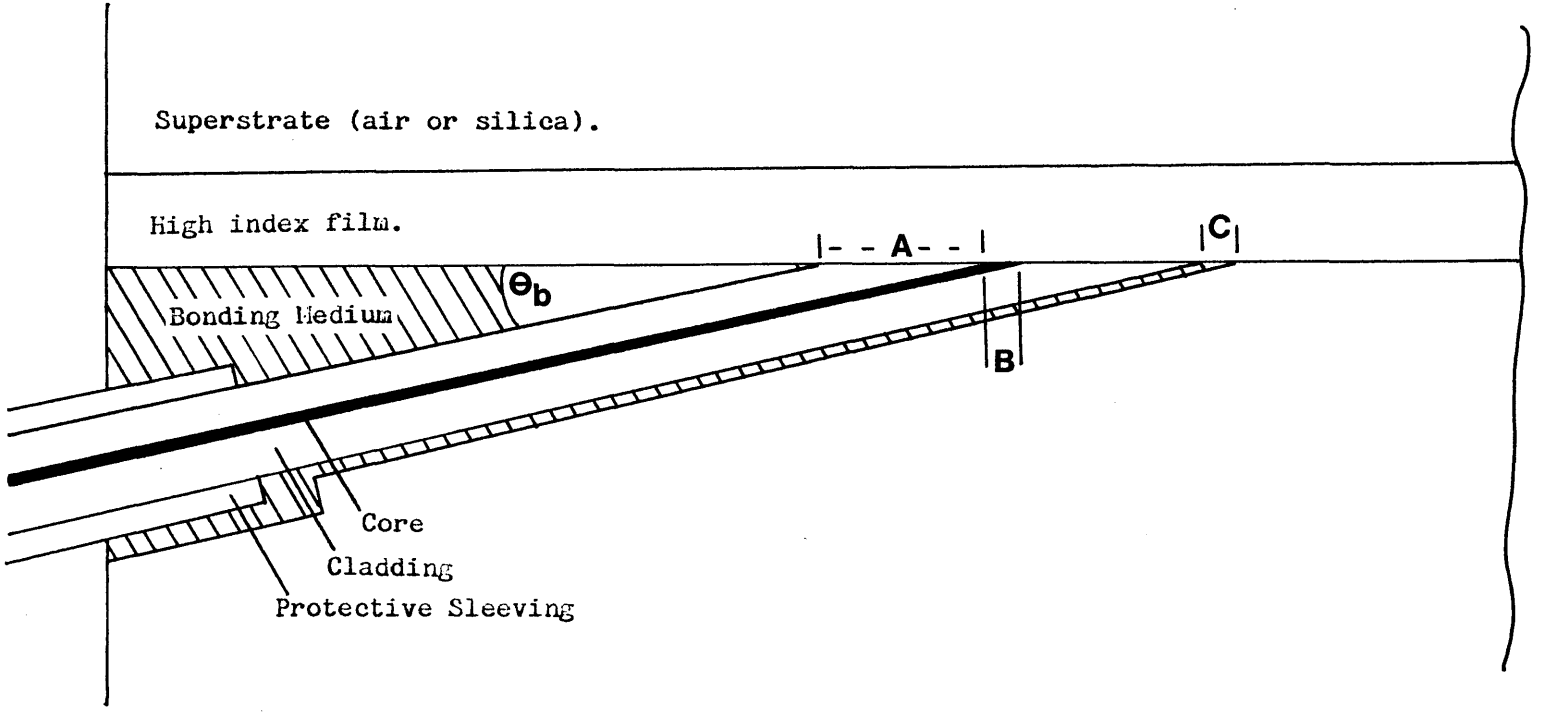

Figure 4.3 Cross-section of TVC showing A-directional coupling region of reduced cladding thickness. B-tapered core region. C-region in which bonding medium becomes guide substrate.

light not coupled into the film is transmitted in the fibre while in the TVC uncoupled light is lost. Light remaining in the fibre at region B (figure 4.3) is no longer guided by the fibre core since the core is now bounded by a high index region. In the geometry of figure 4.3 it is clear that there is zero transmission in the absence of a film while the PDC enjoys a very high transmission level in isolation. In order to build a low insertion loss device using the TVC it is necessary to achieve phase synchronism at both the input and output fibres. With the Stanford coupler it is sufficient to alter the spectral transmission T(λ) of the fibre, by perturbing the evanescent field, to make a device.

A second disadvantage of the TVC lies in the choice of bonding material. It constitutes the film substrate over a length S at the input and output fibres. If the substrate is of high index or is lossy then the film transmission will be reduced. The length of this region in fabricated couplers has been at least 2mm. The bonding material therefore should, be of a similar index and transparency to silica, be suitable for further processing, (e.g. should withstand the elevated temperatures of CVD) and be of a similar polishing hardness to silica.

The most obvious material then is silica, applied in molten form. However the difficulty of accurately handling molten silica (at > 1100°C) and the effect of this temperature on the silica-BASED fibre preclude its use. A fluorine based glass Schott FK54 with an index slightly lower than silica and a glass transition (T_g) temperature of <700°C is available. This temperature was however considered to be impractical with the facilities available. Lower melting point glasses (solder glasses) were available but they had a high lead content to reduce T_g which raised their refractive index.

A number of optically transparent epoxies were avalable. (see e.g. ref 16) These were tested and it was found that those having a low refractive index were too soft while those of sufficient polishing hardness had a high refractive index, typically n_D = 1.54. Other materials such as shellac and various clear waxes were tried as was cynano-acrylate adhesive. None had sufficient strength to retain the fibre in the tapered groove during polshing. In the absence of a material satisfying the criteria listed above a commercial epoxy having excellent polishing hardness and chemical resistance with an operating temperature of up to 300°C was used. The epoxy was white in colour and had a markedly different index from silica. The effect of this index difference was investigated by forming a waveguide on the silica

substrate block and attempting to guide light in the region where the epoxy is the waveguide substrate. This is shown in Chapter 6.

The use of such a compromise material significantly reduced the range of techniques by which thin film guides could be formed and limited the coupler arrangements giving low insertion loss. Epoxy is unsuitable for vacuum processing in general and for 'hot' processes in particular. CVD, r.f. sputter deposition, chalcogenide glass evaporation (with associated post-annealing) and reactive ion beam sputtering were all discounted. Although the experimental arrangement described in Chapter 5 gave low insertion loss for fibre-film-fibre coupling it was entirely unsuitable for the proposed device structure of figure 4.4. Waveguide formation was limited to dip coating and the use of flip-chips.

The future development of the TVC will require a more suitable bonding material. It is probable that a considerable research effort would yield an apparatus capable of handling FK54 glass satisfactorily. This problem was shelved when it became apparent that it would dominate the research effort.

4.3.3 Cutting and polishing

The surface profile of a polished TVC with MCVD fibre is shown in figure 4.5. The profile was examined using a Michelson interference microscope which produces fringes according to the deviation of the (nominally flat) sample surface from the (flat) focal plane of the lens system. A dip in the fringes corresponds to a dip in surface height. The sample was at a small angle to the microscope reference plane resulting in a large number of fringes. The dip in the epoxy region confirmed that its polishing hardness was slightly inferior to that of silica. In addition the central region of the fibre preform deposited by MCVD was marginally softer than the surrounding fibre.

The tapered v-groove was cut with a sharp-faced diamond wheel designed for decoration of crystal glass[17], figure 4.6a. The hardness of the wheel, of silica and the speed of rotation, must be balanced or the diamond impregnation is stripped from the grinding wheel. It quickly emerged that the surface grinder in the Engineering Department workshop was too fast and grooves were therefore cut in BTRL. I am indebted to A.Gotts, of BTRL for the painstaking manufacture of the TVC grooves used in these experiments.

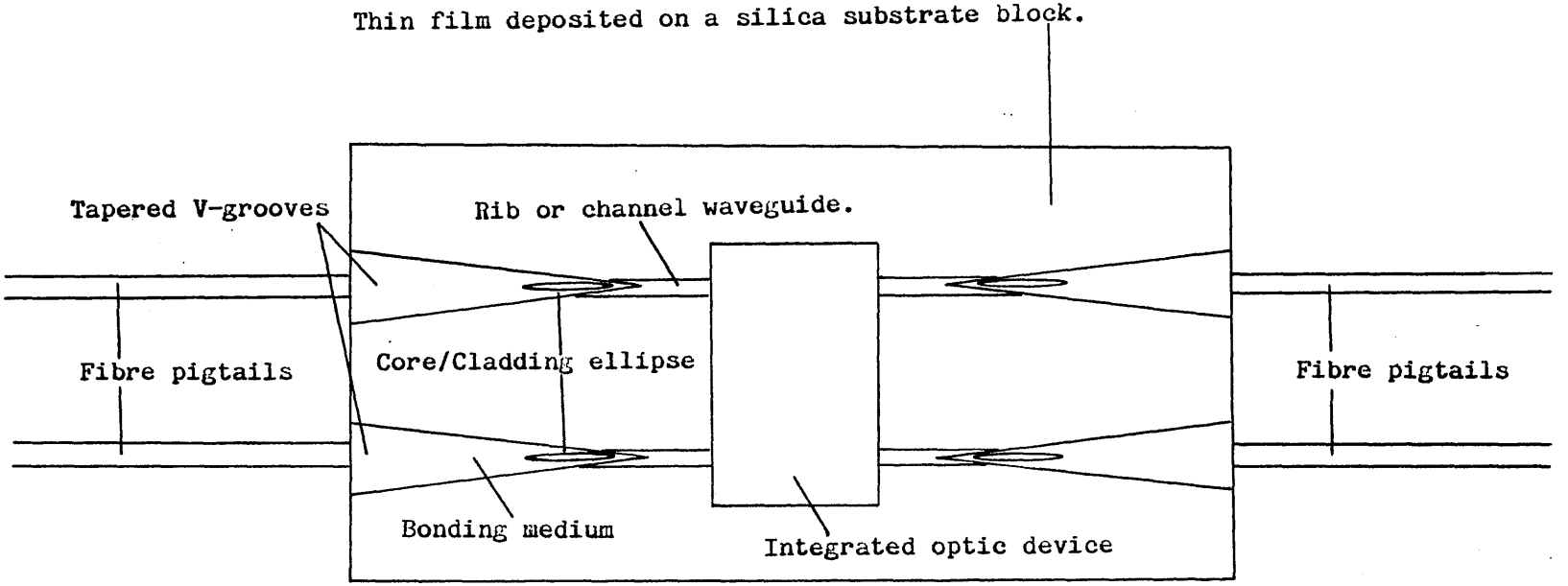

Figure 4.4 Schematic diagram of proposed coupler geometry.

Surface interference fringes

a)

b)

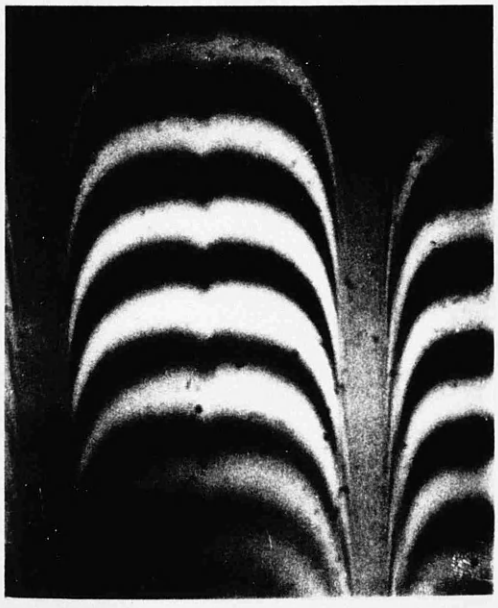

c) TVC fringe pattern

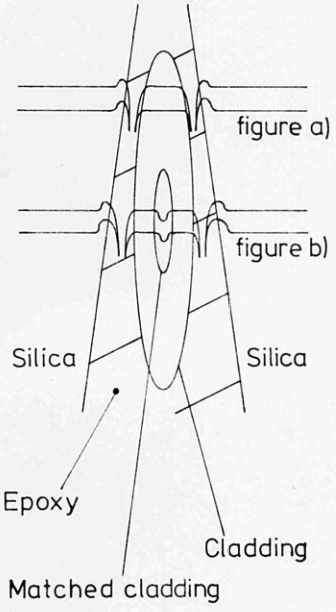

d) Inferred TVC cross-section

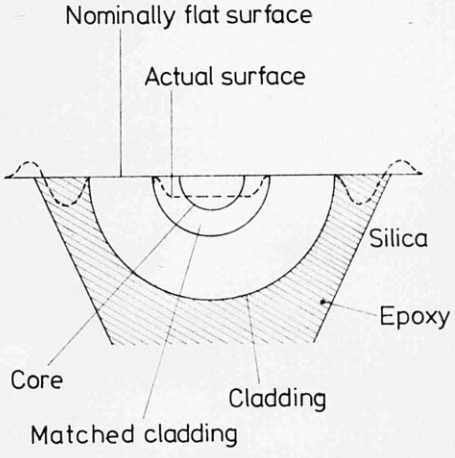

Figure 4.5

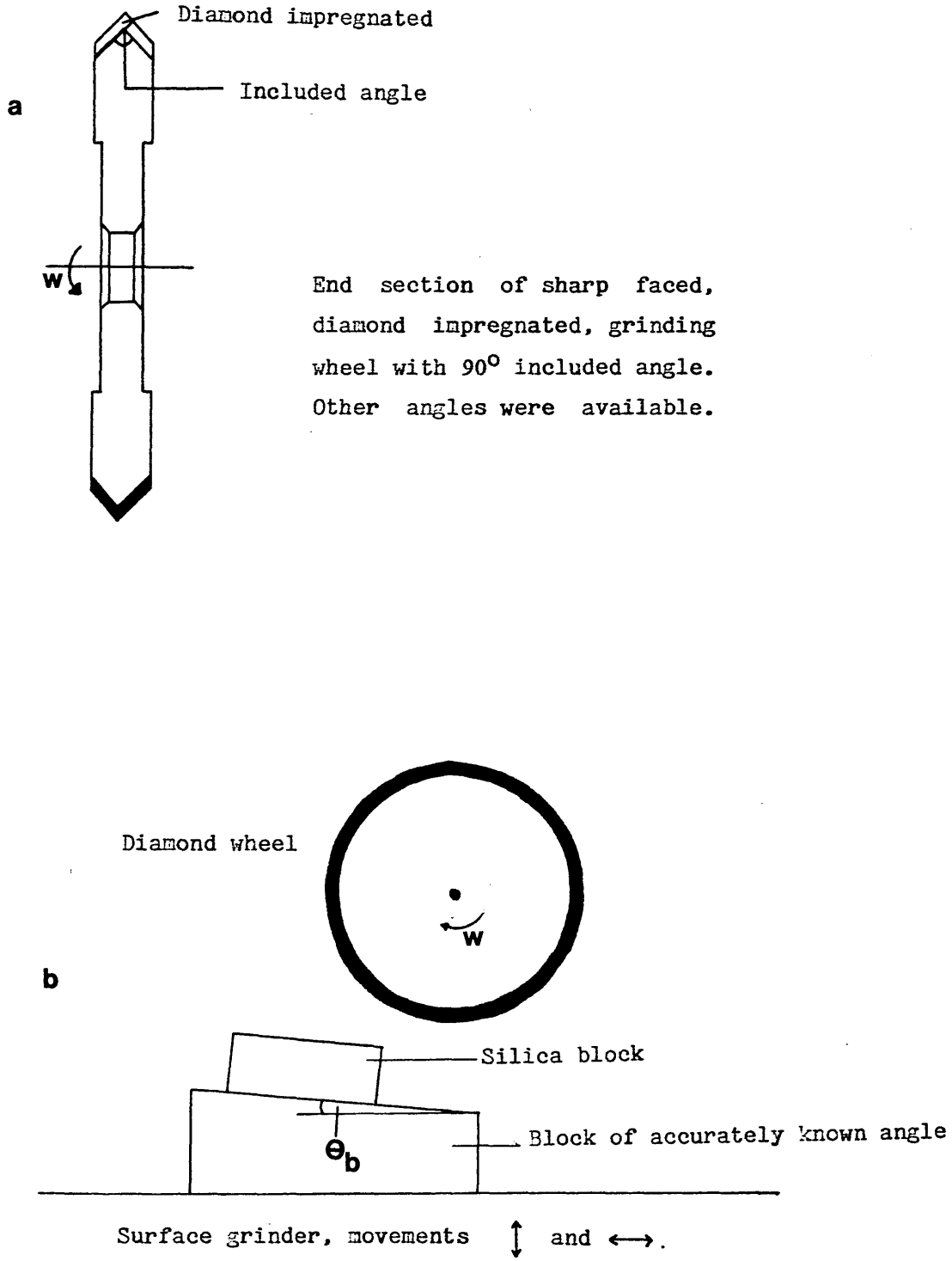

Figure 4.6 Schematic diagram of grinding arrangement for cutting tapered v-grooves.

A third, more minor problem in TVC fabrication was the device length. The longest device, having one-input-output fibre was 110mm long and had a branching angle of $\theta_b = 0.50^o$. At this angle the ellipse length for 125μm OD fibre was 14.324mm. Thus for fibre-film fibre coupling the light had to propagate at least this distance in the film waveguide and a typical distance was 20mm. The device length could be shortened without altering θ_b by the use of bend resistant fibre[18]. A single input single output device with $\theta_b=1.25^o$ and a length of 50mm is shown in figure 4.7.

Once the manufacturing conditions were established, TVC blocks such as that shown in figure 4.7 were made routinely. It was nevertheless a highly skilled and time consuming process. For certain applications such as an in-line fibre filter (see Chapter 5) where the substrate may be any hard material, it may be possible to injection mould the TVC block. This has been successfully demonstrated for the PDC within BTRL[19].

4.4 Mode sinking and ESI measurement

Having established a reliable manufacturing technique, preliminary experiments to characterise the TVC were carried out. In a simple experiment laser light at 633nm was launched into the fibre pigtail. A drop of oil of index $n_D > 1.50$ was placed on the TVC block, over the cladding ellipse and the light was observed to couple entirely into the oil.

Access to the evanescent field of the fibre mode was expected to provide an interesting method of fibre characterisation. As explained in Chapter 2 the effective index or propagation constant of a weakly guiding fibre may be obtained by various methods. These methods derive the longitudinal quantity β from a transverse measurement of mode spot size, refractive index profile etc.[20,21]. By prism coupling light from the fibre it would be possible to obtain β directly, after correcting for the effect of the coupled prism. In the presence of the high index prism, or mode sink, the fibre mode is leaky and power is lost to the mode sink. It was shown in Chapter 3.5 that the radiated light emerges in the prism at a characteristic angle determined by the prism index and the fibre propagation constant β. The experimental arrangement for fibre prism coupling is described below.

4.4.1 Prism coupling to few mode fibres

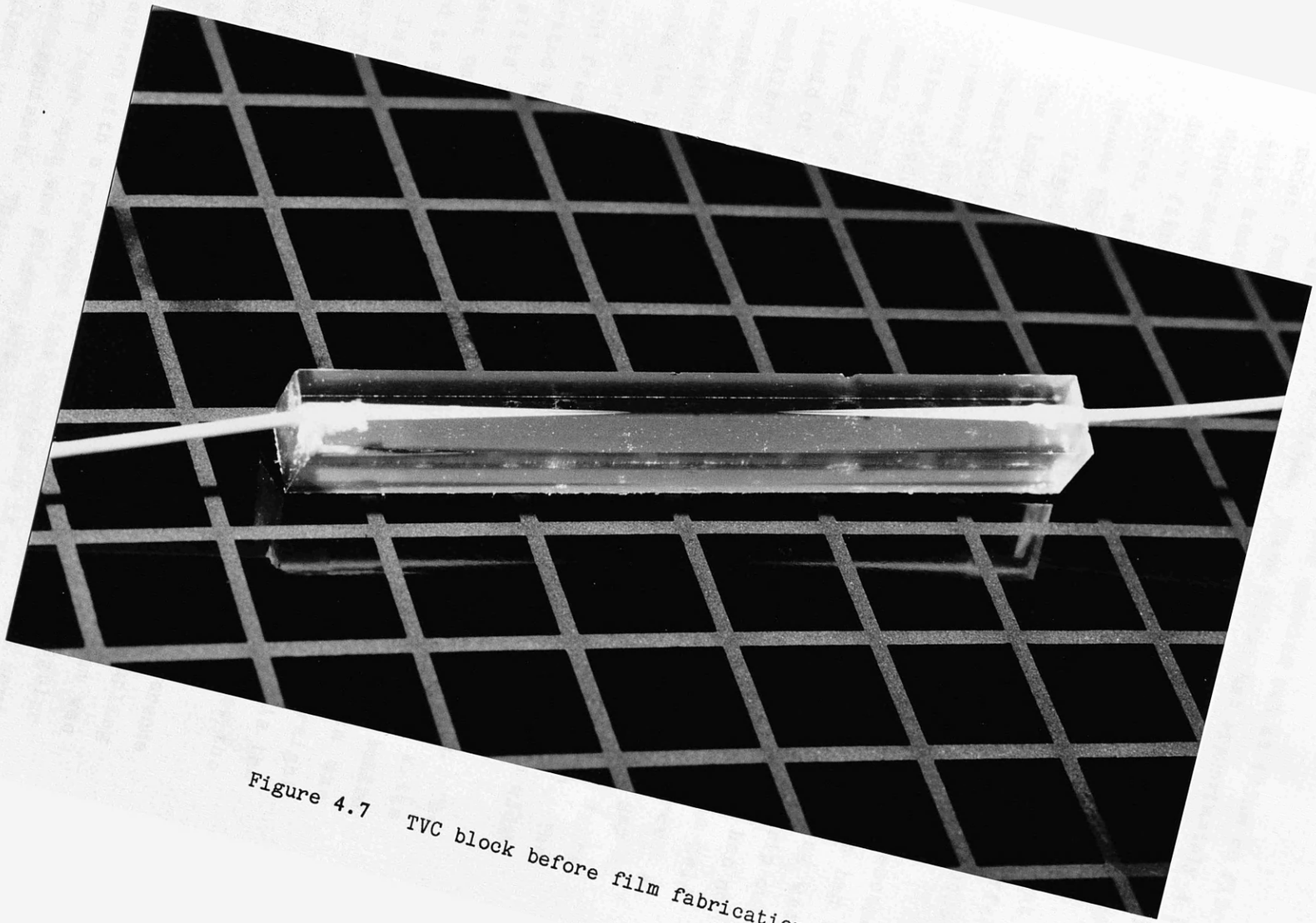

Figure 4.7 TVC block before film fabrication.

Initially experiments were carried out at 633nm on fibres which were single moded at 1.3μm. These fibres had approximately 4 LP modes at this wavelength. By establishing the effective indices of these modes, four points on the fibre dispersion curve are known. Repeating this measurement at longer wavelengths gives the actual fibre dispersion curve. This could then be fitted to some equivalent step index fibre. The apparatus is shown in figure 4.8. Four different fibres, single mode at 1.3μm were incorporated into TVC blocks to assess the sensitivity of the technique.

Light was launched into the cleaved fibre end using a telescope. The launch was optimized by adjusting the x-y-z movement which had a sensitivity of 0.1μm. A short length of the fibre jacketing was removed and the bared section immersed in a high index oil to strip out fibre cladding modes. The remaining part of the fibre pigtail had no small radius bends (< 10cm). The TVC (which had $\theta_b = 1^o$) was held against a small prism by a clamp with a pressure adjusting screw. A liquid of index lower than silica was inserted in the TVC-prism gap by capillary action. This was to increase the extent of the fibre evanescent field which decays according to $\exp(-jk_o(n_e^2-n_a^2)^{1/2})$. The field strength in the prism was also adjusted by varying the gap width using the pressure screw.

In order to couple into the TVC a second laser was used. The output from the prism was spatially filtered using a pair of slits separated by approximately 30cm. The second laser was situated behind the slits in a position where radiated light from the prism was incident on the laser end face. It was then relatively straight forward to launch light from the second laser into the fibre via the prism. In this case the screen was placed at position (a) to view the fibre far field mode pattern.

The second laser was also used to determine an angular reference point (the normal to the exit face of the prism) for prism coupling measurements. Light incident on the prism when normal to the beam was reflected back to the laser and the spot observed. The angular position on the θ_{xy} movement was noted at normal incidence. A semi transparent screen with a reference line marked on it was placed at position b. The laser spot was aligned with the reference line and the second laser extinguished. The radiated lines from the prism were subsequently aligned with the reference mark and the angular reading on the θ_{xy} movement noted. A similar technique, of finding the normal to

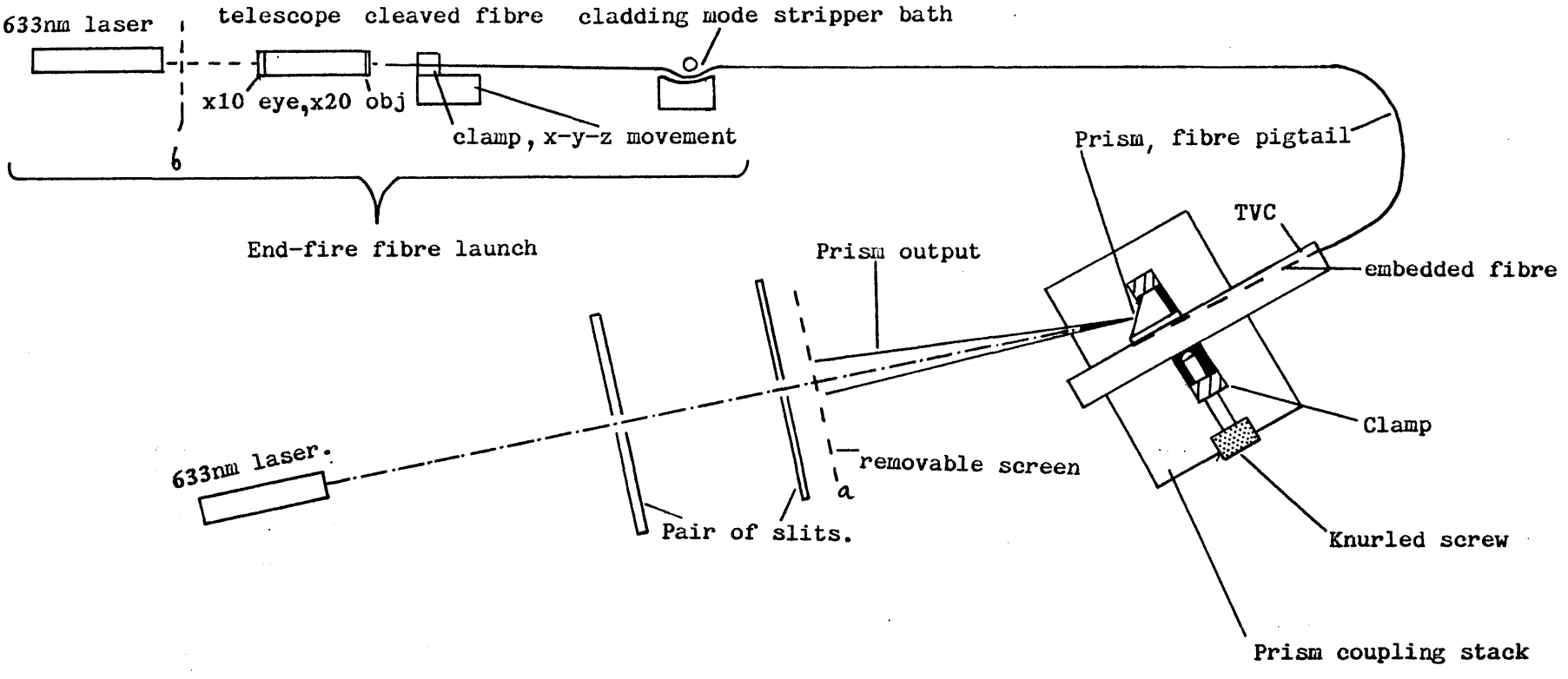

Figure 4.8 Prism coupling arangement.

the prism base and exit face, was used to measure the prism angle θ_p.

Results

The far field radiation from a prism is normally in the form of lines, known as m-lines, since each mode has a characteristic angle and hence gives rise to a characteristic line[22]. For a fibre with 4 LP modes, four distinct lines were expected (figure 4.9a). In fact the prism output consisted of more than 100 resolvable lines. These were clearly not mode lines.

A measurement was made of the intensity of these lines over a central cross section (figure 4.9a) using a photodiode mounted on a motorised stage (figure 4.9b). The resolution of the measurement was improved by placing a slit in front of the diode. A section of a typical plot is shown in figure 4.9c. It was thought that this effect was caused by interference between two (or more) beams and this was supported by interpretation of the coupler geometry (figure 4.10a).

Figure 4.10a shows a schematic cross section of the fibre-prism coupling arrangement. In region A the fibre mode propagation constants were almost identical to those of the fibre in isolation. This gave rise to a beam at the Cerenkov angle θ_{ms} in the film, for each mode m where;

$$\theta ms_m = \cos^{-1}(\beta_m/k_o n_p) \qquad 4.2$$

In region B the tapered fibre region behaved analagously to the planar film taper described in chapter 3.4.3. The light in mode m is less well guided in the taper since the effective core size is smaller. Experiments conducted on fibres which had been heated and pulled into tapers[23,24] have shown a similar phenomenon. As the core radius was decreased the mode was less well guided eventually becoming cut-off and radiating.

In this case, the core tapered asymmetrically and was partly clad with a liquid of index close to but not identical to that of silica. Although this rendered the calculation of the effective index very difficult the central point remained valid, i.e. the effective index of the m^{th} mode decreased. Thus the light evanescently coupled from the tapered fibre region had a larger mode sinking angle θms and crossed the path of the light coupled in region A. This angle θms increased along the taper until the mode was cut-off.

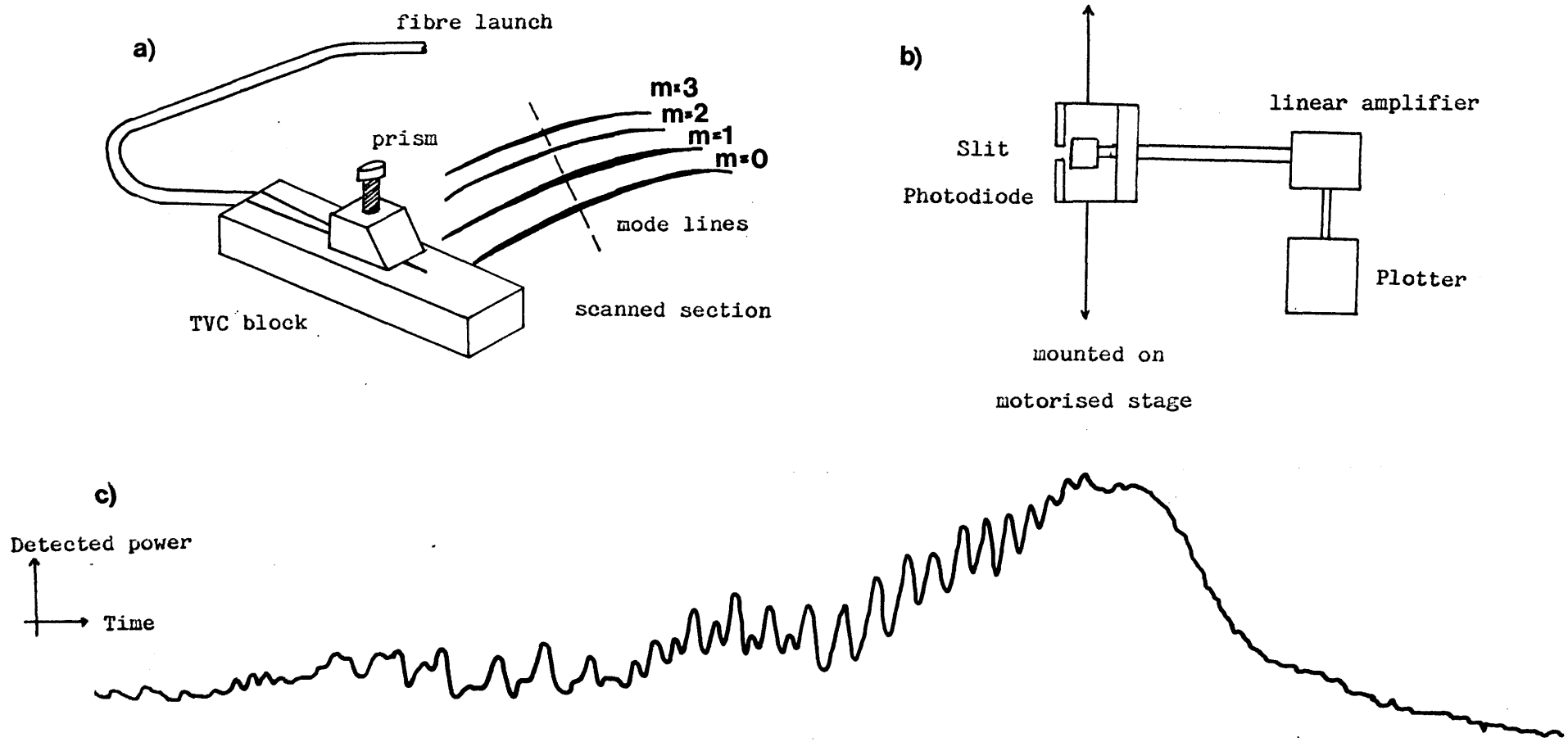

Figure 4.9 a) expected prism output b) scanner arrangement
c) scanner output.

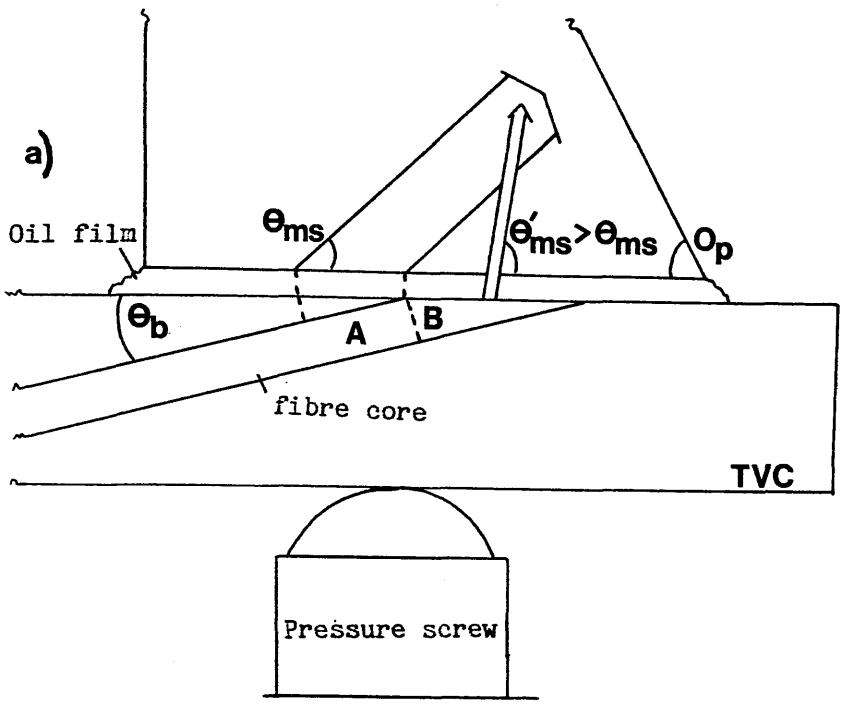

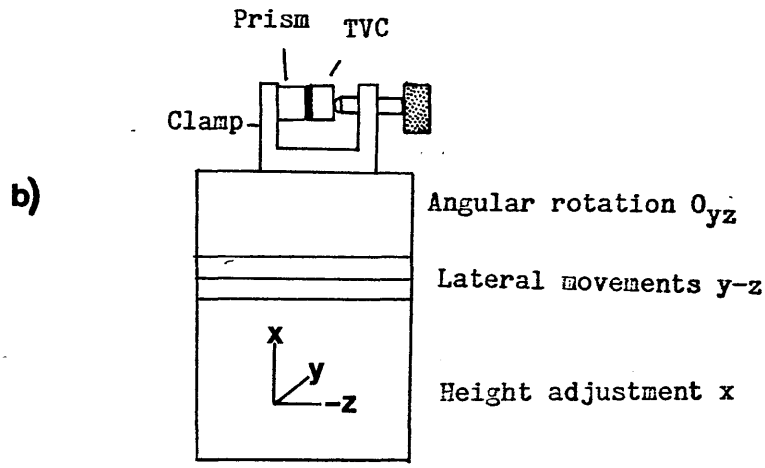

Figure 4.10 a) schematic diagram of light prism coupled from TVC. At A mode-sinking occurs at the characteristic angle O_{ms}. At B the fibre is less confined and β decreases. The angle of radiation therefore increases and light from the two regions interferes.

b) schematic diagram of prism coupling stack.

For each mode m there were two interfering beams, producing a far field interference pattern. The resulting pattern was difficult to analyse and was thought unsuitable for fibre characterisation.

In order to confirm this analysis, further experiments were performed using a fibre which was single mode at 633nm. The fibre was made in BTRL by drawing down a standard fibre and its parameters were unknown. However if the cut-off wavelength of the LP11 mode was 0.6μm compared to 1.2μm for standard fibre, the core diameter would also be approximately halved. (2.14) The ESI core diameter was originally in the region of 8-10μm and a figure of approximately 4-5μm could be expected for the reduced fibre.

4.4.2 Prism coupling to single mode fibres

A TVC with $\theta_b = 1^o4'$ was made using the special single mode fibre to confirm that the observed far field pattern did not arise from interference between modes of different order. Similarly a PDC with radius of curvature 25cm was made using identical fibre to confirm that the interference was caused by light radiated from the taper region.

By adjusting the pressure screw it was possible to have particularly strong or weak coupling. Two regimes were established for the TVC. By tightening the pressure screw to its maximum, radiation-coupling from region A became more dominant (figure 4.11). By loosening the pressure screw more power was coupled in region B extending the observable interference pattern (figure 4.12). The exit radiation pattern for the PDC under the same conditions is shown in figure 4.13 for comparison. These results were obtained using a prism of index $n_p = 1.682$ at 633nm. Matching oil of index $n_D = 1.454$, below that of silica was used to extend the evanescent field. The experimental arrangement was as described in figure 4.8. Accurate measurements ($\pm$ 1' of arc) were made of the mode line position for the TVC and PDC couplers. The TVC was tightly coupled and measurements were made of the dominant mode line (figure 4.11). The TVC was removed and the measurements were repeated for the PDC. These are listed in Table 4.1.

4.4.3 Measurement of effective index

The normal to the prism exit face was established for each coupler. The angular positions of the edges of the mode lines were

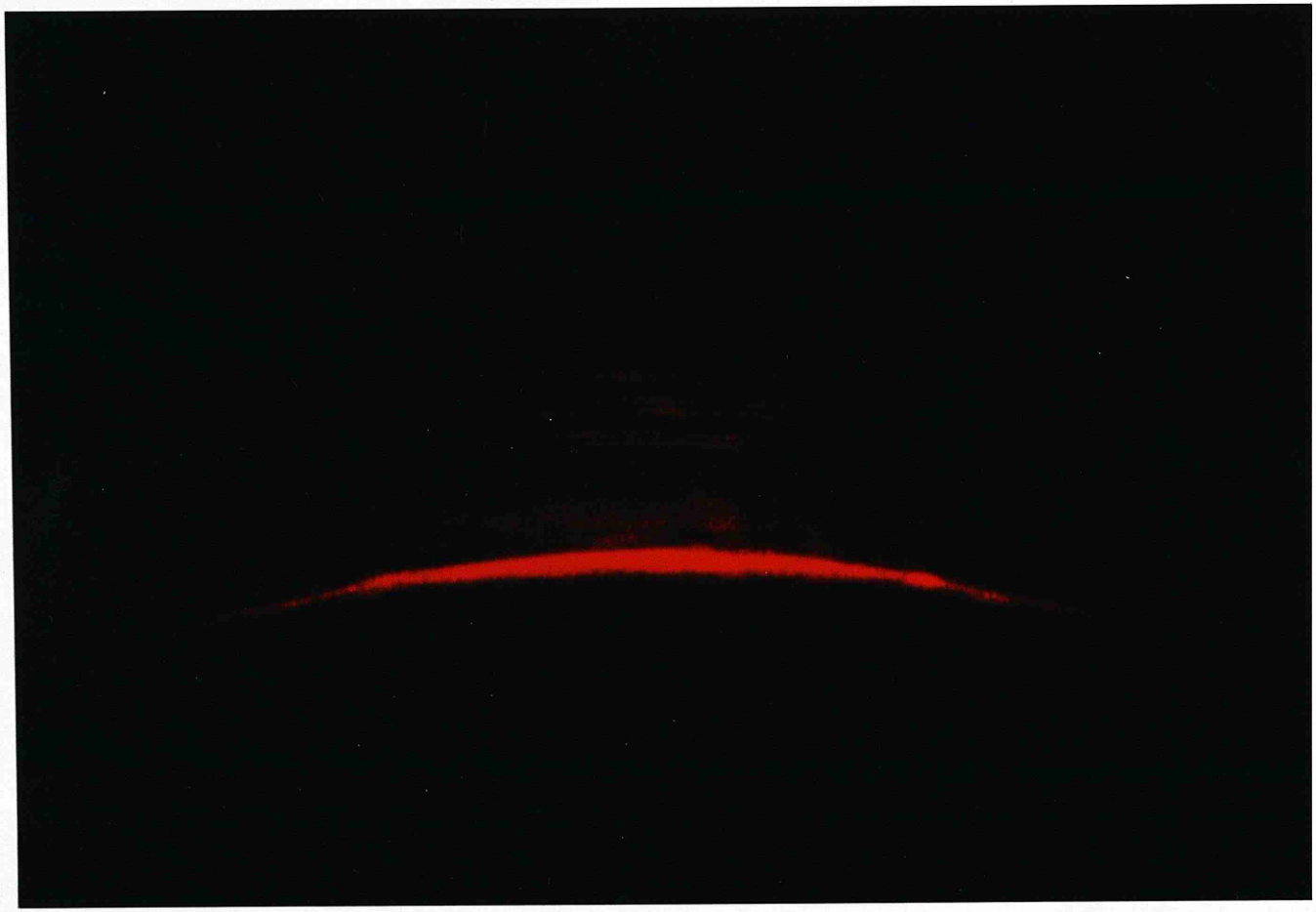

Figure 4.11 Output from TVC, tightly clamped.

Figure 4.12 Output from TVC, loosely clamped.

Figure 4.13 Output from PDC, tightly clamped.

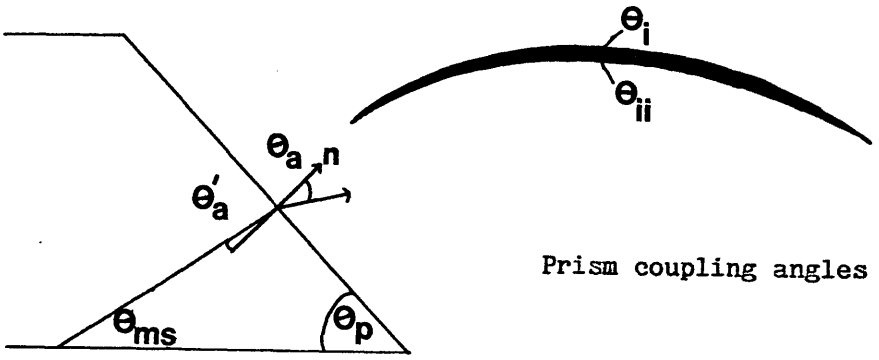

Figure 4.14 a)

Table 4.1 Calculation of effective index from mode angles.

Device	TVC	PDC
Prism normal	356°41'	355°40'
0_i	356°32'	356°20'
0_{ii}	356°46'	356°40'
Average $(0_i+0_{ii})/2$	356°39'	356°30'
0_a	2'	50'
$0_a'$	1'	30'
0_p	59°57'	59°57'
0_b	1° 4'	-
0_{ms}	30° 2'	29°30'
$n_e=n_p\cos(0_{ms}-0_b)$	1.4639	-
$n_e=n_p\cos 0_{ms}$	-	1.4625

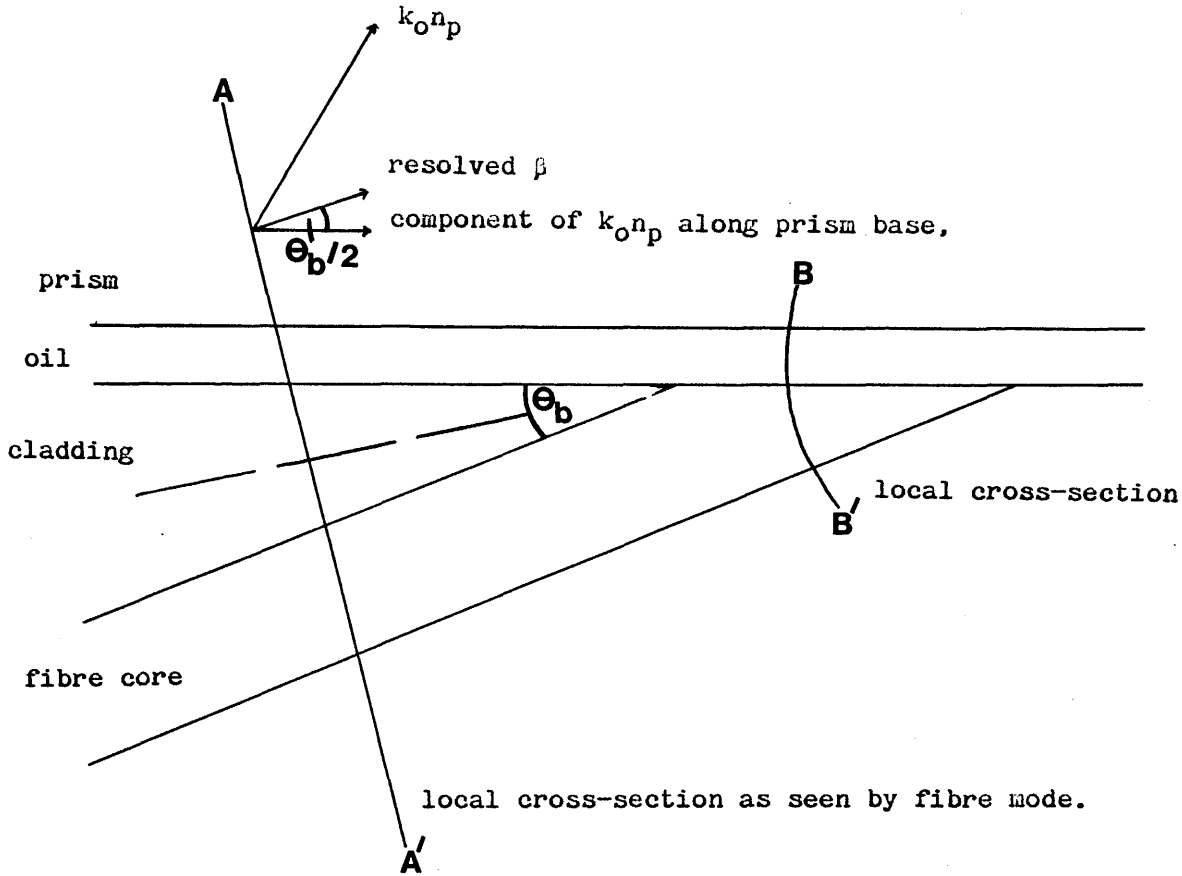

Figure 4.14 Interpretation of local cross-section in TVC during prism coupling

estimated and the average position used in subsequent calculations. The mode sinking angle was calculated and the effective index obtained directly. The prism index was measured with an Abbe refractometer. The measured effective index of the TVC was lower than that of the PDC although identical fibre was used in each. The difference in measured indices ($\Delta n = 1.4 \times 10^{-3}$) was less than the ESI core-cladding index difference $\Delta_s = 4 \times 10^{-3}$. This indicated that the measurements did not give a very accurate indication of effective index but were physically reasonable. Note that there was no overlap in the angular positions of the mode lines.

Interpretation of the measured angles was complicated by the fact that the fibre and prism base were non-parallel. The derivation of 3.25 assumes a z-invariant structure. Figure 4.14b shows the interpretation of the local cross-section in the TVC during prism coupling. In region A this follows Matsuhura as described in section 3.3.5. In region B however it is not possible to define an invariant direction or to define a local normal. There is therefore considerable latitude in the interpretation of coupler measurements.

In the case of the PDC the angle between the fibre and prism base changed slowly and smoothly, allowing a local cross-section to be defined. In the PDC coupling is significant over a length of typically 700μm, for a radius of curvature of 25cm. The change in angle between the fibre and prism over this coupling length was approximately 4.25' The position of the exit radiation (i.e. mode line) arising from each elemental coupling length will similarly alter by about 4.25'. This results in a slightly broader m-line from the PDC compared to the TVC.

The leakage from the fibre into the mode sink occurs over a finite length, i.e. it is radiation from a finite aperture and is diffraction limited. Mode lines therefore subtend a finite angle in general.

4.4.4 Interference

In the case of weak coupling from a TVC the exit radiation pattern was clearly a result of interference (figure 4.12). The pattern was very similar to the far field radiation pattern from plane waves impinging on a slit in an opaque surface. In this section it is shown that the interference pattern obtained was consistent with the concept of two distinct coupling regions in the TVC.

The two interfering beams have a finite cross section, i.e. they are not plane waves. They are diffraction limited and can be

conveniently treated using the paraxial approximation[24]. They may be represented by a superposition of plane waves, analogous to the representation of a finite-duration time function by a Fourier superposition of sinusoids[25]. The Fourier representation of a paraxial ray is derived and the Fresnel diffraction integral is then developed. The Fraunhofer approximation is then obtained to give the far field radiation pattern. The interference pattern is shown to have similar characteristics to that arising from interference between plane waves originating from a slit and a semi-infinite half space. The scalar wave equation describing the propagation of an electromagnetic wave with propagation constant k can be written

$$\nabla^2 \psi + k^2 \psi = 0 \qquad 4.3$$

where

$$k^2 = k_z^2 + k_y^2 + k_x^2 \qquad 4.4$$

and $\psi(x,y,z)$ is the amplitude of the vector potential. If the wave vector k is very nearly directed along the z-axis then the wave is paraxial and

$$k_z = (k^2 - k_x^2 - k_y^2)^{1/2} \simeq k - (k_x^2 + k_y^2)/2k \qquad 4.5$$

using the binomial expansion. The wave amplitude distribution u, is defined as

$$\psi(x,y,z) = u(x,y,z)\exp(-jkz) \qquad 4.6$$

It can be shown that the amplitude distribution u can be built up by plane wave superposition[25].

$$u(x,y,z) = \int dk_x \int dk_y \, U_o(k_x,k_y)\exp -j(k_x x + k_y y)\exp jz(k_x^2+k_y^2)/2k \qquad 4.7$$

The paraxial approximation is valid in the case

$$(k_x^2 + k_y^2)^{1/2}/k \ll 1 \qquad 4.8$$

U_o in equation. 4.7 is the amplitude of the plane wave solution of equation. 4.3 with transverse components kx, ky. At z = 0 the amplitude distribution $u_o(x,y)$ is from equation. 4.7:

$$u_o(x,y) = \int dk_x \int dk_y U_o(k_x,k_y)\exp -j(k_x x + k_y y) \qquad 4.9$$

U_o is therefore the wave amplitude function i.e. the Fourier transform of u_o at $z = 0$. The 2-D fourier transform gives $u_o(k_x,k_y)$ directly as

$$U_o(k_x,k_y) = (1/2\ )^2 \int dx_o \int dy_o\ u_o(x_o,y_o)\exp j(k_x x_o + k_y y_o) \qquad 4.10$$

where 4.9 , 4.10 are Fourier transform pairs. The solution of the scalar wave equation u(x,y,z) can be expressed in terms of the (known) distribution $u_o(x,y)$ at $z = 0$.

$$u(x,y,z)=j/\lambda z \int dx_o \int dy_o\ u_o(x_o,y_o)\exp -j(k/2z)[(x-x_o)^2 + (y-y_o)^2] \qquad 4.11$$

In the case of a plane wave incident on a rectangular aperture in an absorbing screen $u_o(x_o,y_o)$ can be specified simply. In the far field i.e. at large distances from the aperture, the exponential may be approximated by

$$[(x-x_o)^2 + (y-y_o)^2] \simeq [(x^2+y^2) - 2xx_o - 2yy_o] \qquad 4.12$$

For this approximation to be valid the amplitude distribution in the input plane must extend over a transverse dimension s such that

$$s \ll (z/k)^{1/2} \qquad 4.13$$

Substituting 4.12 into 4.11 we obtain;

$$u(x,y,z)=j(2\pi/(\lambda z))^2 \exp[-jk(x^2+y^2)/2z]U_o(kx/z,ky/z) \qquad 4.14$$

The exponential term together with the term exp(-jkz) from 4.6 gives the phase front of the wave. It can be shown that near the axis the phase front is parabolic with a radius of curvature R where $R \to z$ in the far field. We can therefore neglect the phase front in the paraxial approximation, to good accuracy.

4.4.5 Single slit interference.

For a plane wave incident on the narrow slit shown in figure 4.15a the excitation u_o is given by;

$$u_o = 1 \quad x_o < s/2 \qquad 4.15$$
$$0 \quad s/2 < x_o$$

Neglecting the phase front curvature the amplitude u(x) is given by

$$u(x) = j/(\lambda z)\, s \,.\, \frac{\sin kxs/z}{kxs/z} \qquad 4.16$$

with nulls at $x=\pi z/ks$. The far field radiation from two identical parallel slits as shown in figure 4.15b consists of the envelope of the single slit field multiplied by the factor M where;

$$M = 2\cos(kxL/2z) = 2\cos(kL/2.\sin\theta) \qquad 4.17$$

and L is the centre to centre separation of the slits. $\sin\theta=x/z$ where x and z refer to the observation plane. The number of nulls in the 2-slit pattern within each null of the 1-slit envelope increases as the separation of the slits L increases. This is because the phase shift between light incident from each slit is a more rapidly varying function. The number of fringes observed within a given angle is proportional to L. Similarly, oblique incidence of plane waves (figure 4.16a) causes a phase difference in the light originating from each region and the one-slit envelope is spatially modulated.

The far field radiation pattern of the TVC figure 4.12, shows distinct bands of light which are strongly modulated. In this respect the pattern is similar to that arising from two phase separated sources as described above. The two coupling regions A and B have no physical separation. The separation in phase arises from the difference in the fibre mode propagation constants in regions A and B. The mode sinking angles in the two regions are different and this results in a rapidly varying phase in the observation plane. The angle at which the first null of the interference pattern (figure 4.15a) occurs is given by;

$$\theta_x = \lambda/s \qquad 4.18$$

From Table 4.1, $\theta_x = 0^o 7 \pm 1'$ and $\lambda = 0.633\mu m$. The aperture s was therefore $317 \pm 45\mu m$ in length. Since the angle θ_b was $1^o 4'$ the fibre core diameter was $5.9 \pm 0.84\mu m$. Given the approximate nature of the above analysis, this was in good agreement with the expected value of $4-5\mu m$

The imaginary part β of the propagation constant of the light in

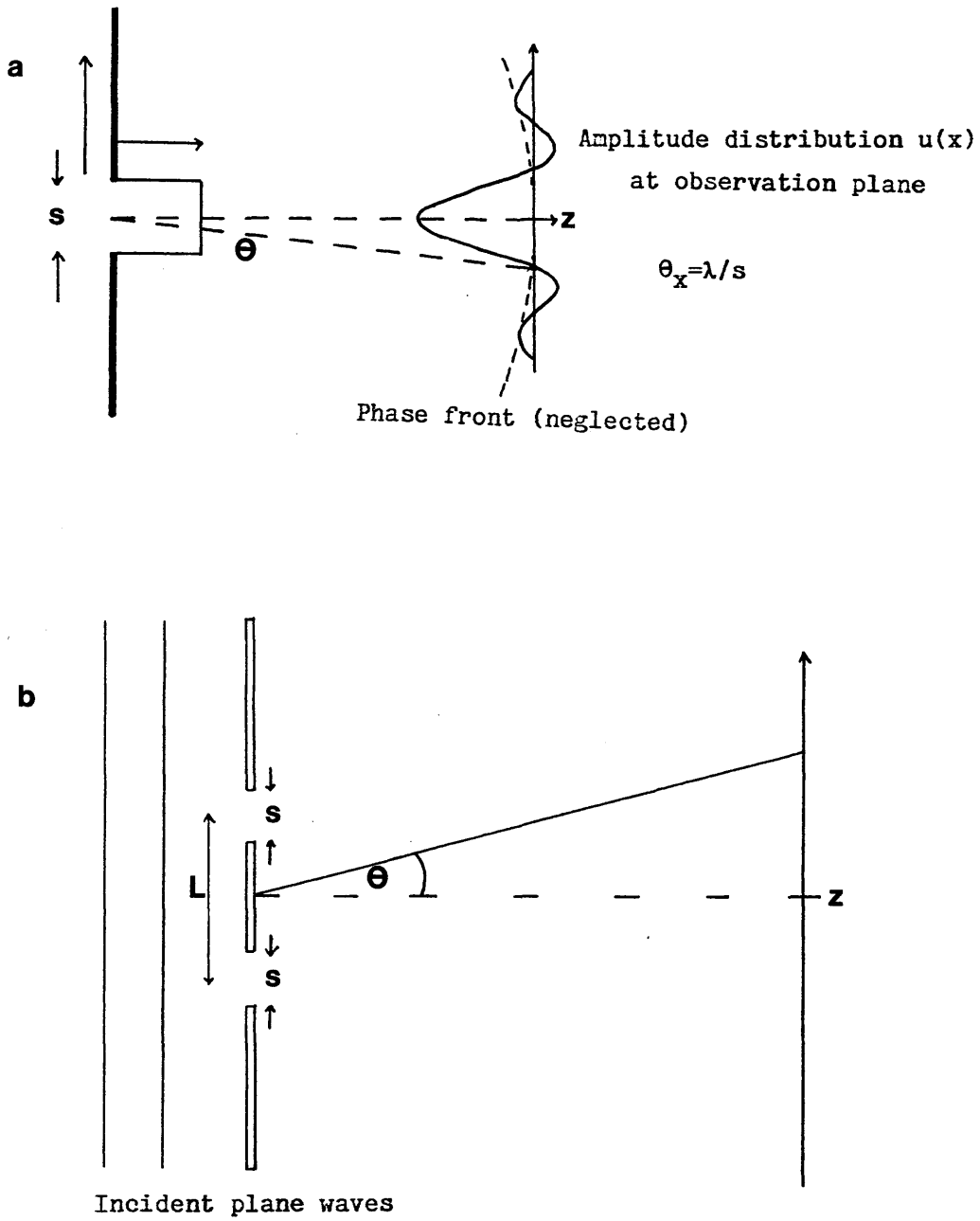

Figure 4.15 a) Plane waves incident on a single slit of width s
b) Plane waves incident on two slits of width s and separation (L-s)

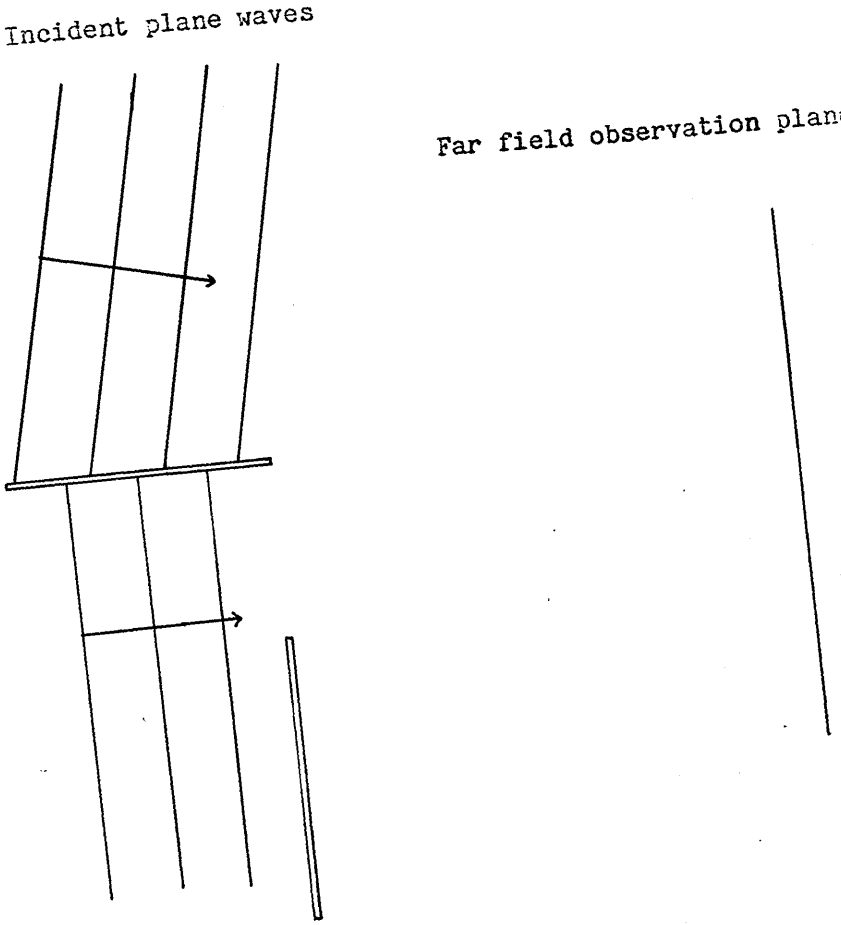

Figure 4.16 Interfering plane waves in a structure analogous to that of the TVC during prism coupling.

the leaky core mode in region B falls smoothly with distance. The angle θ_{ms} at which mode sinking occurs in the prism similarly changes with distance along the fibre. This further complicates the observed diffraction pattern. It is reasonable to suggest however that the band structure observed in figure 4.12 arises from interference from two distinct coupling regions of the TVC which have a significant phase separation.

4.5 Summary

A coupler has been constructed which offers access to the evanescent field of a guided fibre mode. The core of the fibre was polished through completely, tapering to zero at a small angle θ_b. A substantial fraction of the power launched in the fibre apparently remained guided by the core as it tapered, during prism coupling. An experimental investigation of the coupler's suitability for fibre characterisation by prism coupling, was carried out. This revealed that for each guided mode of the fibre the far-field radiation from a mode-sink was a complicated pattern. This pattern had many similarities with that produced by plane waves incident on a single slit and a semi infinite half space in an opaque screen. This suggested that two coupling regions exist in the TVC under prism coupling. The interference pattern was principally a function of the coupler geometry and was not straightforwardly related to the fibre effective index. The TVC was therefore concluded to be unsuitable for fibre characterisation. Experiments were also performed on a PDC constructed of identical fibre. These indicated that a single coupling mechanism was present in the PDC since interference was not observed. The fibre effective index was measured using a prism-coupling technique of good accuracy for both the TVC and PDC. A substantial difference in effective indices was obtained. The most probable explanation of this difference arises from the difficulty of interpreting the prism-measurements from a non-invariant structure.

References

1. Laybourn, P.J.R., Millar, C.A., Stewart, G., Wilkinson, C.D.W., "Optical coupling between thin films and circular fibres", Electron. Letts. 9th January (1975) Vol. 11, No. 1, pp.2-3.

2. Hsu, H.P., Milton, A.F., "Single mode optical fibre pick-off coupler", Appl. Opt., Vol. 15, No. 10, Oct. (1976) pp.2310-2312.

3. Ozeki, T., Kawasaki, B.S., "Optical directional coupler using tapered sections in multimode fibres", Appl. Phys. Letts., Vol. 28, No. 9, 1 May (1976) pp.528-529.

4. Ragdale, C.M., Payne, D.N., De Fornell, F., Mears, R.J., "Single mode fused biconical taper fibre couplers", Proc. Optical Fibre Sensor Conference, London, 1983, 221, pp.75-78.

5. Sheem, S.K., Giallorenzi, T.G., "Single-mode fiber-optical power divider: encapsulated etching technique", Optics Letts., Vol. 4, No. 1, Jan. (1979) pp.29-31.

6. Bergh, R.A., Kotler, G., Shaw, H.J., "Single mode fibre optic directional coupler", Electron. Letts. 27 Mar (1980) Vol. 16, No. 7, pp.260-261.

7. Digonnet, M.J.F., Shaw, H.J., "Analysis of a tunable single mode optical fibre coupler", IEEE J.Quantum Electron. Vol. QE-18, No. 4, Apr. (1982) pp.746-754.

8. Parriaux, O., Gidon, S., Kuznetsov, A. "Distributed coupling on polished single mode optical fibres", Appl. Optics, Vol. 20, No. 14, 15th Jul. (1981) pp.2420-2423.

9. Nayar, B.K., Smith,D.R., "Optical directional coupler using polarisation maintaining monomode fibre", Opt. Letts. Vol. 8, No. 10, pp.543-545, Oct. 1983.

10. Kragness, R.C., Waggener, H.A., US Patent 3506509 (1970).

11. Millar, C.A., UK Patent Application GB 2 080 562 A.

12. Leminger, O.G., Zengerle, R., "Determination of single mode fibre coupler design parameters from loss measurements", J. Lightwave Tech., Vol. LT-3, No. 4, Aug. (1985) pp.864-867.

13. Mao, Z., Fang, X., Li, B., "Polished single mode fibre directional coupler with strong coupling", IGWO 1986 Topical Meeting. Atlanta, Feb. (1986) Post deadline paper PDP-1.

14. Stegeman, G.I., Seaton, C.T., "Non-linear Integrated Optics", J. Appl. Phys. Vol. 58, No. 12, Dec. (1985) pp.57-78.

15. Findakly, T., Chen, C.L., "Optical directional couplers with variable spacing", Appl. Opt., 1 Mar. (1979) Vol. 17, No. 5, pp.769-774

16. Dow Corning Silicones, Reading Bridgehouse, Reading, Berkshire, U.K. Epoxy Technology inc. PO Box 567, Billerica MA 01821, U.S.A.

17. Diamant Boart, Belgium. Supplied by Heathway, Uxbridge Rd. Uxbridge Middlesex, U.K.

18. Ainslie, B.J., Beales, B.J., Day, C.R., Rush, J.D., "The design and manufacture of monomode optical fibre", IEEE J. Quant. Electron. Vol. QE-18, No. 4, (1982) pp.514-523.

19. C.A. Millar, Private Communication.

20. Sabine, P.V., Donaghy, F., Irving, D., "Fibre refractive-index profiling by modified near-field scanning", Electron. Letts. Vol. 16, No. 23, 6th Nov. (1980) pp.882-883.

21. Povlsen, J.H., "Characterisation of graded single mode fibres by fundamental mode spot-size variation", Electron. Letts. Vol. 20, No. 13, 21 June 1984. pp.543-544.

22. Midwinter, J.E., "Evanescent field coupling into a thin-film waveguide", IEEE J. Quant. Electron., Vol. QE-6, No. 10,

October 1970.

23. Snyder, A.W., "Coupling of modes on a tapered dielectric cylinder", IEEE Trans. Microwave Theory β Techniques, Vol. MTT-18, No. 7, July 91970) pp.383-392.

24. Midwinter, J.E., "The prism taper coupler for the excitation of single modes in optical transmission fibres". Optical and Quant. Electron., Vol 7 1975 pp 297-303

25. Haus, H.A., "Waves and Fields in Optoelectroncis" Chapter 4. Prentice Hall Inc. New Jersey.

26. Hecht, E., Zajac, A., "Optics", Chapter 7. Addison Wesley, London.

Chapter 5. Results and Analysis of Transverse Coupling Between A Single Mode Fibre And A Planar Film Waveguide.

5.1 Introduction.

In chapter 3 it was shown that efficient power transfer in directional couplers requires that the guides be very nearly synchronous. There is a rapid fall in maximum power transfer with increasing mismatch and this imposes stringent tolerances on directional coupler manufacture. It is possible to reduce these tolerances by taper coupling but thin film tapers have severe limitations in practice. In an integrated optics context, with a number of devices on a single chip it would be necessary in general to fabricate tapers at different angles and directions. The geometry of the TVC allows fibres to be polished at different angles θ_b to the substrate surface which is equivalent to altering the coupling length of a directional coupler. In addition the fibre core is tapered and the possible reduction of coupler tolerances is discussed in section 5.4.

It was also shown in chapter 3 that a planar film constitutes a mode sink and that optical power is coupled from a fibre into the mode continuum at angles $\pm\theta_{ms}$ to the fibre axis. This phenomenon was experimentally and theoretically investigated and verified. Using TVC blocks a fibre-film-fibre coupler was constructed. The efficiency and wavelength dependence of the coupler was investigated[1] and from this the coupler behaviour, in terms of mode sinking and directional coupling was obtained. The experimental results were confirmed by a BPM analysis of the TVC. The maximum efficiency obtained using the coupler was a fibre-film-fibre transmission loss of 2dB in the near-IR. The mode sinking analyses of Arnaud[2] and Marcatili[3] were further developed to explain the coupling phenomena.

5.2 Directional coupling between a silica fibre and a high index silica clad film.

To gain an understanding of fibre film coupling using the TVC it is convenient in the first instance to neglect mode sinking. The fibre and film are treated as a directional coupler as if both posessed 2-D confinement (chapter 2, table 1, category E). This concept was useful in explaining the initial results described in section 5.2 below. A

local cross-section of the coupler is shown in figure 3.5a.

5.2.1. Theoretical wavelength dependence of directional coupling.

In a directional coupler, significant power transfer occurs only between modes of nearly equal effective index. In weakly guiding fibre the mode index is close to that of the silica cladding. Therefore the film modes which are synchronous with the fibre must also have an effective index close to that of silica. The characteristic equation of the modes of a symmetrical planar guide of thickness t and wavelength λ is (from chapter 2.2);

$$2\pi t/\lambda(n_g^2-n_e^2)^{1/2}=2\tan^{-1}(F(n_e^2-n_s^2)/(n_g^2-n_e^2))^{1/2}+m\pi \qquad (5.1)$$

In the investigation of coupler performance, relatively thick, high index films were used for which the fundamental film mode was not coupled in the near-IR. The synchronous modes of these films are near cut-off and 5.1 can be simplified to;

$$\lambda_m=2t/m(n_g^2-n_e^2)^{1/2} \qquad m\neq 0 \qquad (5.2)$$

The dispersion diagram of the fibre (calculated from equation 2.25) and of an optically thick film (calculated from equation 5.2) is shown in figure 5.1. The film thickness and index were t=43μm and n_D=1.620 respectively. The silica dispersion was calculated from published data[4]. The dispersion of the film index (as used in experiments) was calculated from the manufacturers data[5], measured for the wavelength range 0.3-1.06μm and extrapolated to the longer wavelength region. The film mode effective indices extend to 1.620 but only the modes near cut-off are relevant to this discussion.

From the dispersion diagram it is clear that there is a series of wavelengths λ_m at which the fibre is synchronous with the forward modes of the film, (i.e. the points where the fibre and film dispersion lines cross). The power transfer efficiency is expected to peak sharply at these wavelengths which are given by equation 5.2 with $n_e=n_e(\text{film})=n_e(\text{fibre})$. Around each synchronous wavelength the power transfer efficiency should fall off rapidly with increasing mismatch. This is shown semi-schematically in figure 5.2 as the efficiency of fibre-film-fibre coupling over the wavelength range above.

COUPLING TO SYMMETRIC SLAB MODES

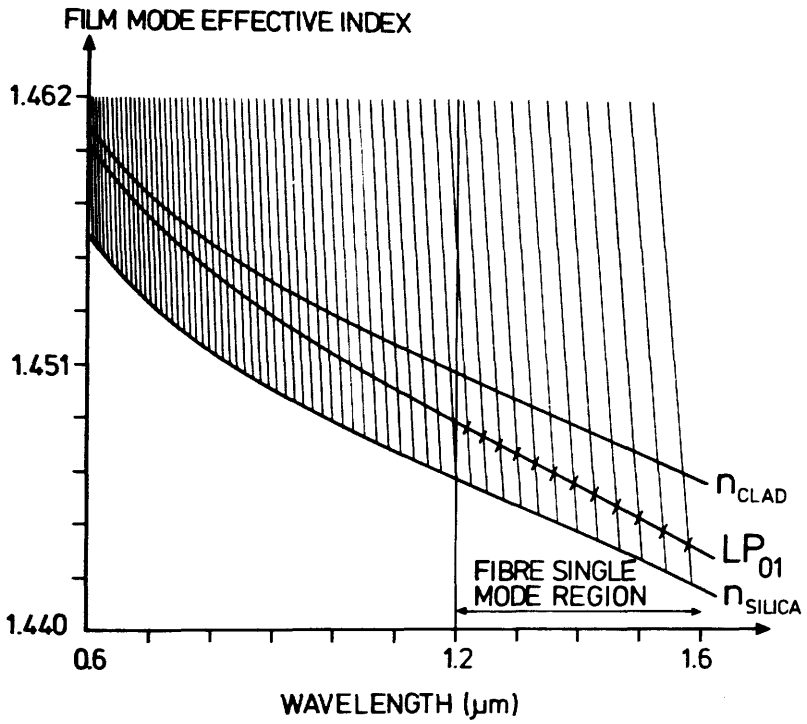

Figure 5.1 Dispersion of standard single mode fibre and high index silica clad planar film.

Film thickness 43 microns,
Index $n_D = 1.620$.

Fibre core 8 microns,
Index difference 0.004.

Fibre-film-fibre coupling with symmetric silica-clad film of index $M_D^{20} = 1.62$ and thickness 43μm

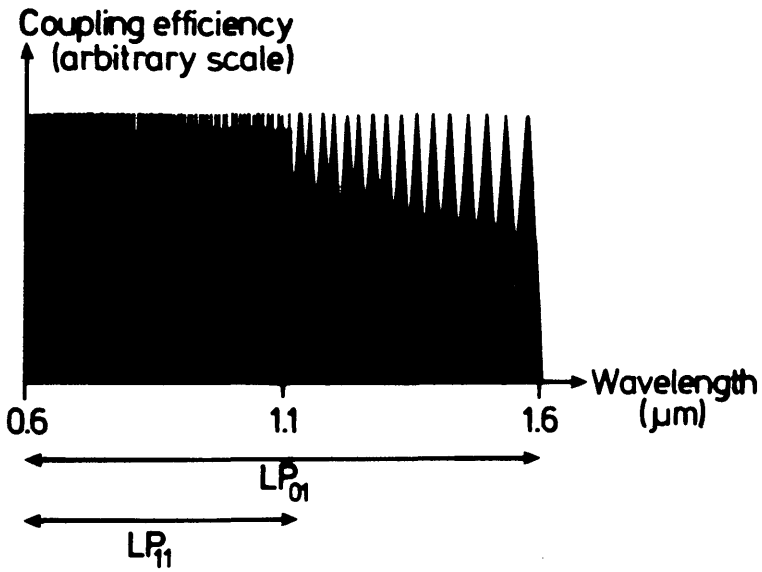

THEORETICAL MODEL

Figure 5.2

The LP_{11} mode of the fibre is guided below 1.2μm. It has a slightly lower effective index (at a given wavelength) than the LP_{01} mode and consequently couples to the forward film modes synchronously at a set of wavelengths λ_m', where for each m, λ_m' is slightly larger than λ_m. The density of synchronous wavelengths is increased below 1.2μm and this results in the reduced modulation of efficiency with wavelength shown in figure 5.2. Experimental verification of this result is discussed below.

5.2.2 Experimental Wavelength Dependence of Directional Coupling

A beam of finite width launched in a planar slab suffers divergence as it propagates since it is unconfined in the direction of the plane. A TVC block with a fibre at each end, aligned such that the groove centres are collinear is shown in figure 5.3. The fibre cores are separated by a distance $(2V_s+L)$ where V_s is the distance between the cladding ellipse and the V-groove end and L is the ellipse length. Typical core separations were 10-20mm for $0.5^o<\theta_b<1.25^o$. An assessment of coupler efficiency using this geometry would be of limited use since the loss due to the region of epoxy substrate and to beam divergence would be difficult to quantify. This geometry was however used with non-planar waveguides as discussed in chapter.6. For initial investigations planar waveguides were simpler to fabricate and the problems of beam divergence and epoxy loss were largely overcome by using the geometry of figure 5.4.

Two TVC blocks were placed face to face such that the two fibre axes lay in the same x-z plane.The blocks were held in a jig which was originally designed for studying the polished directional coupler[6]. The jig provided controlled relative movement of the TVC blocks only in the direction of the y-axis. The blocks were adjusted by hand in the z-direction and by placing a large weight on the upper TVC the block spacing in the x-direction was adjusted. A schematic cross-section of the coupler arrangement is shown in figure 5.5 A planar waveguide was formed by inserting oil of known dispersion into the space between the polished block surfaces by capillary action. The film index was changed by removing the blocks and cleaning them with alcohol before applying the appropriate oil.

A white light source (quartz-halogen lamp) and an optical spectrum analyser (OSA), (Anritsu MS96A) were used for launch and detection. This allowed measurements to be made over the wavelength range 0.6-

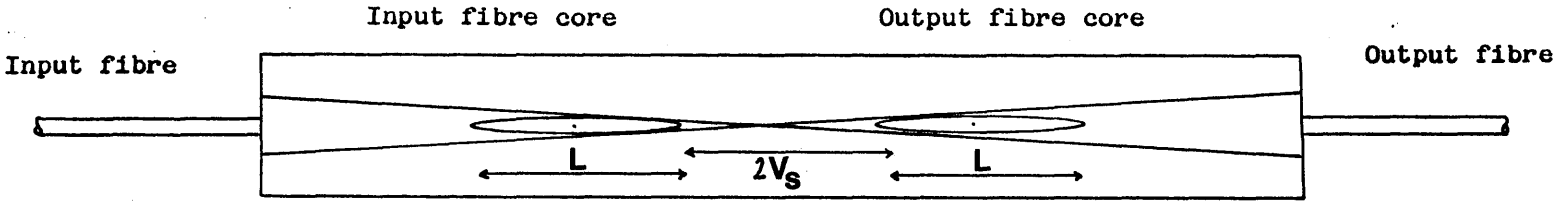

Planar film deposited on TVC block.

For O_b=1.25°, L=5.7mm
O_b=0.50°, L=14.3mm

Key
L - Ellipse Length
V_s- Separation of V-groove End from Ellipse End.

Figure 5.3 Minimum separation of collinear polished fibre cores in a single-input/single-output TVC. V_s is typically a few mm. The core separation is approximately $2V_s$+L.

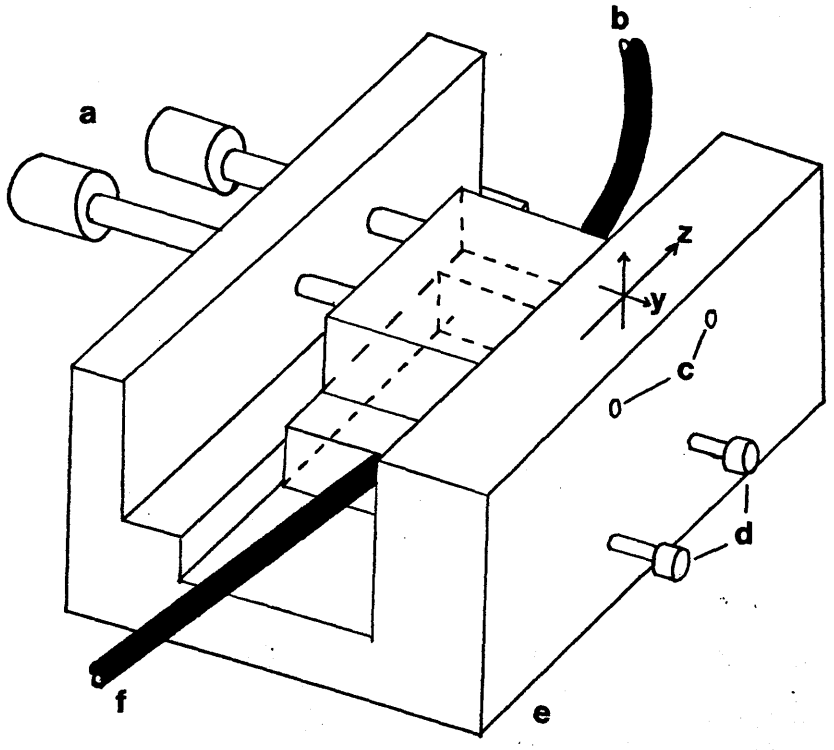

Figure 5.4 Experimental apparatus for relative positioning of two TVC or PDC blocks.

a) Upper TVC position adjustment by micrometer screws.

b) Output fibre and upper TVC block.

c) Return springs, coaxial with micrometer screws.

d) Lower TVC clamping screws.

e) Solid brass mounting.

f) Input fibre and lower TVC block.

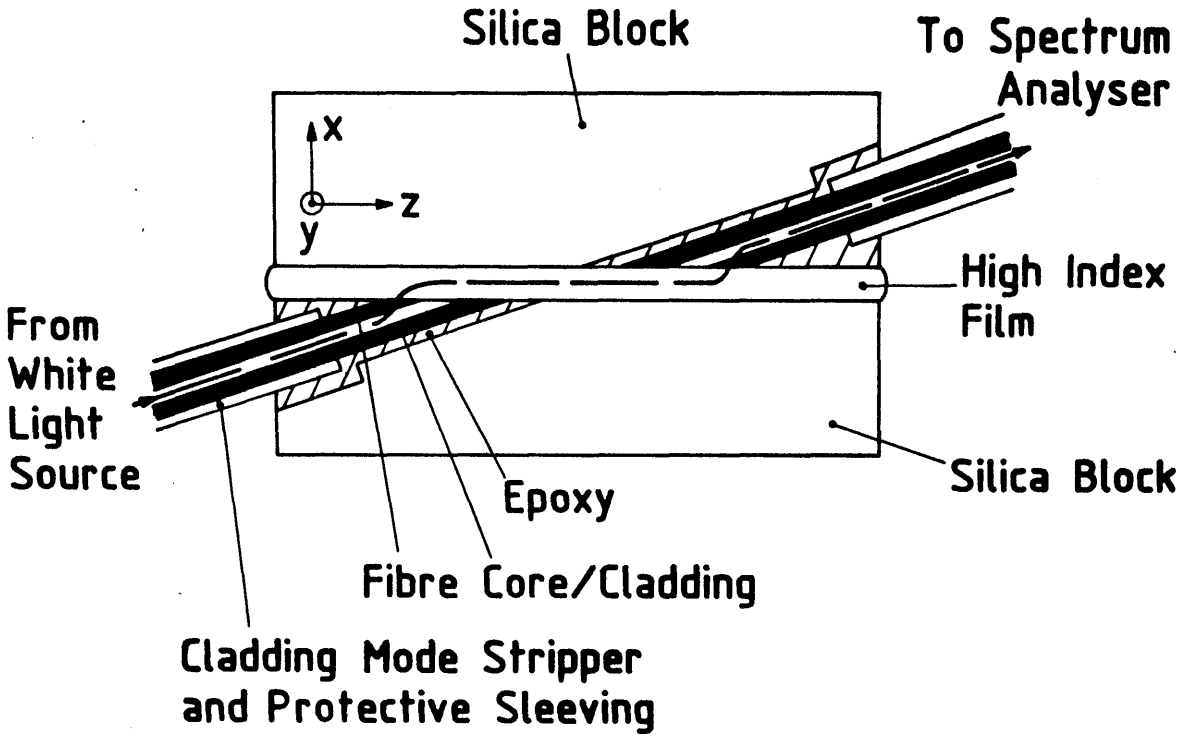

Figure 5.5 Schematic diagram of experimental arrangement used to investigate the wavelength dependence of fibre-film-fibre coupling using the TVC.

1.6μm although the most useful information was obtained over the fibre single mode region (1.2-1.6μm).

Positioning of the coupler blocks in the z-direction was performed in a darkroom by manually adjusting the upper TVC block while estimating (by eye) the point at which the maximum brightness of the output fibre was obtained. For this reason the film waveguide was short, estimated to be 1mm or less. From this position it was noted that if the blocks were moved in the positive z-direction the optical power output (perceived brightness) fell very sharply. Moving the blocks in the negative z-direction (from the position of maximum brightness) resulted in a slow decay of the optical power output. This asymmetry indicated that light was coupled from fibre to film to fibre rather than being directly radiated from fibre to fibre. This indication of transverse coupling was confirmed by measuring the wavelength dependence of the coupler.

A typical result(for which the dispersion curve 5.1 was calculated) is shown in figure 5.6. It shows clearly the coupling maxima associated with the synchronous wavelengths in the single mode region. The density of synchronous wavelengths increases below λ_{co} and the reduced modulation of efficiency with wavelength shown in figure 5.2 is apparent. This measurement was performed with a grating resolution of 10nm i.e. the power over each 10nm interval was measured and plotted. The graph shows the actual power level at the output fibre. It was not normalised for the source and fibre transmission characteristics. The dynamic range of measurement was limited by the noise floor of the detector to about 15dB. The TVC blocks were fabricated with $\theta_b=1.25^o$. The film thickness was calculated from the positions of the coupling peaks in figure 5.6, using equation 5.2.

For two peaks at λ_m and λ_{m+n} we have;

$$\lambda_m/\lambda_{m+n}=(m+n)/m*(n_g^2(\lambda_m)-n_e^2(\lambda_m))^{1/2}/(n_g^2(\lambda_{m+n})-n_e^2(\lambda_{m+n}))^{1/2} \qquad (5.3)$$

The variation of the dispersion term over a few hundred nm is small since both terms, n_g and n_e decrease slowly with wavelength compared to the large difference in their magnitudes. Neglecting dispersion we have simply;

$$\lambda_m/\lambda_{m+n}=(m+n)/m \qquad (5.4)$$

Equation 5.4 is useful in understanding the wavelength spacing of film

Fibre-film-fibre coupling with symmetric, silica-clad film of index $n_0 = 1.62$ and thickness 43μm

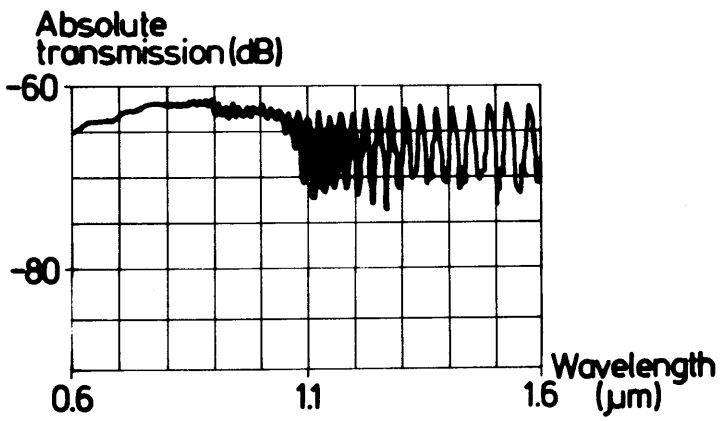

EXPERIMENTAL RESULT

Figure 5.6

modes but since the dispersion term must be evaluated in order to calculate film thickness the full equation 5.3 was normally used. From the peaks at λ_m=1.58μm and λ_{m+1}=1.54μm the film parameters were calculated to be m=38.5, t=43.2μm. m was non-integer because the peak position measurements were of limited accuracy as was the dispersion data. It was concluded that light was evanescently coupled from fibre to film to fibre and that coupling peaks corresponded to wavelengths at which the forward film modes were synchronous with the fibre modes. However it was decided that a purpose built jig giving continuously tunable film thickness and full (3-axis) range of movement was required to facilitate alignment and independently confirm the film thickness measurements. In order to increase the total coupling strength (section 3.3.4) TVC's were made with θ_b=0.50° and were used in the experiments described in the remainder of this chapter.

5.2.3 Improved experimental apparatus

A dedicated jig was designed for accurate relative positioning of coupler blocks. The three axis positioner on which it was based[7] provided movement by stressing flexible plates. For each axial control, movement occurred over a parabola (with a large radius of curvature) rather than strictly along a single axis. This was a small disadvantage in comparison to the load bearing capabilities offered by the stage, which had negligible play and backlash. Under suitable conditions the movement had submicron accuracy.

The jig shown in figure 5.7 was designed to be compatible with the PDC's which had larger cross-sectional dimensions. Collars were therefore constructed of silica which adapted the TVC's to the jig. Four micrometer screws with a nominal sensitivity of 0.1μm were incorporated to provide relative tilt between the blocks to correct any residual offsets. Three piezoelectric positioner sensors with a nominal sensitivity of 0.1μm were incorporated to measure directly the relative movement of the micropositioner stage. The faces of the two clamps (figure 5.7d) were precision ground and were assembled to be parallel to within measurable accuracy. Viewing ports were bored into each clamp assembly so that initial alignment could be performed by eye. The jig was solidly constructed from heavy gauge material to minimise flexing. The range and accuracy of mechanical movement required to mechanically tune and align optical waveguides in this manner were of an extremely high standard. I am indebted to

N.Vankoningsveld of BTRL for the patient and skilled construction of this jig.

As an initial experiment, the polished surface of a TVC block was coated with a thick layer of meltmount[5]. This was a low (65°C) melting point, optically transparent material of known refractive index (at Sodium D). The two coupler blocks were then clamped into position and heated using a hot air blower , to approximately 75°C. It was then possible to align the blocks in the manner described in section 5.2.2. The blocks were allowed to cool and were removed from the jig. The detected power at the output fibre was measured using the OSA and is shown for the single mode wavelength region in figure 5.8. The linear scale 5.8b has a vertical division of 200picoWatts.

To obtain better noise discrimmination, 1000 samples were taken at each 10nm interval and averaged. The result shows the coupler transmission to be a maximum at a set of synchronous wavelengths. It also showed that the device, removed from the jig (figure 5.9) acted as an in line fibre filter. The FWHM of the peak at 1.48μm was 15-20nm. The loss of the coupler at each peak was unknown but in later experiments it was found that no more than -54dBm over a 10nm interval could be detected from a fibre connected directly betwen the QH lamp and OSA . The peak power detected in this experiment (figure 5.9, λ=1.48μm) was -61dBm. This indicated that the fibre to film to fibre loss at λ=1.48μm was, at most, 7dB. This loss was attributed partly to mechanical misalignments betw een the blocks. The experiment showed that the TVC in this configuration had the potential to be an in-line fibre-filter with low insertion loss.

Using this jig the experiment described in section 5.2.2 was repeated for a film of the same index and similar thickness (n_D=1.620, t=53.8μm).The result of the spectral measurement is shown in figure 5.10. The dispersion diagram of the two guides is also shown. The positions of the synchronous wavelengths are slightly different from the theoretical predictions because of the limited accuracy of the oil dispersion measurements in this wavelength region. It is important to note that coupling was through one single mode of the film. For example, light of wavelength 1.54μm was coupled through the 47^{th} film mode. The improvement in accuracy of the jig and the reduction in branching angle θ_b gave a greater dynamic range of measurement by reducing the coupler insertion loss. The loss at 1.54μm was estimated to be less than 6dB. This result showed the wavelength filter characteristics of coupled dissimilar waveguides[8] having two

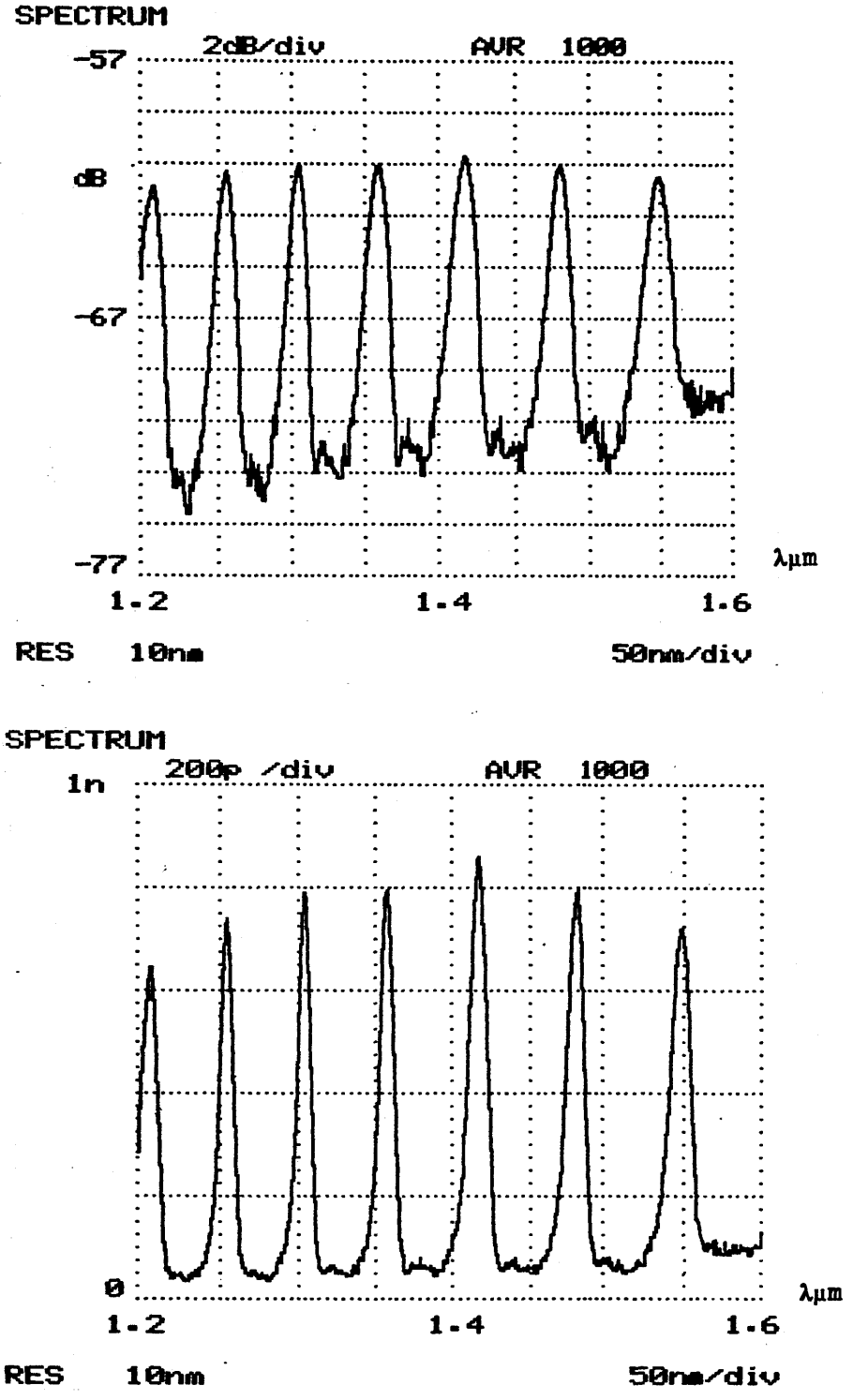

Figure 5.8 Fibre-film-fibre transmission using two 0.50° TVC's with a Meltmount[5] film of index n_D=1.70 and thickness t=20.5μm. The film modes are 21 and upwards.

dimensional confinement. The loss was attributed to mechanical misalignment of the two polished fibres and to beam divergence in the film. Beam divergence is discussed in section 5.4.1.

5.2.4 Confirmation of film thickness measurements.

It was not physically possible to clamp the two TVC blocks together with zero (i.e. a small fraction of a micron) spacing. This would have provided a reference point for thickness measurement using the piezoelectric sensor operating in the x-direction. Instead relative physical movements measured by the sensor were compared with calculated optical thicknesses. Using the apparatus described in the experimental section, light was coupled from fibre to thick-film to fibre. As the film thickness was decreased in stages the coupled spectrum and position transducer reading were recorded. The full dispersion equation 5.3, was used with modes m and m+3. These modes were used in preference to m,m+1 to reduce the innacuracy caused by an error in estimating peak position. The results are shown in table 5.1.

Table 5.1 Film Thickness Measurements.

Calculated Optical Thickness μm	Change in Optical Thickness μm	Change in Mechanical Thickness μm
93.1		
77.0	-16.1	-16.5
25.5	-51.5	-52.0
16.7	-8.8	-10.5

For large thickness changes in a thick film the agreement between the two figures was excellent, but worsened for thinner films. The reason for this error was that the polished surfaces were adjacent over a length of several cm. Although they were smooth they were not perfectly flat over this length. Before the TVC's were finally clamped they were pressed together by tightening the x-movement of the positioning stage. This meant that the polished faces were nominally parallel to each other.

However because the top and bottom faces of the TVC blocks were not exactly parallel, the plane of the polished TVC faces did not lie exactly in the y-z plane of the micropositioner. At low film thicknesses, this resulted in the TVC's coming into contact with each

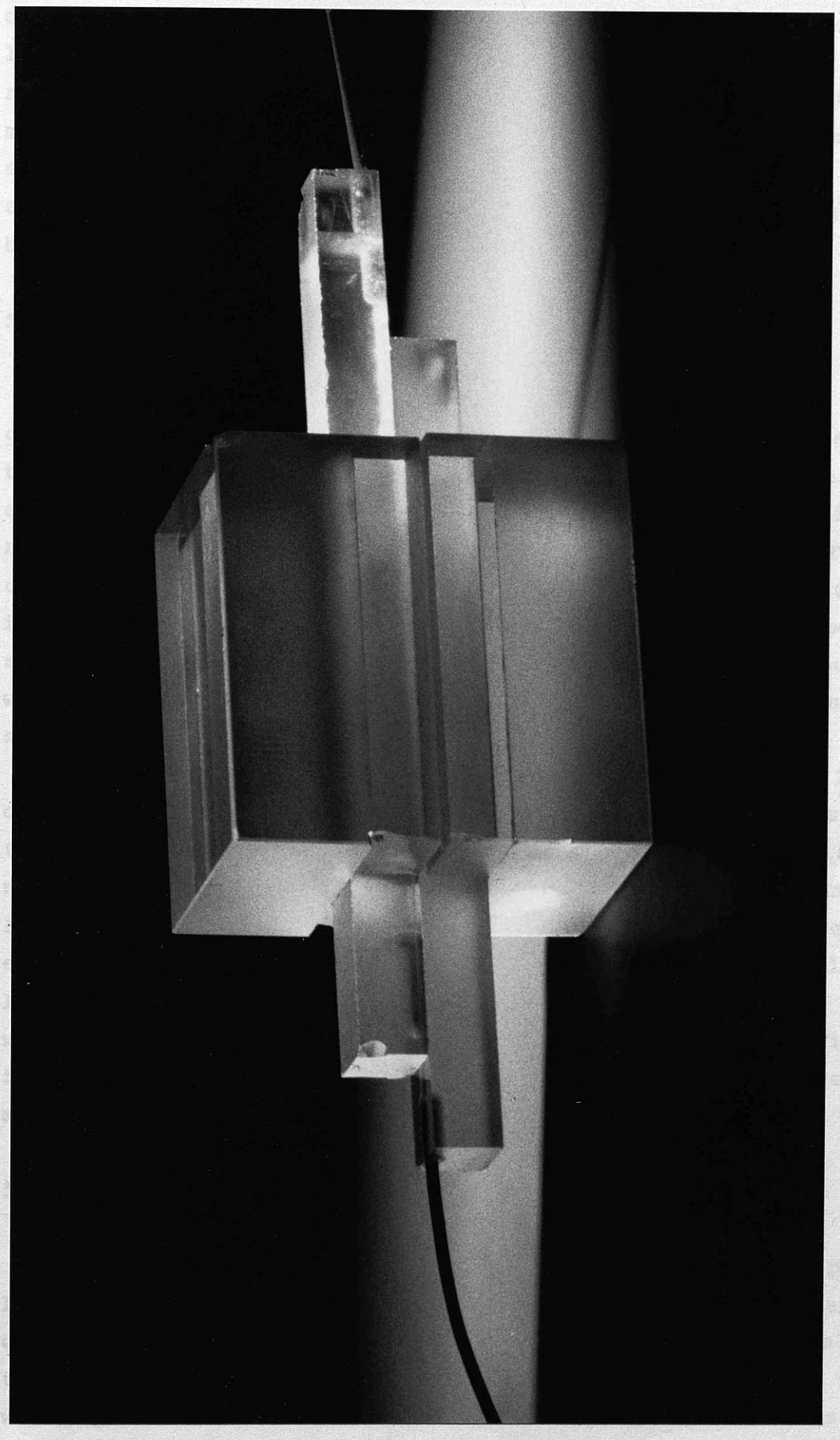

Figure 5.9 In-line fibre filter.

other at their extremities. Mechanical movement in the x-direction at low separations produced movement in other directions and was responsible for the error in table 5.1. This showed the difficulty of mechanically creating optical waveguides of low mode order. Accurate alignment of the two single mode fibres was not possible in this configuration at film thicknesses below 10μm. The measurement showed however that the optical thickness measurements were accurate.

5.2.5 Measurement of Coupler Loss

It was important to establish the efficiency of the fibre film coupling process. A 4m length of identical fibre was fusion spliced to the fibre pigtail of the TVC connected to the white light source. The experiment above was repeated with an optically thinner film of index n_D=1.500 and thickness t=12.5μm. The output power spectrum of the coupler was measured and stored then the input fibre was cleaved (to include the splice) and connected to the OSA giving the input power spectrum. By subtraction the loss through the fibre-film-fibre coupler was obtained at each wavelength. This is shown in the transmission spectrum of figure 5.11.

Coupling was through the 6^{th} and higher modes and the minimum loss, occurring at 1.36μm was 2dB. The transmission of higher order modes (m=7,8) was progressively less efficient. Intuitively this is reasonable since the fibre mode extends further into the cladding at longer wavelengths and the overlap integral for lower order modes is expected to be larger, giving increased coupling. This effect would be less pronounced for differences between the m^{th} and $(m+1)^{th}$ modes as m was increased. The insertion loss of this device, as an in-line fibre-filter of 2dB showed that efficient evanescent field coupling between a monomode fibre and a thin film waveguide was a practical reality.

5.3 Investigation of mode sinking and of coupled beam shape.

In the experiments detailed above there was little evidence of power leakage by mode sinking from the fibre. Consider the dispersion diagram of figure 5.10b. At λ=1.58μm, the fibre mode effective index equalled that of the m=47 film mode. The effective index of the m=46 film mode was larger than that of the fibre mode at this wavelength. Thus the mode-sinking condition described in chapter 3, $k_s > \beta$ was satisfied and power leakage was expected to occur from the fibre into this film mode.

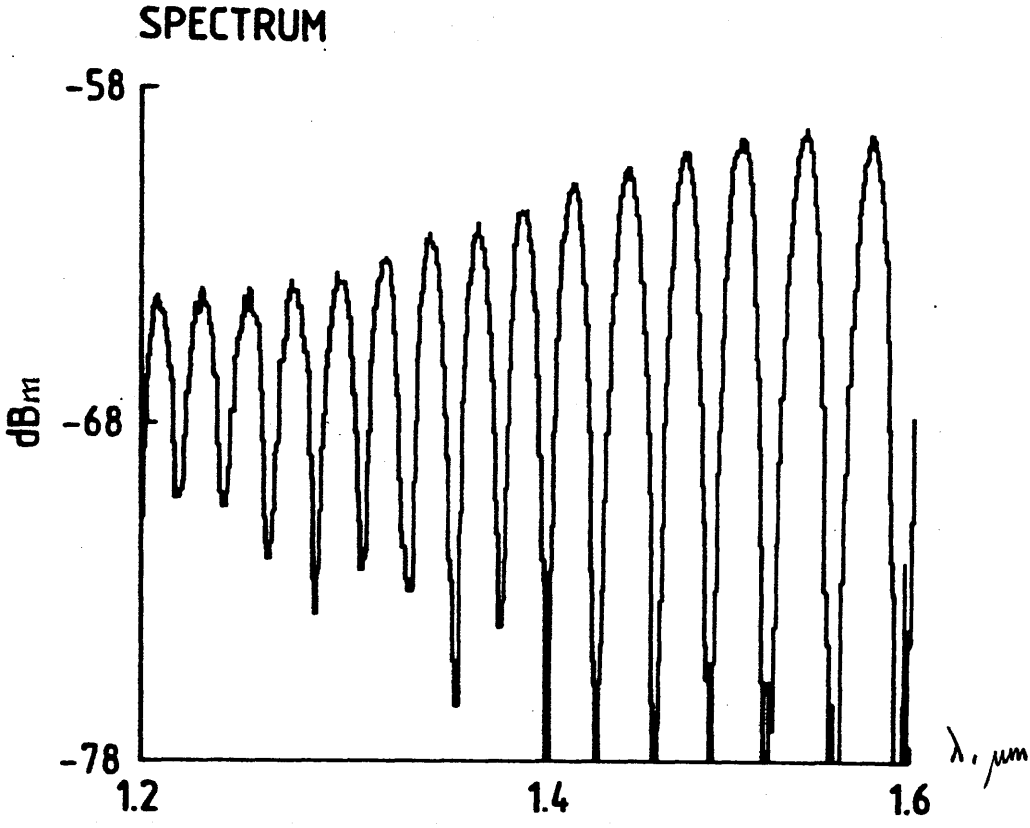

Actual transmission levels from fibre to film to fibre showing synchronous coupling to film modes (film thickness 53.4 μm, index n_D = 1.620).

Figure 5.10 a)

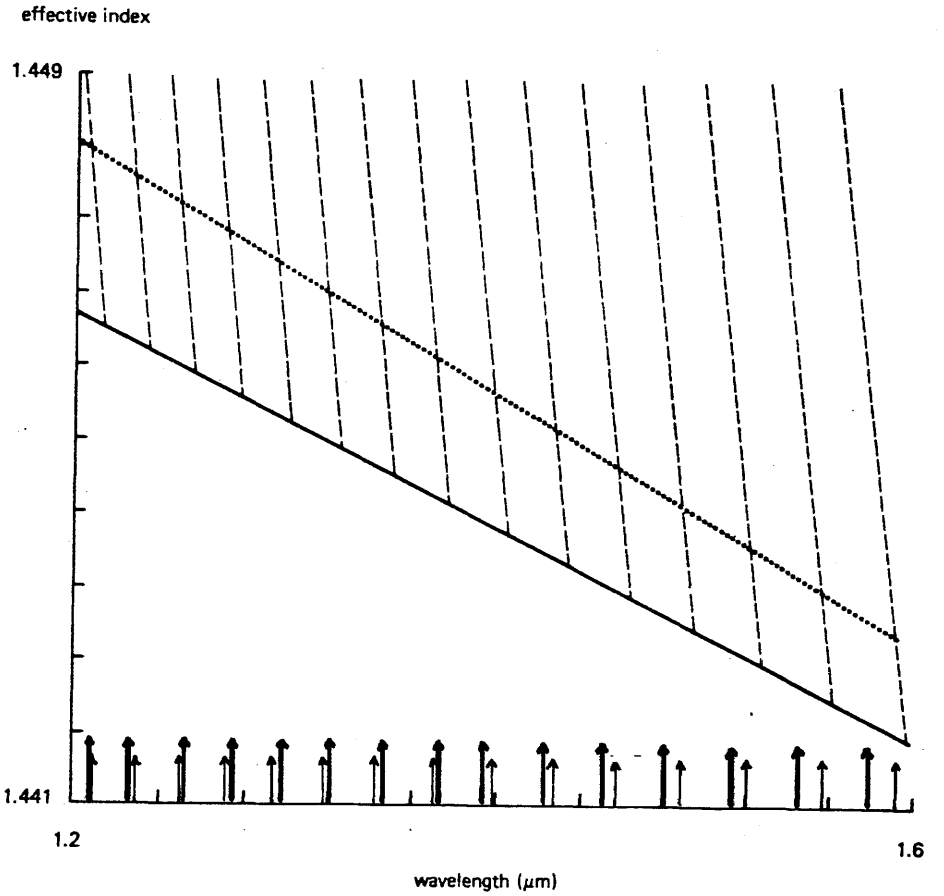

Dispersion diagram of planar film (index n_D = 1.620, thickness 53.4 μm) and single-mode fibre, including material dispersion. The dashed lines show the individual film modes, the dotted line is the fibre LP_{01} mode and the solid line is the silica cladding.

Figure 5.10 b)

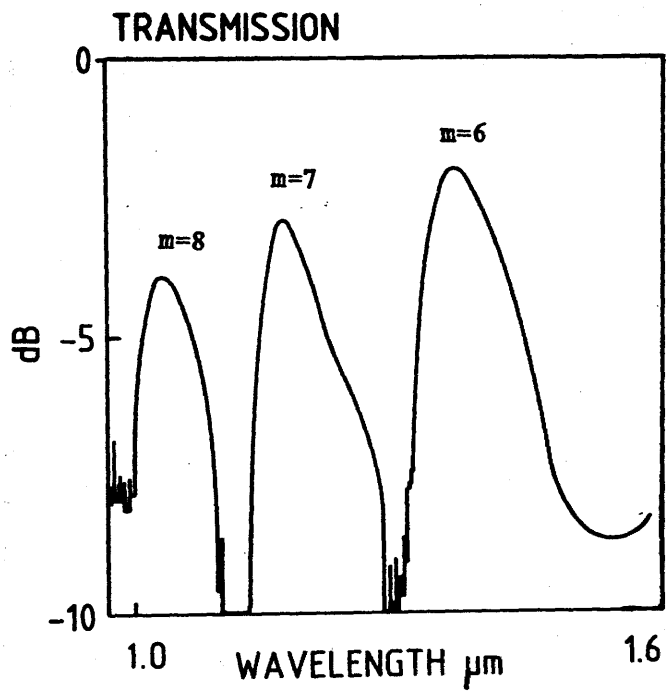

Figure 5.11 Normalised transmission from fibre to film to fibre (film thickness 12.5μm, n_D=1.500)

However if the rate of leakage was e.g. a few dB per km, then over a coupl length of several hundred microns, this effect would have been negligible. We refer to this as mode sinking to a mode of lower order than the synchronous film mode.

In the following section we consider in more detail weak coupling of the fibre mode at wavelengths around the synchronous wavelength (which is denoted λ_s) to the film mode which is synchronous at λ_s. In section 5.4 we interpret the actual coupler behaviour from an "exact" BPM calculation. The weak coupling behaviour described here is a useful intermediate step in the understanding of the actual coupling described later.

5.3.1 Theoretical wavelength dependence of weak coupling.

(i) At a wavelength λ_s, β(fibre)=k_s(film) the fibre is synchronous with the forward mode of the film and power is coupled from the fibre into this film mode. At a small angle (in the y-z plane) $\pm\theta$ to the z-axis, $k_s\cos\theta$ is slightly less than β. Power is coupled less efficiently to the mode propagating at this angle, $k_s^m(\theta)$ since coupling is non-synchronous. As θ and the off-axis component k_y increase, the mismatch between k_s and β increases, rapidly reducing the efficiency with which power is coupled into the mode $k_s^m(\theta)$; Figure 5.12 a,c.

The power coupled into each mode k_y is directly related to the wave amplitude function of the beam in the slab guide. The Fourier transform of the wave amplitude function (in the paraxial limit) gives the beam shape. This is shown in figure 5.12 c,d. Since $U(k_x)$ is monotonically decreasing, u(x) also decreases monotonically, i.e. the beam has effectively a finite width as required by power considerations. Power is coupled from the fibre into a beam of finite width, travelling in the z-direction in the film. This is referred to as synchronous coupling.

(ii) At a wavelength λ_{pm}, slightly larger than λ_s, $\beta > k_s^m$ and the fibre is phase mismatched to the mode continuum in the film. The minimum mismatch occurs for $k_z=k_s$ and the power transferred to the axially propagating mode will be greater than that transferred to modes propagating off axis in the manner described for λ_s above. In total the rate of power coupling from the fibre will be significantly less than for the synchronous case and will fall very rapidly with increasing mismatch. The coupled beam in the film will similarly propagate along the z-axis and will be of finite width but with reduced amplitude. This

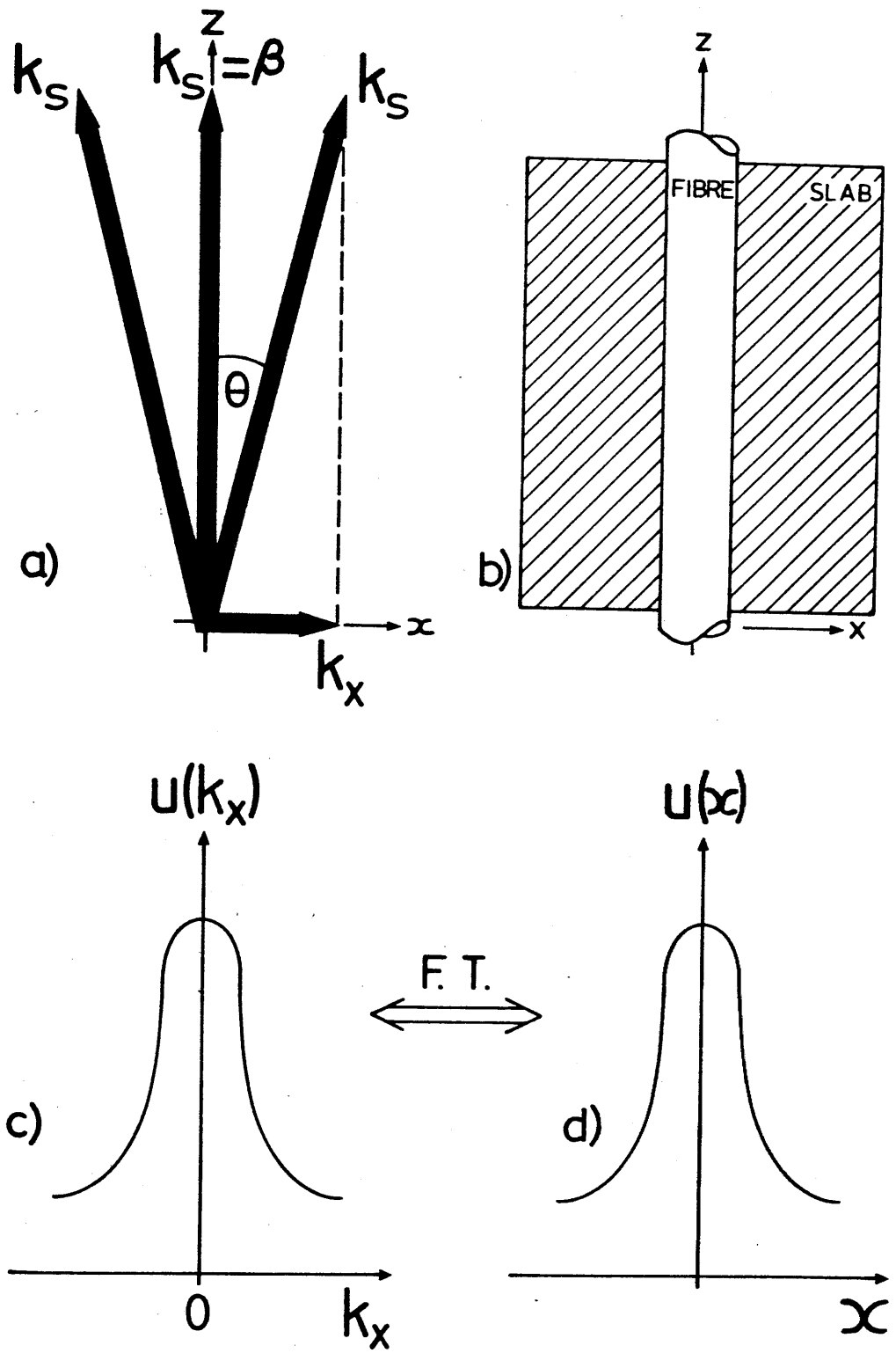

Figure 5.12 a) Angular mismatch at synchronous wavelength.

b) Coupler geometry (parallel guides).

c) Beam amplitude function.

d) Beam shape.

is referred to as phase mismatched coupling.

(iii) At a wavelength λ_{sm}, slightly shorter than λ_s, $\beta<k_s^m$ and the fibre is matched to a point in the mode continuum (of the m^{th} mode). Power is synchronously coupled off axis at angles $\pm\theta_{ms}$ given by;

$$\theta_{ms}=\cos^{-1}\beta/k_s \qquad (5.5)$$

In a similar manner to the above, film modes propagating at an angle $\pm\delta\theta$ to the mode sinking angle $\pm\theta_{ms}$ are slightly mismatched. Correspondingly less power will be coupled to these modes. We therefore expect two beams of finite width propagating at angles $\pm\theta_{ms}$ to the z-axis. This is referred to as mode sinking. The phase fronts of the mode sinking beams are parabolic with a large radius of curvature (paraxial approximation) and are effectively normal to the propagation direction $\pm\theta_{ms}$. The phase fronts of the fibre modes are normal (Gaussian approximation - see ch.2.3.5) to the fibre axis. As the difference $(k_s^m-\beta)$ increases, the angle θ_{ms} increases and the angle between the fibre and coupled beam phase fronts increases. This intuitively reduces the overlap integral between the fibre and film modes and reduces the rate of power leakage from the fibre. The mismatch $(k_s^{m-1}-\beta)$ is very much larger than $(k_s^m-\beta)$ and leakage to lower order modes than the synchronous mode is therefore expected to be much lower.

To summarise, for weak coupling the fibre loss and coupled beam shape depend on the relationship between β and k_s^m according to;

$\beta>k_s$	phase mismatch, axially propagating beam.	(5.6)
$\beta=k_s$	synchronous, axially propagating beam.	(5.7)
$\beta<k_s$	mode-sinking, two beams propagating at an angle $\pm\theta_{ms}$ to the fibre axis.	(5.8)

The fibre mode is expected to be effectively decoupled from the film modes k_s^{m-1} and k_s^{m+1} by the large mismatch between the axial effective indices.

5.3.2 Experimental Wavelength Dependence of Mode-Sinking.

It was realised that if mode sinking occurred then it would be observed by increasing the spacing between the input and output fibres. In this case (figure 5.13) the mode sinking beams would not be coupled to the output fibre since they would no longer be in proximity to it.

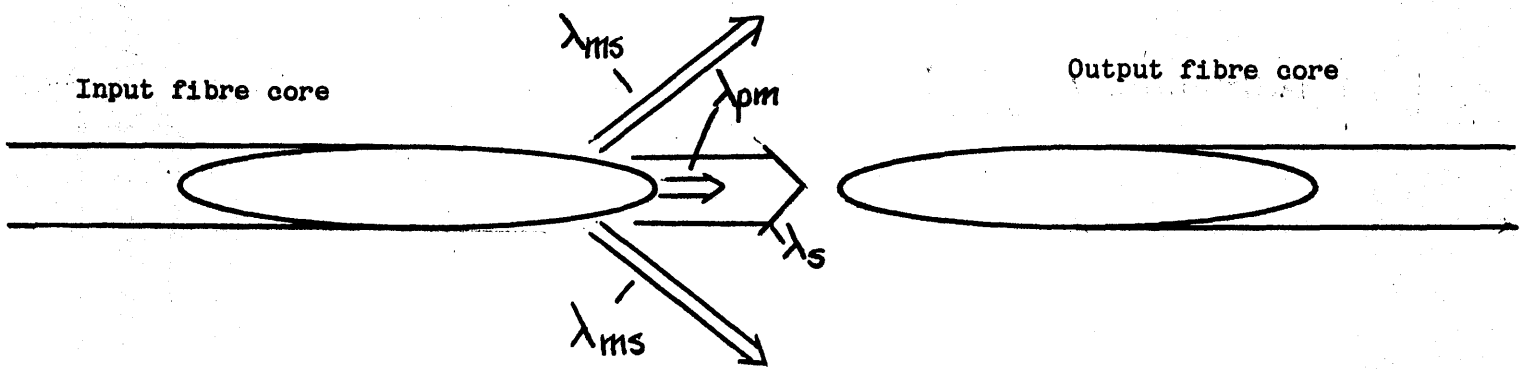

Figure 5.13 Wavelength dependent coupling.

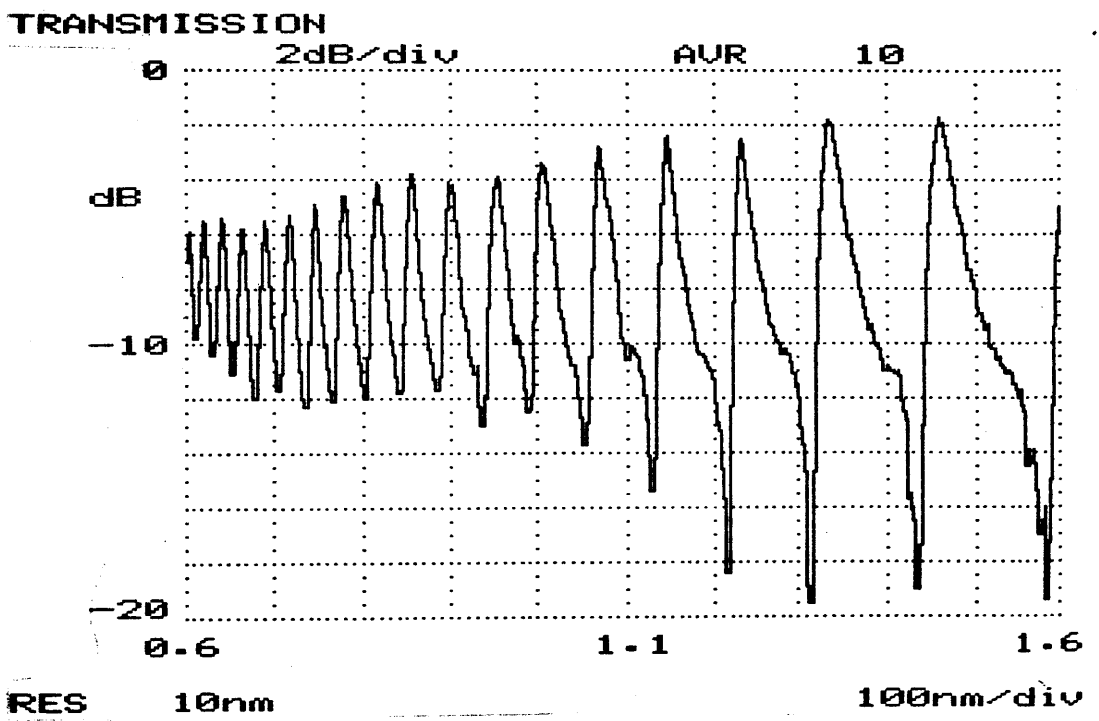

Figure 5.14 Sharp cut-off filter characteristic caused by mode-sinking Fibre-film fibre transmission through two 0.50° TVC blocks . Film thickness 12μm, modes 11 and upwards.

The synchronous and phase mismatched beams, directed on axis would be efficiently coupled. Using the experimental arrangement and normalisation technique described above, the insertion loss spectrum of two 0.50^{o} TVC's with a core separation s of approximately 1mm was recorded (figure 5.14). The film thickness and index were t=12μm and n_D=1.620. The film modes were m=11 and upwards.

The sharp cut-off filter characteristic observed, supported experimentally the theoretical explanation based on weak coupling given in section 5.3.1. Over the wavelength range 1.33-1.32μm the transmission of the coupler dropped by more than 17dB. This figure was limited by the dynamic range of measurement available.

A second experiment was performed at 633nm using a TVC with standard, type B fibre as above. The fibre supported 4 LP modes at this wavelength. Laser light at λ=633nm was end fire launched into the cleaved fibre endface using the apparatus described in section 4.4.1. A ''flip-chip'' was clamped to the polished face of the TVC to provide the thin film waveguide. The flip-chip consisted of a polished silica disc on which was deposited a low index passive material (approximate index n=1.51 (at 633nm) and t=2.5μm). I am grateful to B.J.Ainslie of B.T.R.L. for supplying this material. The film supported two modes at 633nm[10]. Mode sinking was observed and can be clearly seen in figure 5.15. The photograph shows the plane of the slab guide.

The higher order fibre modes were closely spaced in effective index and had a lower effective index than the LP_{01} mode. Thus their mode sinking angles were smaller and more closely spaced. The fundamental fibre mode suffered leakage at the largest angle. This single wavelength experiment supported the evidence of mode-sinking reported in section 5.3.2 above and demonstrated transverse coupling from a single mode fibre to a flip-chip. These experiments showed that the concept of mode sinking from a 2-D confined guide to a 1-D confined guide was valid and of practical interest.

5.4 BPM Analysis of fibre-film coupling using the TVC.

Coupling between the TVC and a thin film was analysed using a 3-dimensional BPM program. The propagating field was analysed at 1μm intervals over a 900μm length (figure5.16a). This technique used substantial computing time and therefore only one run was possible. I am indebted to J.V.Wright of B.T.R.L. for performing these calculations.

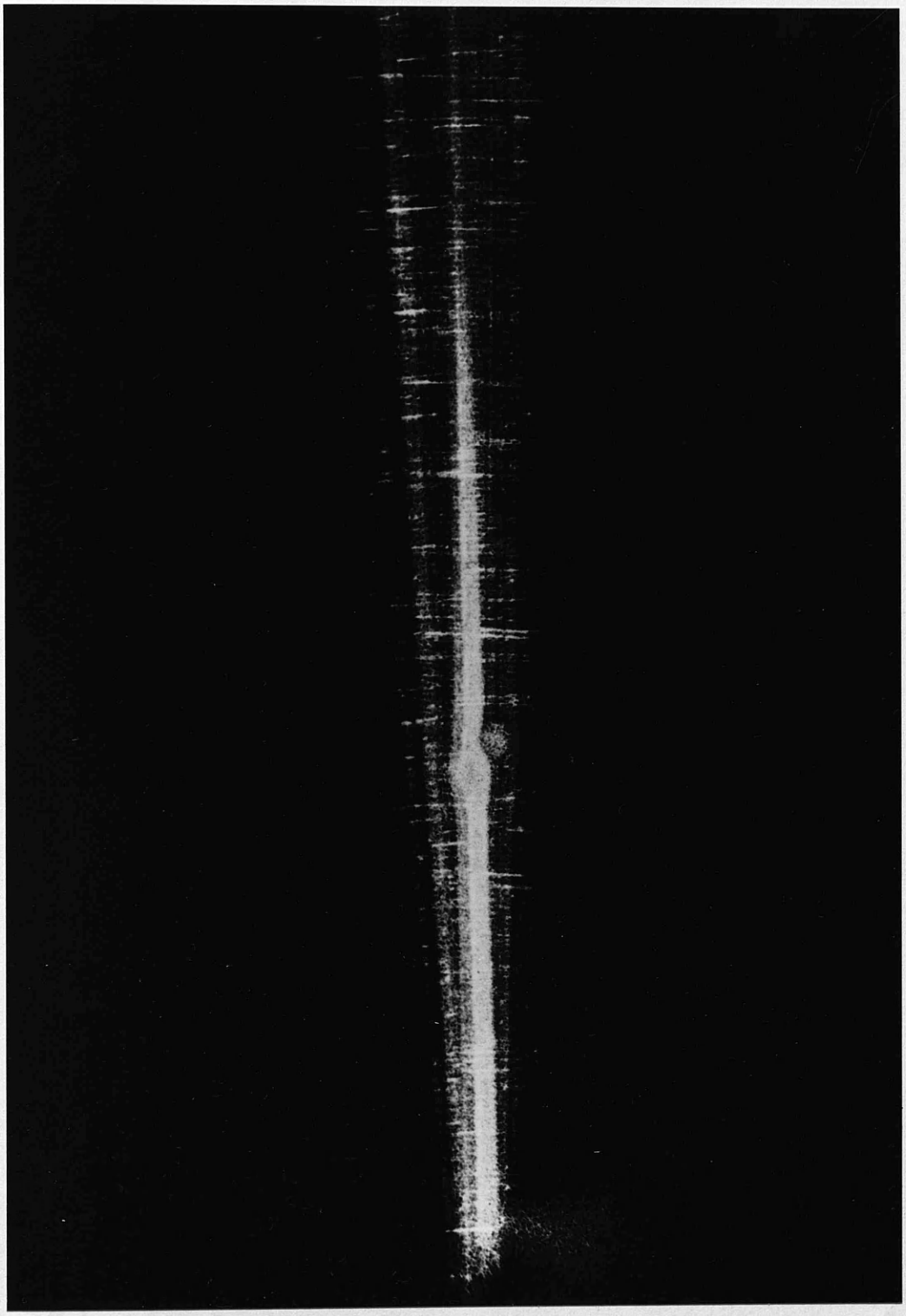

Figure 5.15 Mode sinking to a planar flip-chip.

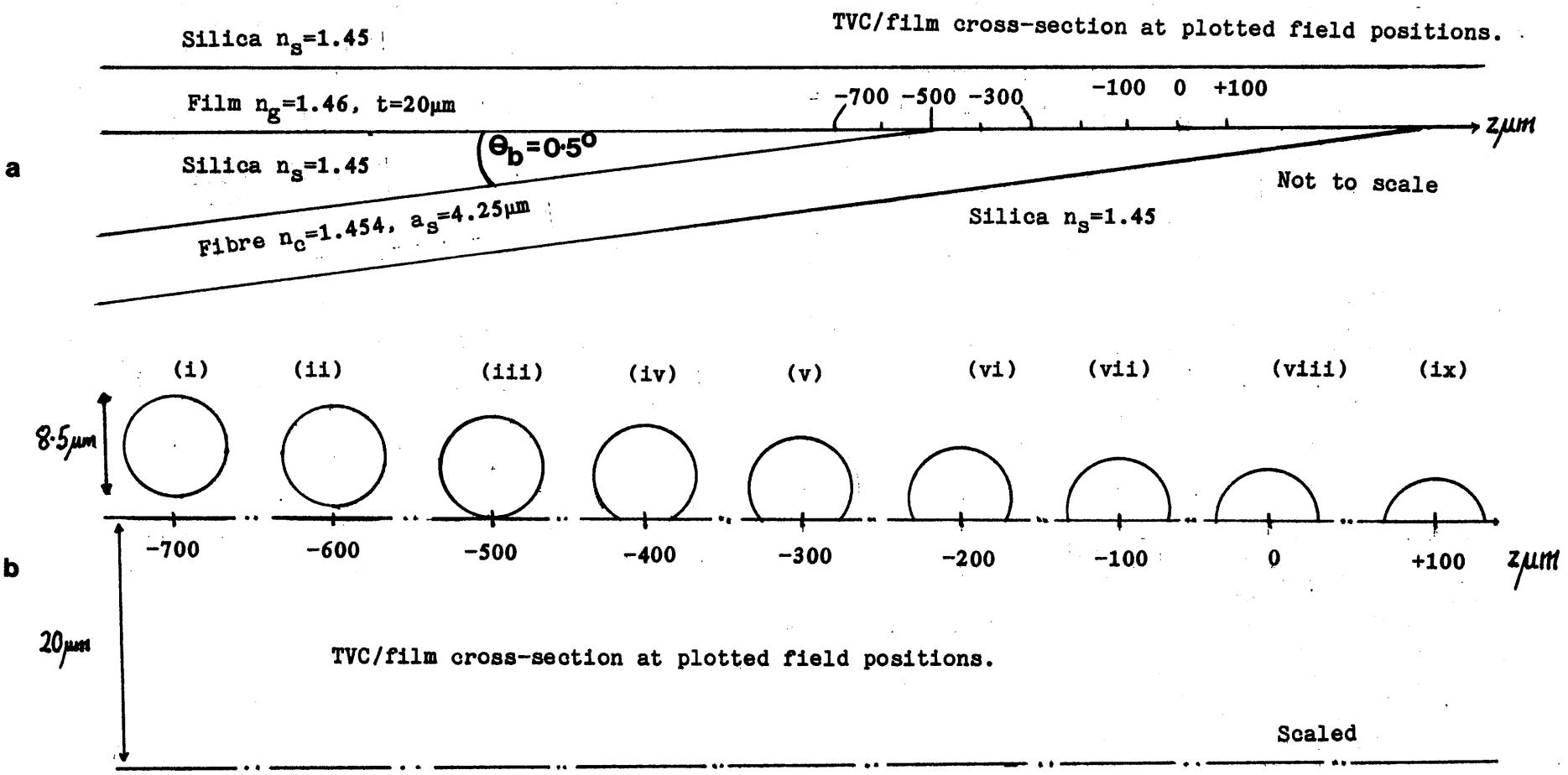

Figure 5.16 Base data for BPM program.

The coupler structure is shown in figure 5.16a. The initial field was that of the fibre LP_{01} mode, launched at -800μm. The field of the composite waveguide was calculated at 1μm intervals for 900μm thereafter. z=0 corresponds to the point at which exactly half of the fibre core remains. Plots of the field at 100μm intervals are shown in figures 5.17(i-ix). The cross-sections of the composite fibre-film guide at each of the plotted field positions are shown (to scale) in figure 5.16b. The field plots were normalised by setting the peak field in the fibre to a constant level. The film and fibre mode propagation constants are listed in table 5.2. The film thickness and index were t=20μm and n=1.46. The wavelength was 1.3μm and the fibre parameters were Δ_s=0.004, a_s=4.25μm. A low moded film was used to save computing time. The TE_5 mode was sufficiently near cut-off to be negligible.

Table 5.2 Effective indices of guide modes for BPM calculation.

Mode	Effective index.	
Film TE_0	1.4597	
Film TE_1	1.4588	
Film TE_2	1.4574	
Film TE_3	1.4555	
Film TE_4	1.4531	
Fibre LP_{01}	**1.4519**	
Film TE_5	1.4504	negligible

The mode sinking condition was satisfied by the TE_0-TE_4 film modes but leakage to the TE_4 mode was expected to be dominant.

5.4.1 Interpretation of field plots.

Figure 5.17(i) shows weak coupling from the fibre to the TE_4 mode. The amplitude of the coupled beam in the transverse y-direction decreases monotonically from a central peak as predicted by Figure 5.12c,d. The core film separation is 1.86μm. It was not possible to calculate separately the propagation of the field at this particular cross-section. However it is apparent from the field plots that a beam of finite width propagates axially as the guide cross-section changes.

Figure 5.17(ii) shows the field a further 100μm along the coupler. The guide separation is now 0.99μm and the coupling characteristics are similar to those above. There is no evidence of mode-sinking. Figure

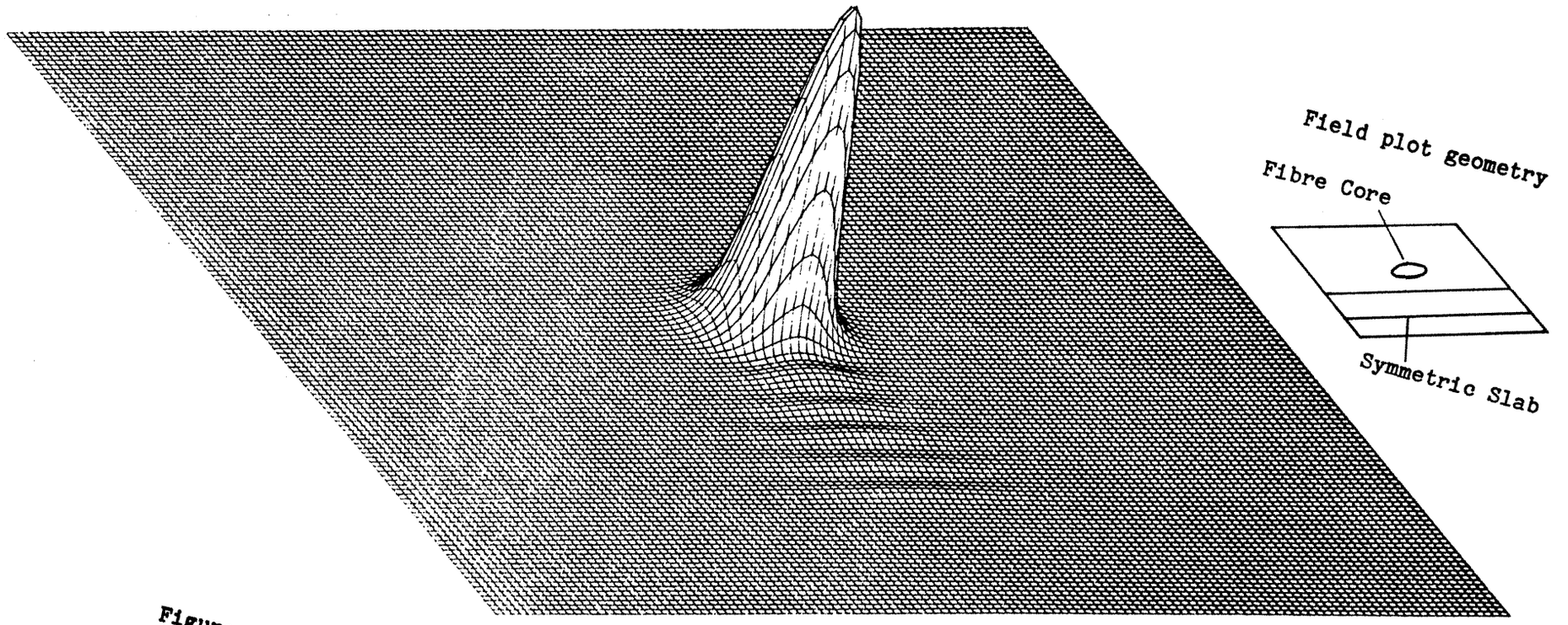

Figure 5.17.(i) Optical power distribution over TVC/film cross-section, z=-700μm, core film gap=1.86μm.

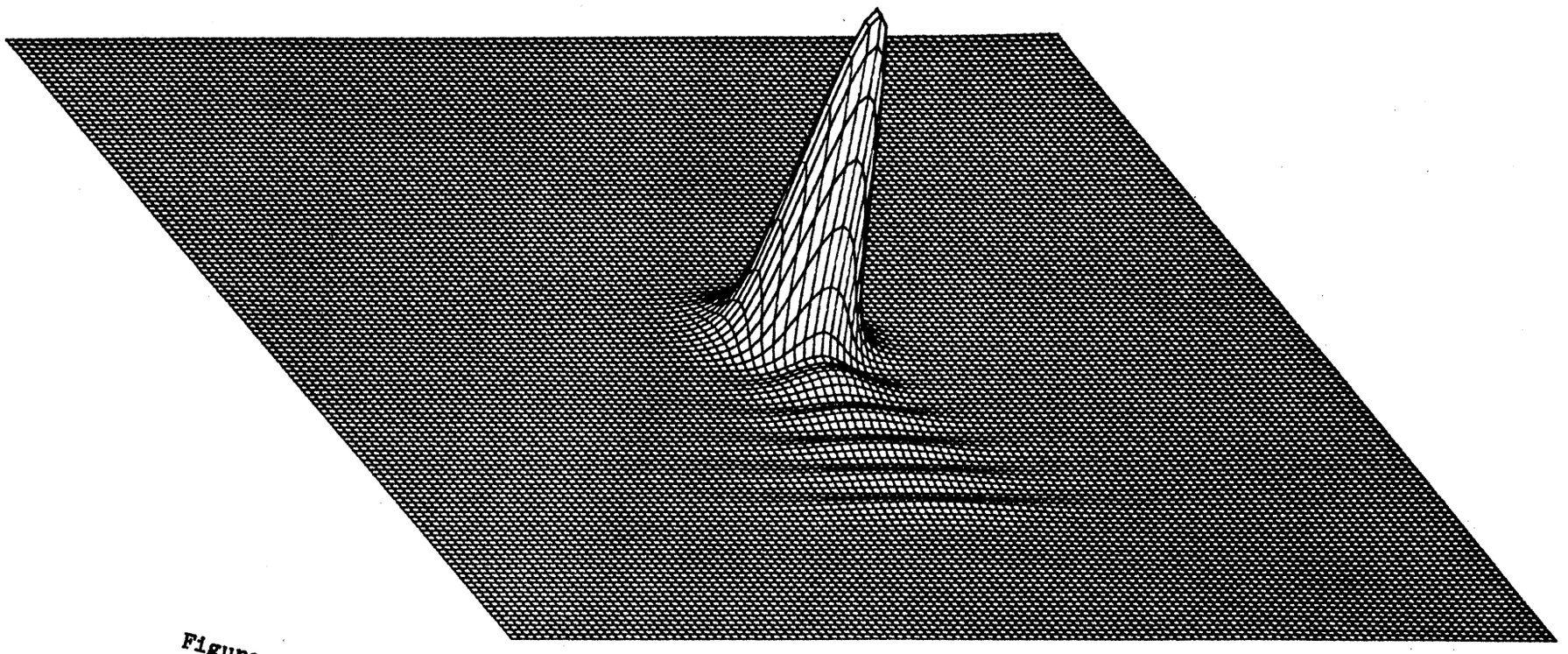

Figure 5.17.(ii) Optical power distribution over TVC/film cross-section, z=-600μm, core film gap=0.99μm.

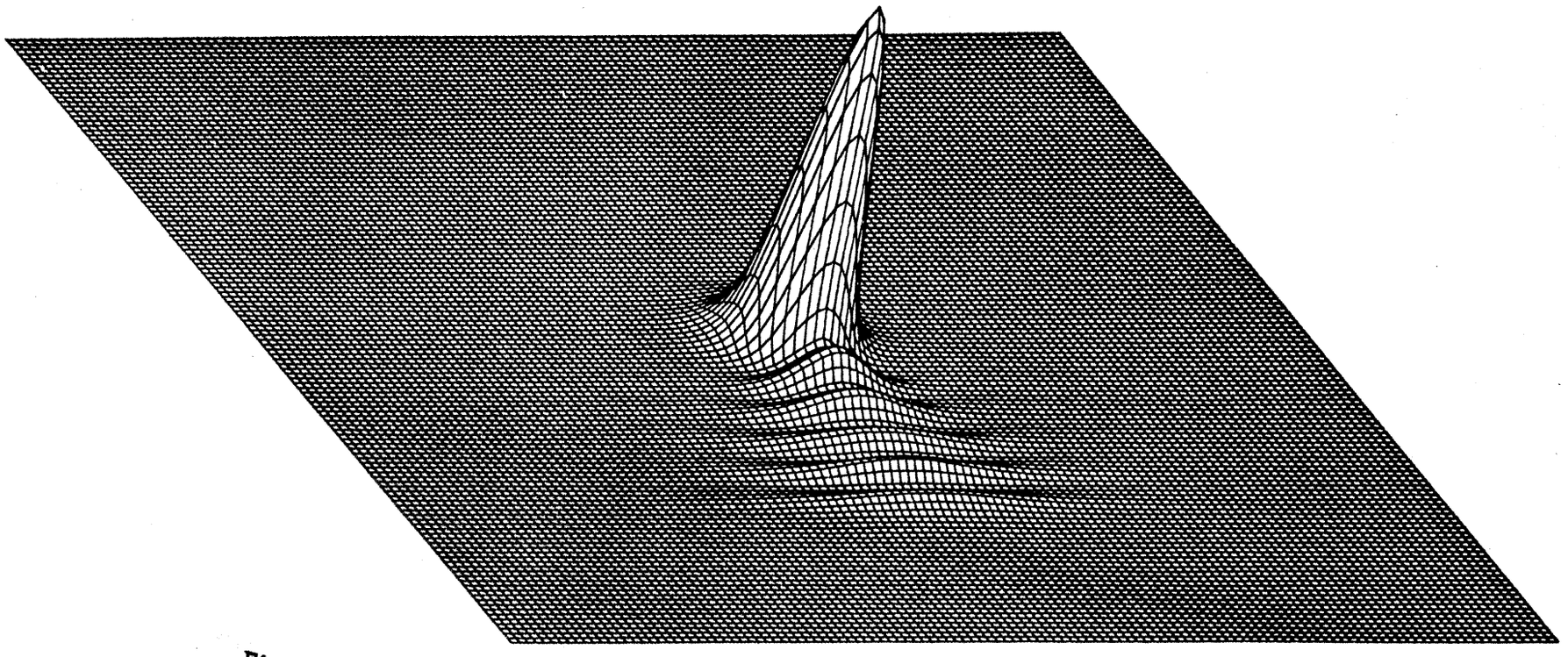

Figure 5.17.(iii) Optical power distribution over TVC/film cross-section, z=500μm, core film gap=0.11μm.

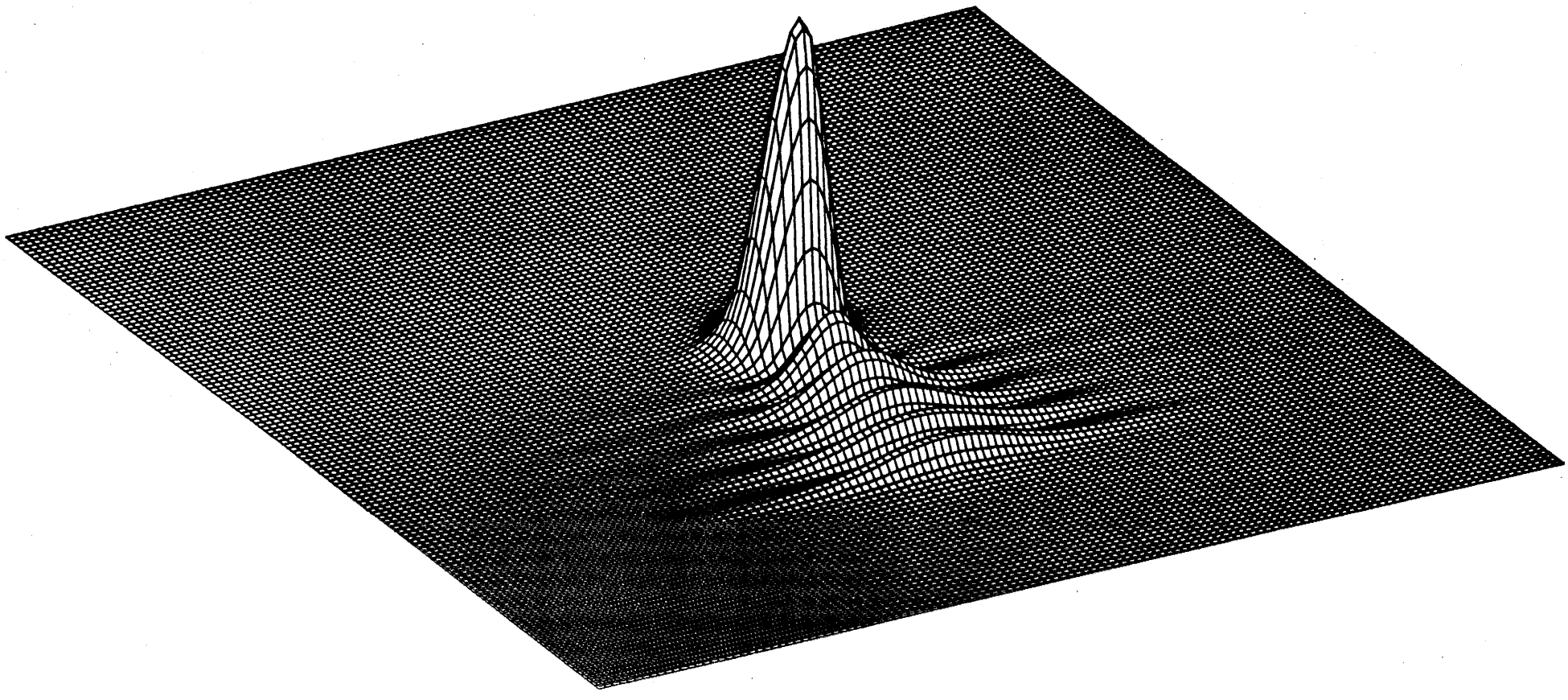

Figure 5.17.(iv) Optical power distribution over TVC/film cross-section, z=-400μm, 94% of core area remains.

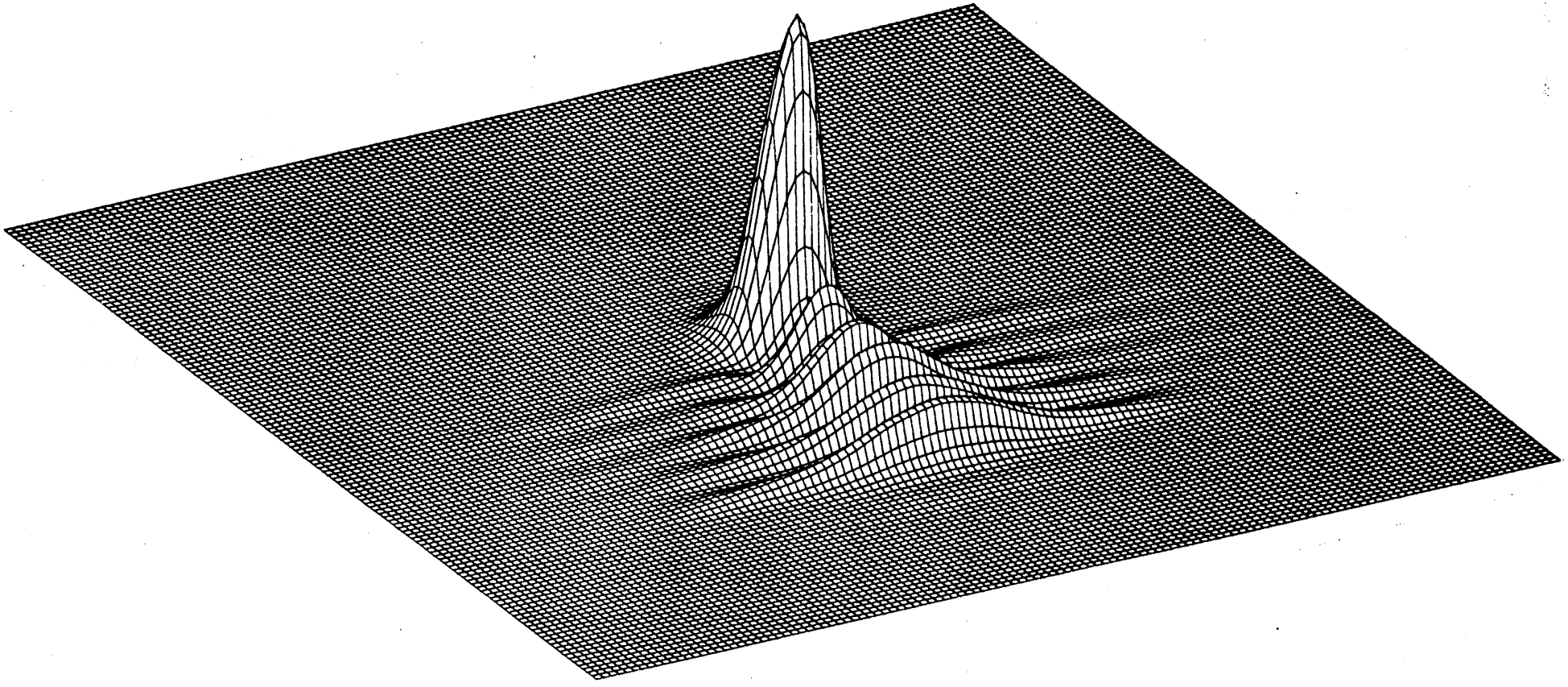

Figure 5.17.(v) Optical power distribution over TVC/film cross-section, z=-300μm, 86% of core area remains.

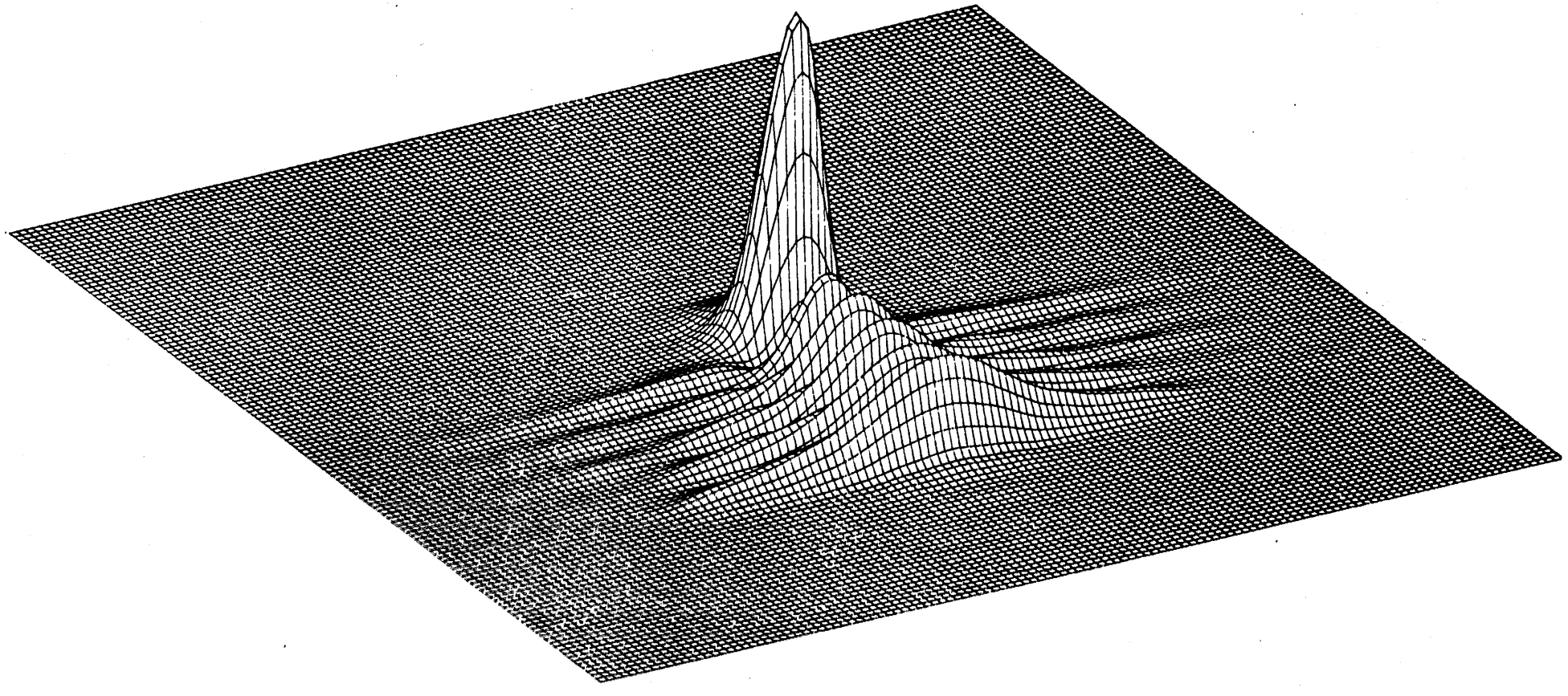

Figure 5.17.(vi) Optical power distribution over TVC/film cross-section, z=-200μm, 76% of core area remains.

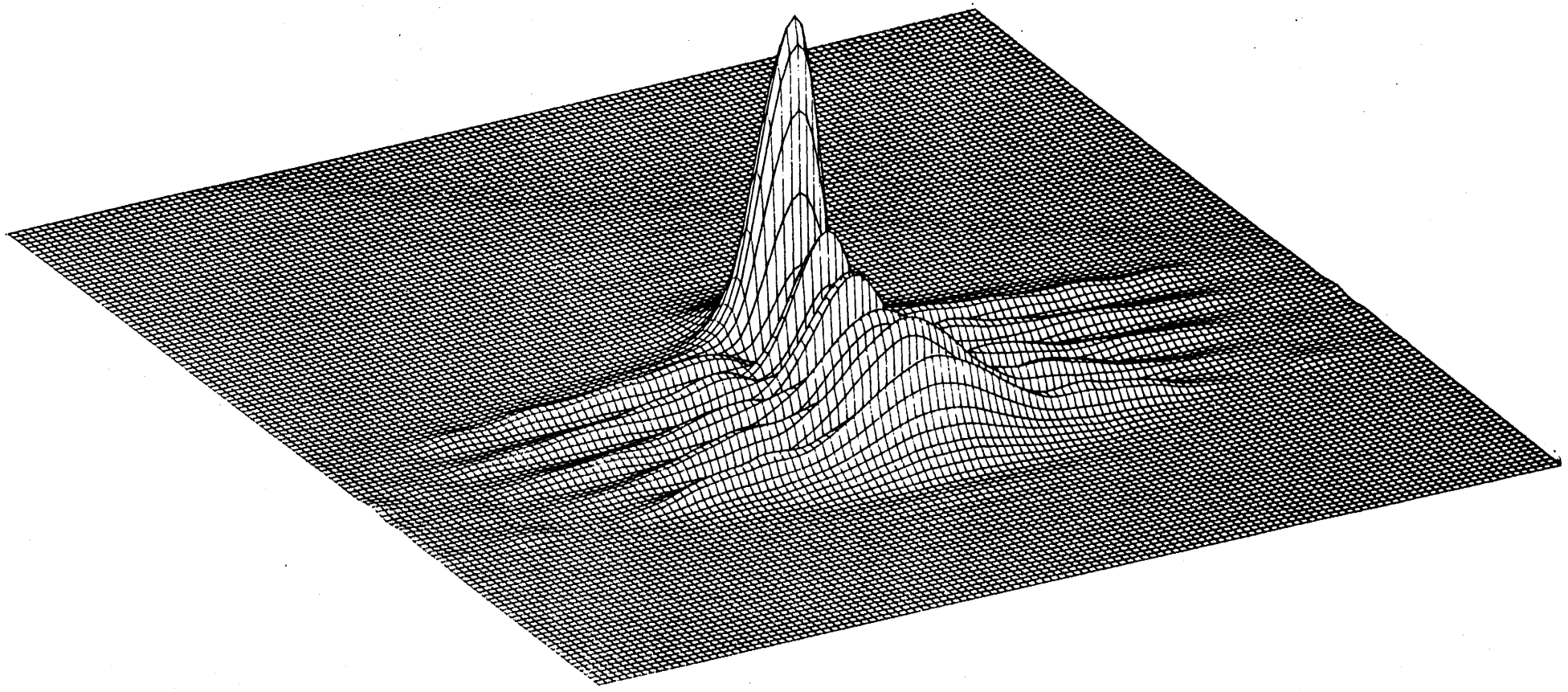

Figure 5.17.(vii) Optical power distribution over TVC/film cross-section, z=-100μm, 63% of core area remains.

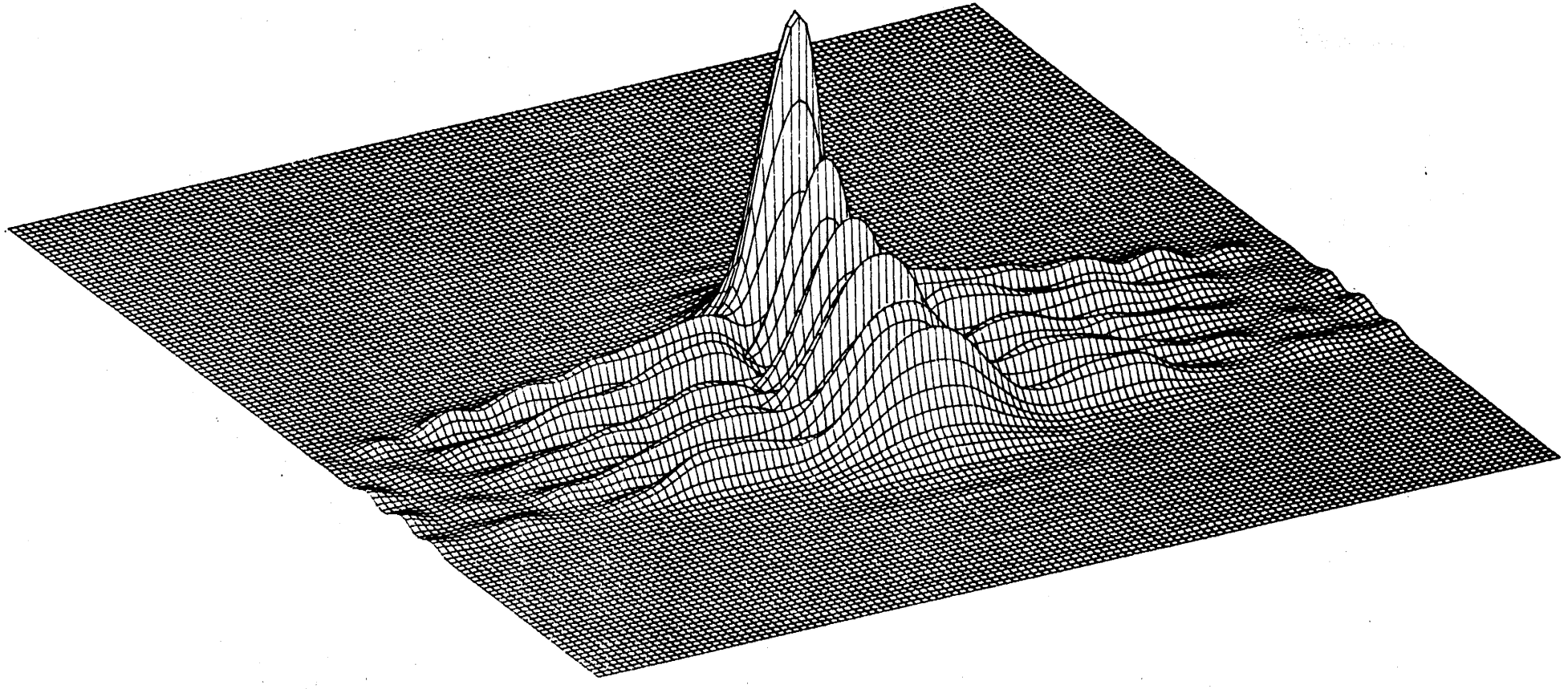

Figure 5.17.(viii) Optical power distribution over TVC/film cross-section, z=0μm, 50% of core area remains.

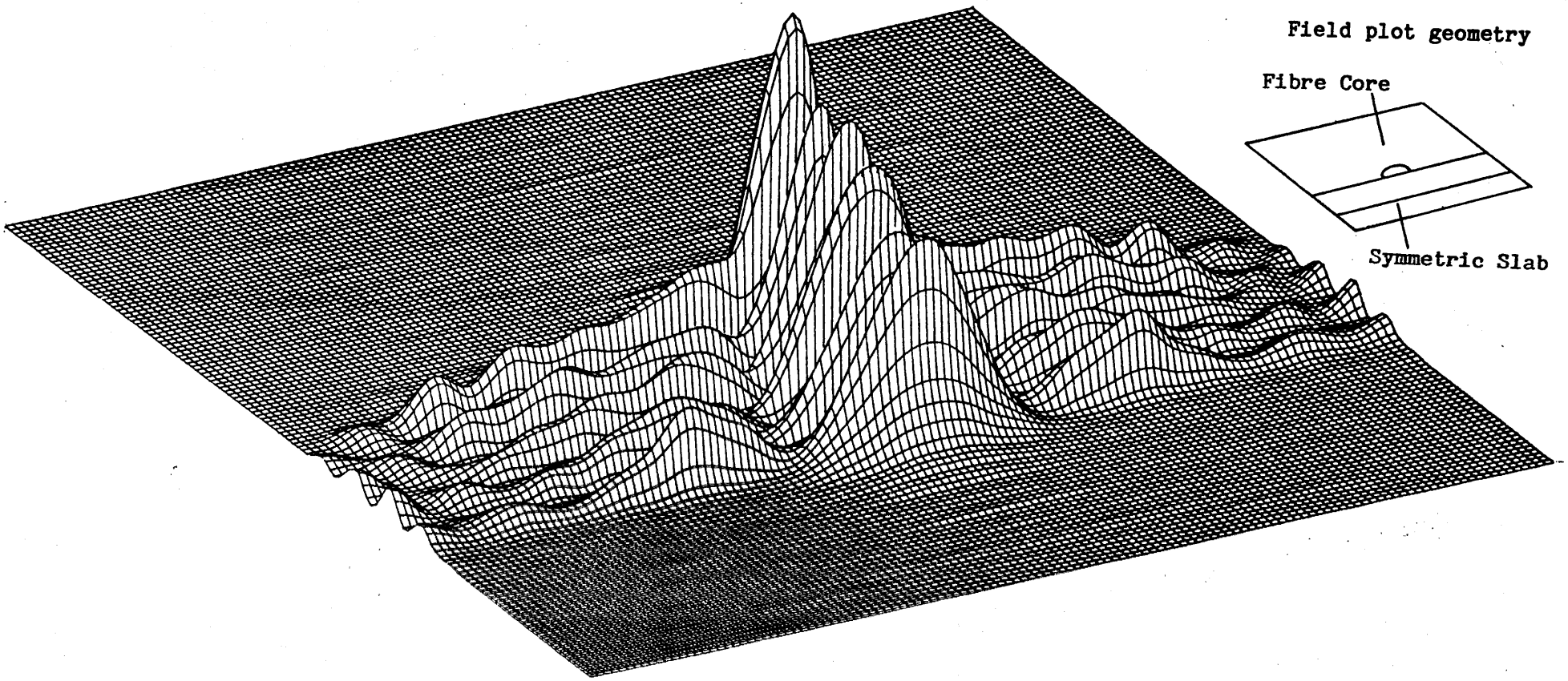

Figure 5.17.(ix) Optical power distribution over TVC/film cross-section, z=+100μm, 37% of core area remains.

5.17(iii-iv) The field amplitude in the film continues to grow and there is no evidence of off-axis propagation.

Figure 5.17(v) The power coupled to the TE_4 mode has increased but the beam in the film is no longer monotonically decreasing in the y-direction. The film mode peak nearest the fibre core has a turning point (~~arrowed~~). This is leakage due to mode sinking. Figure 5.17(vi-viii) The forward propagating beam and the two off-axis beams are now established. Figure 5.17(viii) The core region has now been halved but continues to guide a significant quantity of power. Figure 5.17(viii-ix) The complex pattern of turning points in the y-direction indicates inter-modal interference. This means that the leakage of power from the fibre core into TE_4 and TE_3 modes (at least) is now occuring. This effect would be smaller for higher order modes of a high index film since the mismatch between modes would be larger.

In order to interpret the field amplitude profiles it is preferable to consider the fibre and film, at each cross-section to be a composite rib-waveguide rather than two seperately coupled guides. The assumption of weak coupling is no longer valid in this case. The fibre core acts as a perturbation to the planar guide and provides a degree of transverse (y-axis) confinement. The modal solutions at arbitrary directions in the slab are loaded by the fibre to give a propagating field in the z-direction. Similarly the planar guide perturbs the fibre since it is a mode-sink. This gives rise to two separate and diverging beams in the film as power is coupled from the fibre.

The field initially launched in the isolated fibre is a guided mode solution at that cross-section. As the core film separation decreases the guides become coupled and the fibre mode field is no longer a guided mode solution at the new cross-section. Now the coupler cross-section changes slowly and smoothly. Therefore the overlap [11] between the transverse mode fields at any two, closely spaced cross-sections is very nearly unity. Thus power is efficiently transferred from the mode field at one cross-section to the new mode field at a later cross section. The axially propagating mode Figure 5.17(i-ix) is the solution of the angularly degenerate slab fields, transversely loaded by the fibre. The off-axis mode-sinking can be thought of similarly as the solution of the fibre mode loaded by the mode sink. i.e. there are two solutions present for each wavelength.

As the remaining core area falls, the degree of transverse confinement the fibre provides also falls and the field solutions have a larger transverse extent. Ultimately the core area is zero and the

field solutions have an infinite extent, i.e. the beam diverges. If a beam of identical amplitude distribution but with a convergence equal to the divergence of the original was launched in the film it would couple totally into the fibre. However the output fibre in the face to face TVC arrangement of figure 5.4 sees a divergent field which cannot therefore couple totally to the fibre. This is a fundamental source of loss in the oil film experiments described and partly explains the coupler insertion losses measured.

At any particular wavelength the two sets of solutions could be plotted, for each cross section, forming two "branches". The change in coupling characteristic with wavelength is the result of changes in power distribution between the solution branches. At a synchronous wavelength, more power would initially couple into a rib mode of the composite guide. Conversely, at a phase mismatched wavelength less power would be initially coupled into mode sinking beams.

These results show that mode sinking occurs to beams of finite width, composed of plane waves propagating at angles $\pm\theta$ to the beam axis. In this respect they extend the mode sinking analyses of Arnaud and Marcatili who considered coupling to only one plane wave.

5.5 Summary

The wavelength dependence of transverse coupling between a single mode fibre and a multimode planar waveguide has been investigated using the TVC. Initial investigations indicated that the coupling behaviour was similar to that of guides having equal confinement (figure 5.2,5.6) but this was later shown to be a special case (figure 5.14). A theoretical explanation based on the early analyses of Arnaud and Marcatili was developed. This gave a qualitative rather than quantitative description of the coupling process and was limited by the 'weak-coupling' assumption in what was essentially a 'strong coupling' problem. The essence of the weak-coupling theory was that mode-sinking and on-axis coupling occurred at different wavelengths according to the mismatch in the longitudinal propagation constants (figure 5.1). A BPM analysis of the coupling process showed that in the case of strong coupling, both elements, mode-sinking and on-axis coupling were present at a single wavelength. Two solutions were indicated for each wavelength; a perturbation of the fibre mode by the film and similarly a perturbation of the film modes by the fibre.

Prism coupling from the TVC, described in chapter 4, had indicated that coupling occured both in the tapered core region and in the region of thin cladding preceding it. This was confirmed by the BPM analysis which also showed that the majority of power transfer took place in the taper region. This is an important observation since the tolerances for taper coupling are less stringent than for simple directional coupling.

A jig was constructed which allowed continuously tunable film thicknesses, for a range of refractive indices to be used in coupling experiments. Using this jig, fibre-film -fibre coupling was demonstrated with an insertion loss of 2dB.

References, Chapter 5.

1. Bradley L.,Millar C.A.,"A new method of fibre-film coupling" IOOC Conference on Lasers and Electro-optics (CLEO-86), Paper MF-5.

2. Arnaud J.,"Transverse coupling in integrated optics part II, coupling to mode-sinks," BSTJ, Vol.53, No.4, April(1974), pp675-6

3. Marcatili E.A.J.,"Slab Coupled Waveguides," BSTJ, Vol.53, No.4, April (1974), pp645-674.

4. Wood D.L.,Fleming J.W.,"Computerised Refractive Index Measurements for Bulk Materials at UV, Visible and IR Wavelengths," Rev. SciInstrum. Vol.53, No.1, Jan (1982), pp43-47.

5. R.P.Cargille Laboratories Inc. 55 Commerce Rd., Cedar Grove, N.J.07009 U.S.A.

6. Digonnet M.J.,Shaw H.J.,"Analysis of a Tunable Single Mode Optical Fibre Coupler," J.Quant.Electron., Vol.QE-18,No.4, April(1982) pp746-754.

7. Module MD102, Manufactured by Martock Design Ltd., Water St., Martock, Somerset, TA12 6JN.

8. Whalen M.S.,Walker K.L.,"In-line Optical Fibre Filter for Wavelength Multiplexing," Electron.Letts. 15th Aug(1985) Vol.21, No.17, pp724-725

9. Haus H.A."Waves and Fields in Optoelectronics," Chapter 4. Prentice HallInc. New Jersey.

10. Ainslie B.J. Private Communication.

11. Louisell W.H.,'Analysis of the single tapered mode coupler,' B.S.T.J. Vol.34, No.6, (1955) pp853-866.

Chapter 6 Coupling from the TVC to Rib Waveguides

6.1 Introduction

In chapter 5, it was shown that light could be efficiently coupled between the TVC and individual modes of a multimode planar waveguide. In this chapter coupling to polymer and flip chip waveguides is described, with details of the guide fabrication. The range of waveguide fabrication techniques suitable for use with the TVC was limited as explained in chapter 4.

Passive polymer waveguides were developed as early as 1970[1] and doped polymer guides exhibiting lasing were reported in 1972[2]. Since then their use has become widespread particularly in non-linear optics[3]. Channel waveguides have been made by doping the polymer matrix with photochromic compounds[4]. Although they do not in general have the high environmental resistance of glass waveguides they are useful in device development since they are relatively simple to fabricate. The polymer guides used in these experiments were undoped and were made using a dip-coating technique.

6.2 Dip-coating

The dip-coating technique[5] for fabricating thin films is relatively simple and inexpensive. For polymers it does not require greatly elevated temperatures although these are required for solution deposition of silicate glasses[6]. The dip-coating apparatus is shown in figure 6.1. The basis of the technique was that a sample was withdrawn at a steady speed from a bath of polymer solution. The solvent was volatile and as the sample emerged from the bath it evaporated leaving a polymer film, coating the sample. The sample was then placed in an oven to drive out residual solvent leaving a hard transparent film. High draw-speed stability was obtained by the use of reduction gears between the d.c. motor and travel screw. The polarity of the motor driving voltage was changed by the lower microswitch and the supply switched off by the upper microswitch. The speed range of the sample holder was 0.1-0.64cms^{-1}, obtained by varying the motor driving voltage. The solution was kept in a temperature controlled water bath at 23.5^{o}C. The solvent tray, shown in figure 6.1, contained the same solvent as the bath and provided a solvent rich atmosphere around the sample as it was withdrawn. This reduced the initial rate of

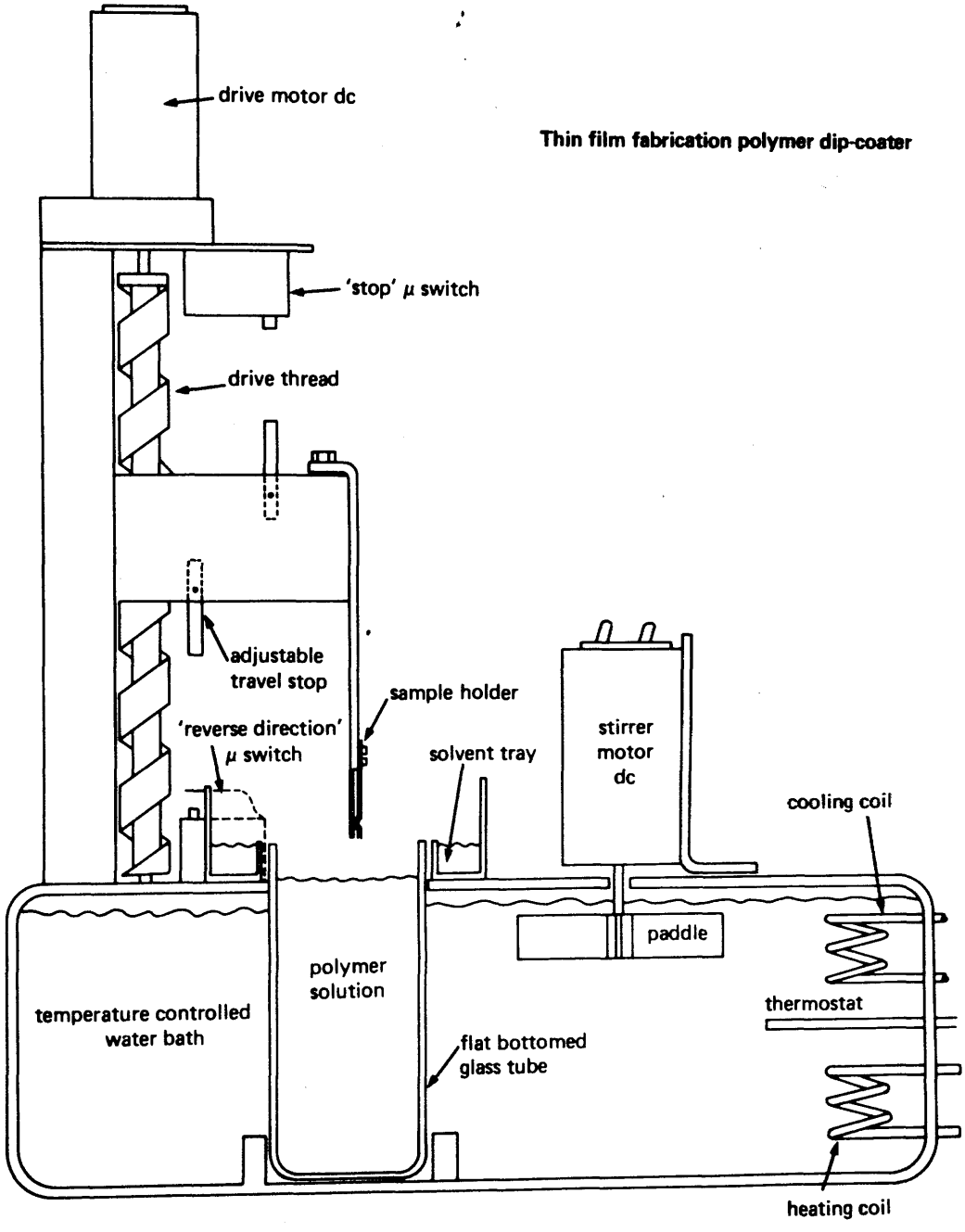
drive motor dc
Thin film fabrication polymer dip-coater
'stop' μ switch
drive thread
adjustable
travel stop
'reverse direction'
μ switch
sample holder
solvent tray
stirrer
motor
dc
cooling coil
paddle
polymer
solution
temperature controlled
water bath
flat bottomed
glass tube
thermostat
heating coil

Figure 6.1

evaporation allowing the films to stabilise. Without the tray a skin formed on the films which had poor surface quality. The solvent 'dichloromethane' - CH_2Cl_2 was used throughout these experiments for polymer films and the proprietary solvent, Cellosolve, was used for photoresist films.

6.2.1 Solution preparation and thickness calibration

Polymer solutions were prepared as follows; A 200ml bottle was cleaned in soap and water then rinsed in deionised water. It was then rinsed in CH_2Cl_2 and dried. The desired mass of polymer was accurately weighed and added to the bottle. 100ml of CH_2Cl_2 was then measured and added to the bottle, together with a magnetic stirrer which had been similarly cleaned. The solution was then stirred at room temperature overnight. The solutions were found to have excellent clarity and were free of bubbles. The percentage weight of polymer in solution was calculated using equation 6.1. Since the density of CH_2Cl_2 is $1.326kgl^{-1}$ the mass of 100ml was 132.6g. The mass of polymer, x grammes, for an n% w/w solution was given by;

$$x/(x + 132.6) = n/100 \qquad 6.1$$

For a given solution concentration (or given viscosity) the speed range of the driving motor corresponded to a fixed film thickness range (at constant temperature). By dip-coating a series of microscope slides at different draw speeds it was possible to calibrate the dip-coater for that particular solution. Film thicknesses were measured by Talystep. A typical calibration plot is shown for 6% w/w solution of Poly Methyl Meth Acrylate (PMMA) in figure 6.2. After dip-coating the slides were dried at 130°C for 6 hours then allowed to cool before being measured. The slide cleaning procedure was relatively standard[7];

Scrub in soapy water
Rinse in de-ionised water.
Ultrasonic for 10mins in Acetone
Ultrasonic for 10mins in isopropyl alcohol(IPA)
Rinse, blow dry, leave on hotplate for 20 minutes

The same procedure was employed in cleaning the TVC blocks prior to coating. The films were pinhole free and very uniform. The

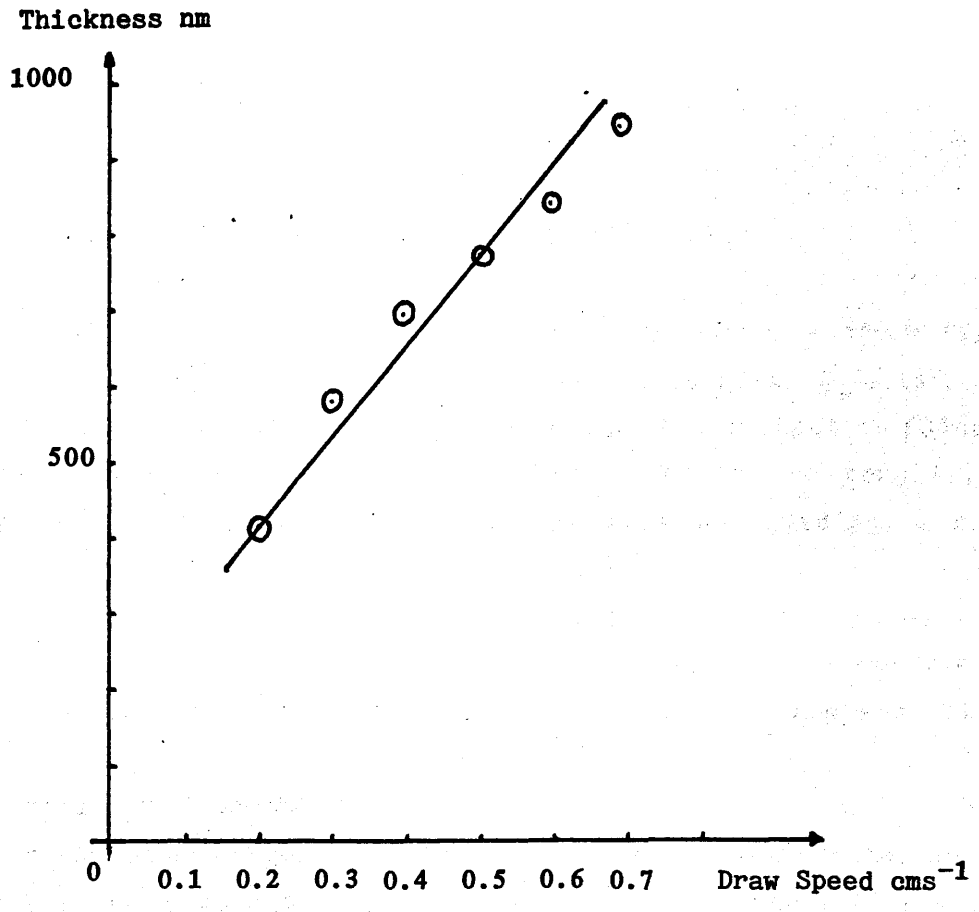

Figure 6.2 Calibration curve for dip coating a 6% w/w solution of PMMA in CH_2Cl_2. Draw speed was calculated from the motor driving voltage and thicknesses were obtained from talystep measurements.

calibration procedure was repeated as required for different solutions allowing a desired thickness to be obtained.

6.2.2 Single mode PMMA film deposited on TVC

Using the dip coating apparatus described above, a 580nm film of PMMA (N_D = 1.490) was deposited on a TVC block with θ_b=1.25°. The film supported the TE_0 and TM_0 modes only. Laser light at 633nm was launched into the fibre pigtail of the TVC but no coupling was observed. In order to verify that the film was guiding, a narrow beam (focused using a long focal length lens, f = 1m) was prism-coupled into the film. The laser was aligned to launch the TE mode. By manipulating the micropositioning stack to which the prism/TVC were attached the direction of the coupled beam in the film was altered. The results are shown in figure 6.3 (a-e).

Figure 6.3a shows the TVC in the prism clamp, mounted on the micropositioning stage. The rear face of the TVC was painted black to increase the contrast during observation. Figures 6.3c,e show an attempt to couple from a launched film mode into the fibre. The launched beam was unable to continue propagation in the epoxy region between the groove end and the fibre core. Two beams can be clearly seen making small angles with the V-groove. Figures 6.3 b,d show the result of coupling a beam such that it propagated across the fibre cladding ellipse in the region where the epoxy substrate extended over the shortest distance. The beam was observed to be partially transmitted and partially reflected. This experiment showed that the epoxy was incompatible with the silica fibre and silica block as an optical substrate material.

There were two possible reasons why fibre-film coupling was not observed. Firstly the imaginary part of the epoxy index (i.e. the loss) may have been sufficiently high that all the power coupled into the film was absorbed. Secondly the real part of the epoxy index may have been significantly higher than that of silica such that the PMMA-epoxy combination did not constitute a waveguide. Optically thicker films were used in further experiments to minimise the field strength at the film-epoxy interface.

From figure 5.17 it was clear that where a substantial fibre-core area remained (i.e. z < 0μm) in the TVC, the guided power was concentrated in its vicinity. The same was expected of an overlaid rib

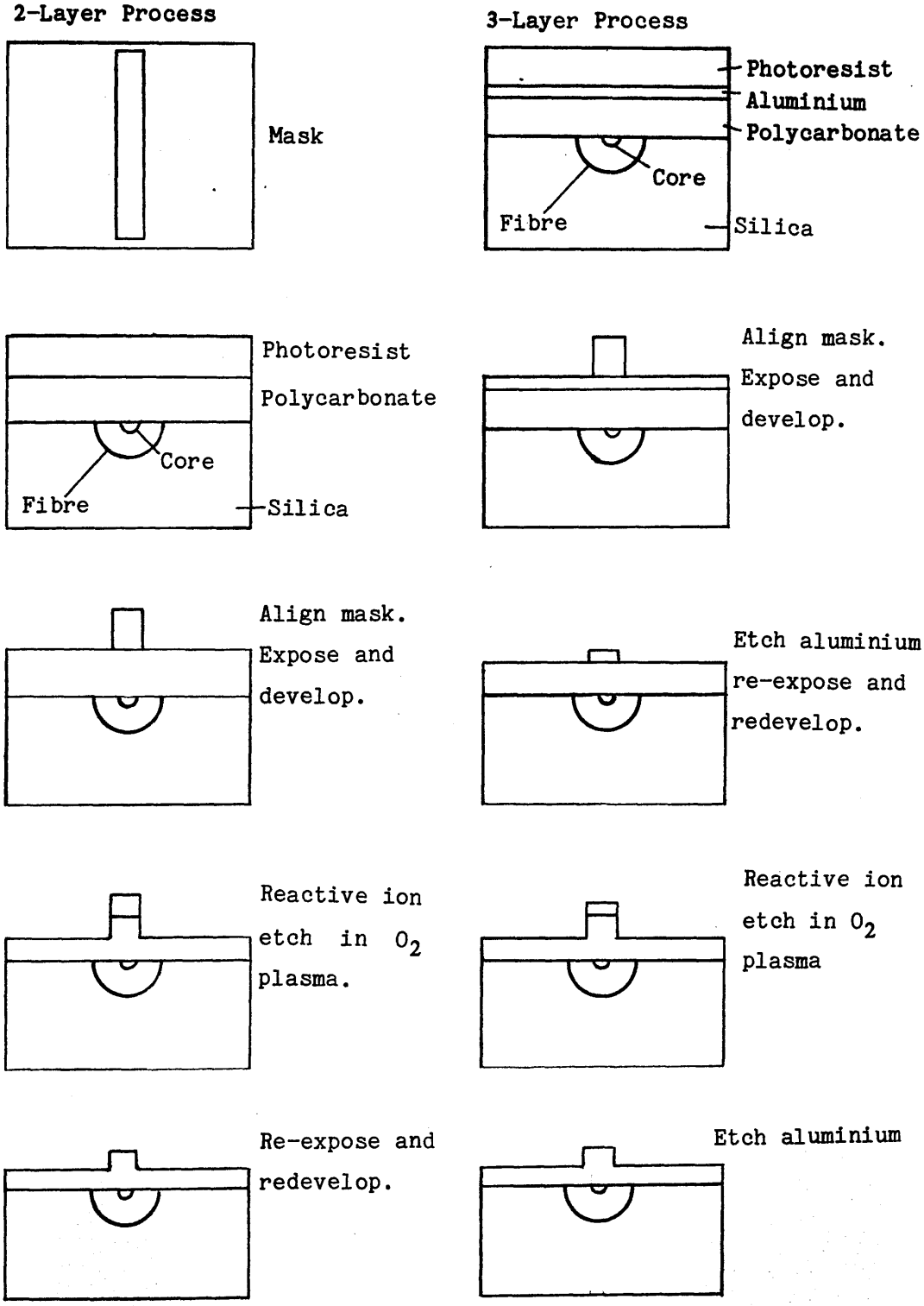

Figure 6.4 Two and three layer processes for formation of a rib waveguide on a polished fibre block. The mask is common to both processes.

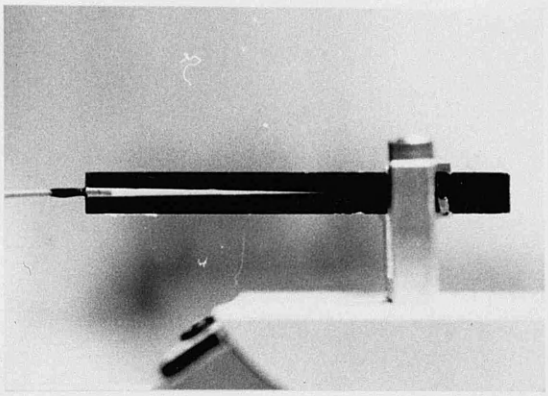

(a)

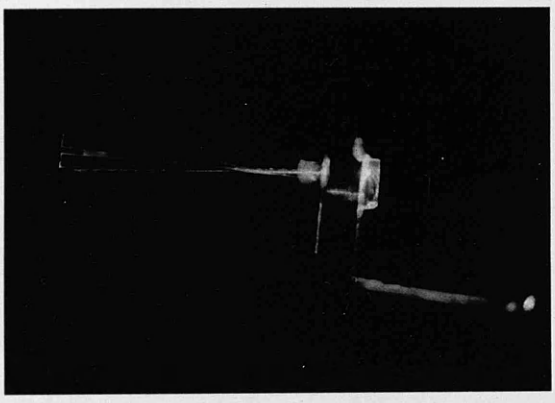

(b)

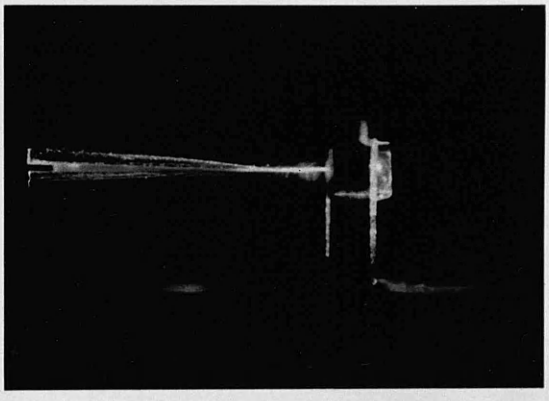

(c)

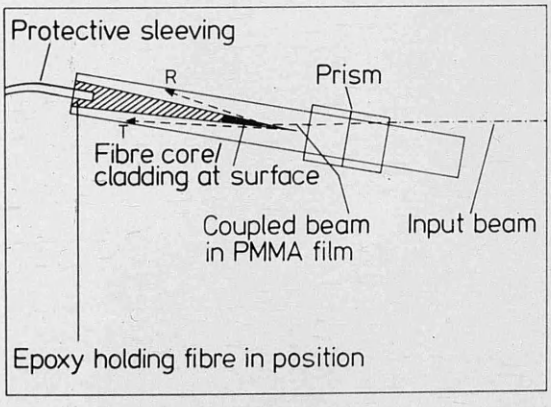

(d)

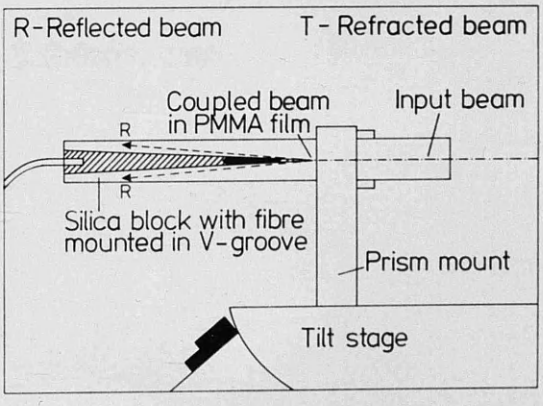

(e)

Figure 6.3

The effect of a high index epoxy substrate region on light guided in a PMMA film with Silica as a substrate, showing reflection and refraction.

guide coupled to the fibre i.e. power would initially be concentrated near the fibre-film interface. As the core area was decreased the guided mode shape would alter and power would become concentrated in the rib region of the rib guide. It would then have only weak field strength at the film-epoxy interface.

6.2.3 Fabrication of rib waveguides.

Two methods of rib fabrication were considered and these are shown in figure 6.4. In the two layer process a film of Polycarbonate (PYC) N_D = 1.5850, was dip-coated onto a TVC block (of the geometry shown in figure 5.3). It was then baked at 130°C for 6 hours to remove residual solvent before a layer of photoresist (Shipley AZ1350J) in Cellosolve thinner was overlaid by dip coating. Within a few seconds the surface became blistered and after drying the film was completely blistered. The polycarbonate film was clearly soluble in the photoresist thinner. This and similar 2-layer processes were therefore inapplicable to the polymers used although this procedure is standard in dip-coating anti-reflection coatings of glass layers from solution[8]. The 3-layer process, figure 6.4b, was devised with an aluminium film used to separate the two dip-coated films. The aluminium film was applied by vacuum evaporation and had good adhesion to the polycarbonate. The three layer film was formed on the TVC block, after cleaning, as follows;

1. Dip coat 3.9μm film of PYC, bake at 130°C for 6 hours.
2. Place sample in evaporator and rough out, to outgass sample.
3. Pump to full vacuum and perform evaporation. Aluminium thickness 40-150nm.
4. Dip coat 1.8μm film of photoresist, bake at 86°C for 30 min.

The film quality was a marked improvement on that of the 2-layer process but a few randomly spaced blisters were still present. These were traced to pinholes in the aluminium film. The pinholes were small (<0.5 μm diameter) and were found to be caused by dust. The filtration in the clean room cabinets used was designed to collect particles of > 0.3 μm diameter. No large dust particles (> 0.5μm) were observed on samples cleaned with particular care but it was found impossible to eliminate the small particles completely. Their effect which was out of proportion to their size is evident from figure 6.5 which shows a

blister extending to over 40μm in diameter. It was not possible to evaporate a 0.5μm film of aluminium nor was it possible, within the timescale of the project to establish an alternative polymer-solvent-resist combination. This would have been of lower priority than establishing an alternative to the epoxy used, which would have introduced alternative film fabrication options.

6.2.4 Alignment of polymer rib waveguide

The surface texture of the polished epoxy and polished fibre ellipse were markedly different. Very uniform films were obtained by dip coating and it was found that these films followed the surface contours i.e. they did not fill indentations leaving a flat surface. The aluminium films, similarly followed the surface contours and the cladding ellipse could be readily identified under an optical microscope, figure 6.6. Using the microscope on a Nikon mask aligner, the rib mask was positioned such that the line coincided with the ellipse ends of both the input and output fibres. The rib was (in theory) then aligned with the fibre core ellipses. However the mask aligner was designed to accept 3" dia. wafers and the TVC samples were 11cm long with 1m pigtails at each end. It was therefore necessary to make some minor modifications to the mask aligner. The pigtails affected the self levelling stage incorporated in the mask aligner, reducing its accuracy. The mask and substrate surfaces were not therefore parallel and movement along one axis resulted in small movements on other axes. In practice it was found difficult to align a 40μm wide rib in the centre of the 125μm wide cladding. In order to align single mode (typically 2-6μm) ribs it would be necessary to extensively modify a mask aligner which would then be dedicated. This would be technically feasible.

After alignment and resist exposure (20 sec. exposure using integral UV lamp) the resist was developed (1:1 Shipley developer and deionised water for 1 min.) and then the unprotected aluminium was etched. The TVC was then re-exposed and developed, without a mask, removing the remaining photoresist. Normally the photoresist is removed during photolithography by immersing in acetone but it was found that this also removed the polymer layer. The samples were then rinsed and blow dried.

The samples were next etched, by reactive ion etching[9,10], in oxygen. In this technique a directional etch is obtained by

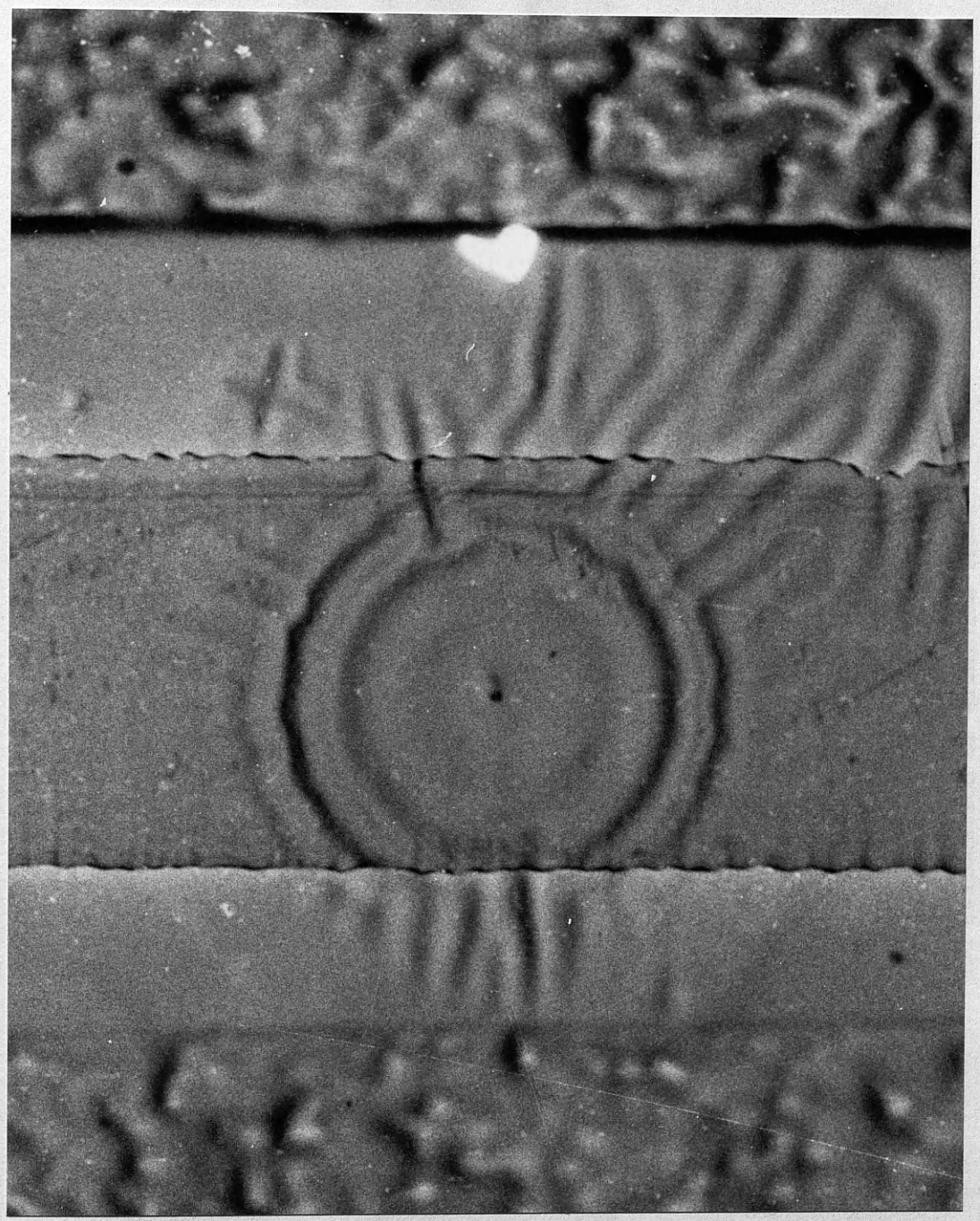

Figure 6.5 Effect of sub 0.3μm pinhole on rib waveguide. Blistering of the rib region is evident and the pinhole can be clearly seen at the centre of the blister. The rib width is 40μm.

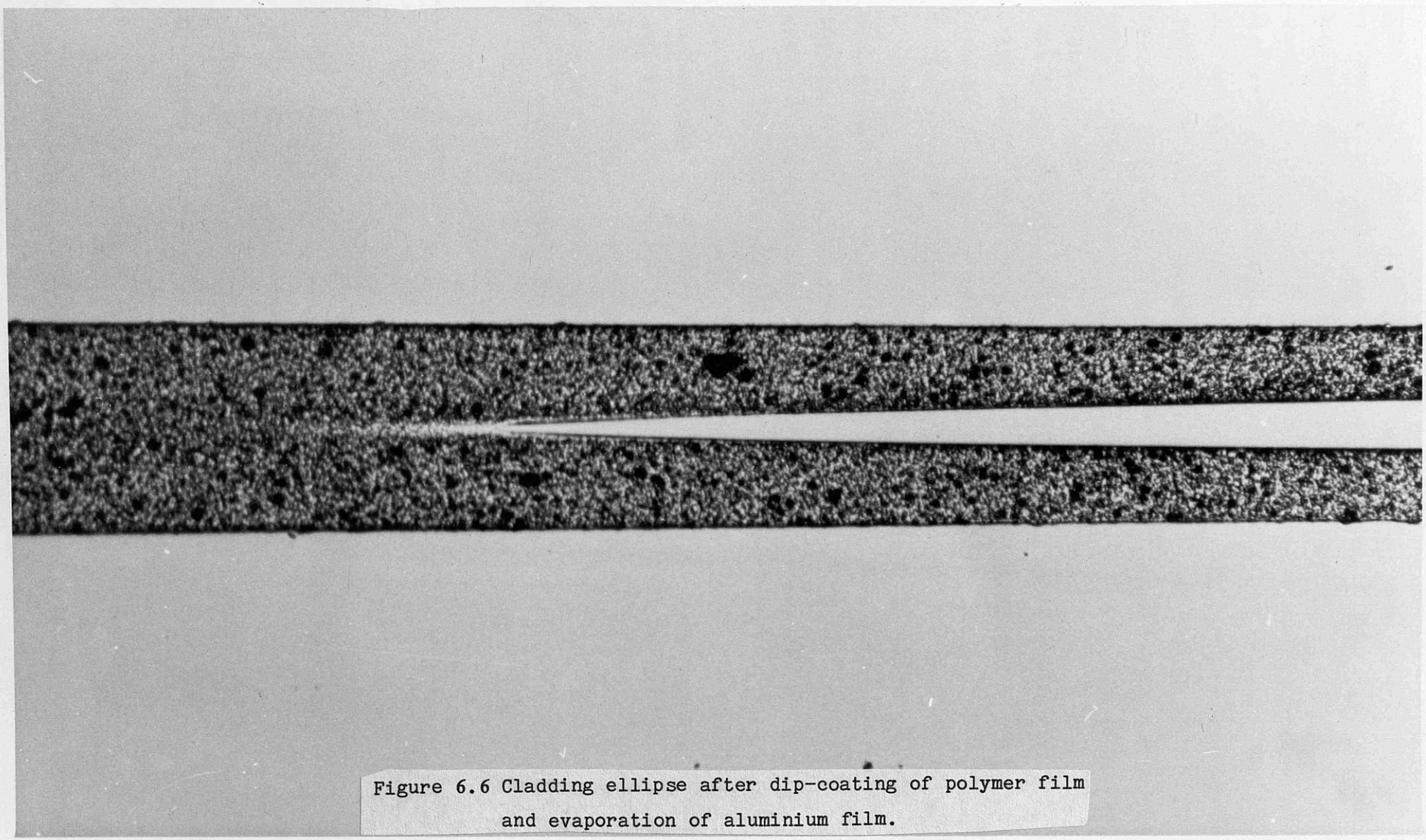

Figure 6.6 Cladding ellipse after dip-coating of polymer film and evaporation of aluminium film.

accelerating charged particles towards a target substrate, in a moderate vacuum where they react chemically and/or physically to etch the target materials. In RIE, a high percentage of reactions are chemical, the end products are gaseous and are pumped out of the vacuum chamber[11]. Related systems have a high percentage of physical reactions and are referred to as sputtering systems[12]. The reaction products of such systems are often redeposited before they can be pumped from the reaction chamber[13]. RIE was more suitable for giving a clean etch profile, with vertical walls and was used in preference to sputter etching.

The charged particles are maintained in a glow discharge or plasma, using an RF signal. The discharge is confined by a self generated d.c. electric field to a region above the target. The d.c. field also accelerates ions from the plasma towards the target. This bias potential can be controlled to vary the etch rate. The etch rate also depends on the flow rate of gas in the chamber since the reactive species become less populous as the flow rate falls[14]. Flow rate is measured in standard cubic centimetres per minute ($sccm^{-1}$). A third factor affecting etch rate is the RF power coupled to and generating the plasma. Many of the electrons have a high energy, corresponding to temperatures of 10^4 to 10^5K but the plasma is normally only a few degrees above ambient. It is therefore a suitable technique for etching a wide range of films, provided that a suitable gas mixture giving gaseous reaction products can be found. Oxygen is particularly suitable for etching polymers. The etch parameters in this instance were;

Initial pressure	1.5×10^{-4} mbar
Flow rate O_2	20 $sccm^{-1}$
Plate Voltage	500V
RF power coupled to plasma	20W
Etch time	10 min.

This etch time at these parameter values gave an etch depth of 1 μm, measured by Talystep.

6.2.5 Coupling to polymer rib waveguides

After fabrication the samples were examined under an optical microscope to assess the film and line quality. Laser light at 633nm

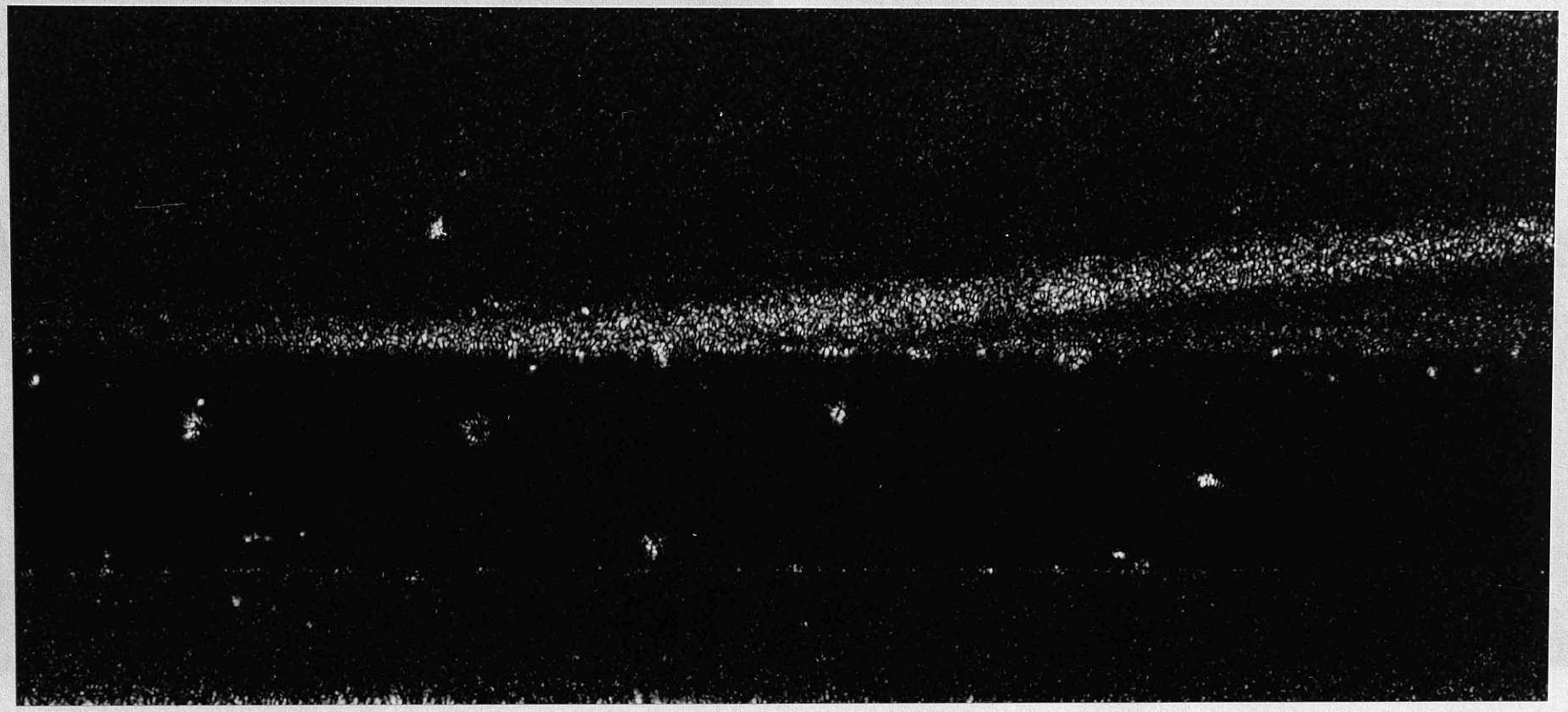

Figure 6.7 Mode-sinking from a rib-guide, caused by a defect in the rib.

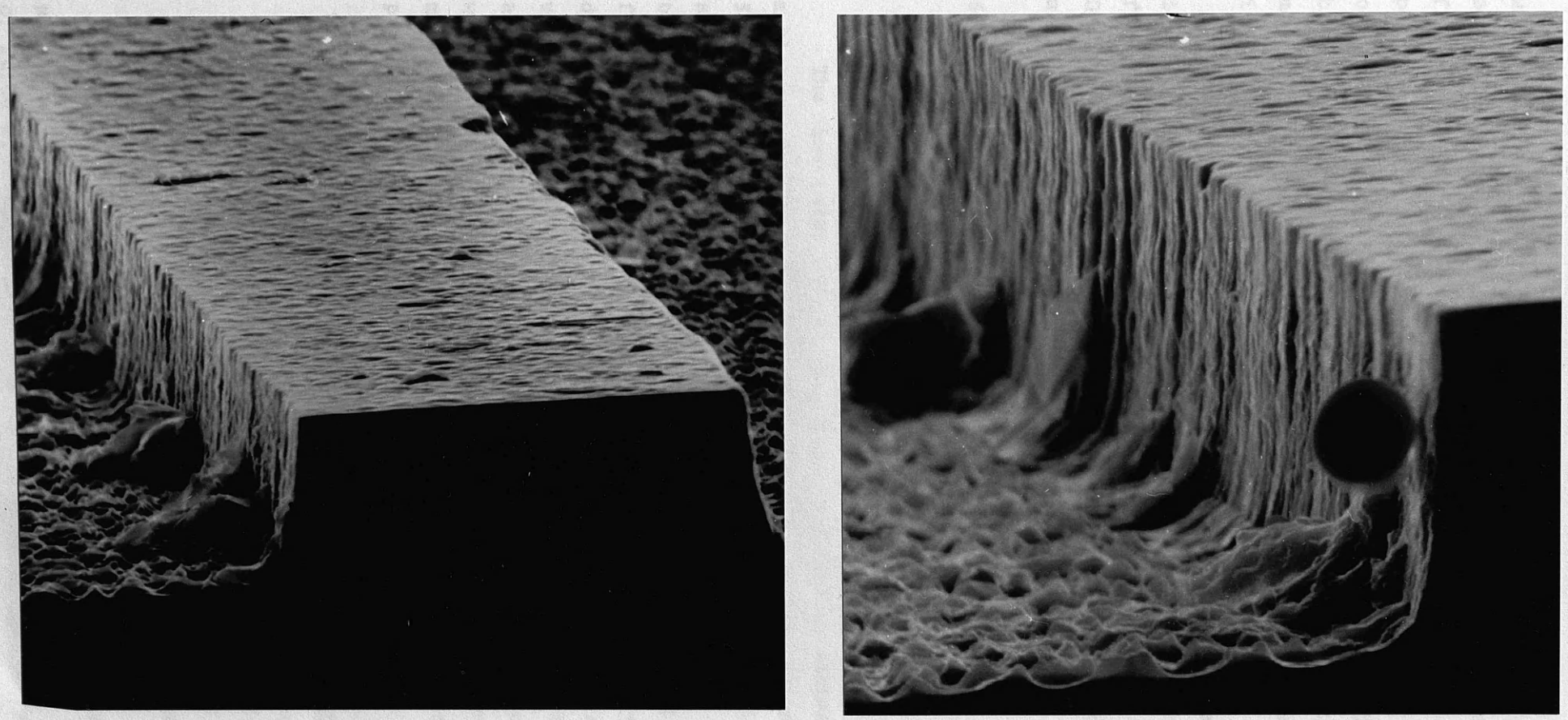

Figure 6.8 a) Rib guide, 6μm wide. b) Detail of rib wall.

was then launched into the end face of each fibre to examine the coupling behaviour. A typical result, for a 40μm guide is shown in figure 6.7. This photograph shows mode sinking from a defect in the polymer rib into the polymer film. The mode sinking beam is well confined. Minor defects such as this and major defects such as the blisters shown in figure 6.5, together with alignment difficulties meant that fibre-polymer rib-fibre coupling was not demonstrated, nor its efficiency measured.

In order to reduce the effect of the film/rib defects, oil of index slightly lower than that of silica was applied to the device of figure 6.7. Unfortunately this completely removed the polymer film. Due to the fabrication and alignment difficulties described above, the alternative of flip-chip coupling was pursued.

6.3 Rib waveguide flip-chips

6.3.1 Fabrication

The 'low-index passive material' deposited on silica substrates as a planar waveguide, (and to which mode-sinking was observed in chapter 5) was used to form rib-waveguides. Their fabrication, which was similar to that of the polymer guides but without the alignment and blistering difficulties was as follows. After cleaning, an aluminium film was vacuum evaporated onto the samples. A photoresist film was dip-coated onto each sample then dried at 86°C for 30 min. The mask was transferred to the resist by contact printing then the unprotected aluminium was etched leaving an aluminium line. The photoresist mask was subsequently removed in acetone. The aluminium served as an etch mask during reactive ion etching in a CF_4/O_2 plasma. The etch parameters were;

Initial pressure	200mTorr
Flow rate 80:20 ratio of CF_4/O_2	35sccm^{-1}
Plate voltage	500V
RF power coupled to plasma	100W
Etch time	10 min.

This etch time at these parameter values gave an etch depth of 2 μm. The aluminium was then etched leaving a rib guide. Various widths of guide were made and figure 6.8 shows scanning electron micrographs

of a 6μm rib. Wall verticality was good with small undulations in wall thickness visible.

6.3.2 Alignment and coupling

After fabrication, the flip chips were placed on the TVC samples and aligned **by hand** while viewing under an optical microscope. They were then clamped lightly in position with G-clamps. Further manual adjustments were performed with progressive tightening of the clamps until the rib guide and ellipse ends were collinear and tightly clamped. Low index oil (N_D = 1.44) was then inserted into the space between the flip-chip and the TVC by capillary action. The rib boundary was no longer visible when the oil was applied. Therefore any subsequent adjustments required the flip-chip and TVC to be first separated, then cleaned and dried. Fibre-rib-fibre coupling was observed using both 20μm and 40μm ribs, at 633nm. The coupling efficiency was observed to be low but it was felt that this would be improved with a more sophisticated alignment apparatus and a longer wavelength source. It was not possible to record this experiment because a fire in the engineering building destroyed both the samples and associated fabrication facilities.

6.4 Conclusions

These experiments demonstrated transverse coupling between an integrated optical waveguide and a standard single-mode fibre. The film fabrication options were limited, by the epoxy used in the TVC construction, to the use of polymer waveguides and glass flip-chips. The polymer waveguides were unsuitable for conventional multilayer processing and suffered from blistering. Alignment of a lithographic mask, with the interpolated position of the fibre core was achieved but with limited accuracy. The glass waveguides were relatively straightforward to pattern but also proved difficult to align. The experiments showed that while the TVC gives rugged and straightforward alignment between a fibre and a planar film, it requires a sophisticated apparatus to perform the alignment necessary to couple to rib waveguides of low mode order. The coupling efficiency could not be measured.

References

1. Harris, J.H., Shubert, R., Polky, J.N., 'Beam coupling to films', J. Opt. Soc. Am., Vol. 60, No. 8, Aug (1970), pp.1007-1016.

2. Ulrich, R., Weber, H.P., 'Solution-deposited thin films as Passive and Active Light Guides', Appl. Opt., Vol. 11, No. 2, Feb (1972).

3. Hetherington, W.M., Van Wyck, N.E., Koenig, E.W., Stegeman, G.E., Fortenberry, R.M., 'Coherent Raman Scattering in thin-film waveguides', 7th Topical Meeting on Integrated and Guided Wave Optics (IGWO) Apr (1984).

4. Bennion, I., Hallam, A.G., Stewart, W.J., 'Optical waveguide components in organic photochromic materials', Radio and Electron. Eng., (1983), Vol. 53, p.313.

5. Gibson, M., Frejlich, J., 'Dip-coating method for fabricating thin photoresist films', Thin Solid Films, Vol. 128, (1985) pp.161-170.

6. Tiefenthaler, K., Brignet, V., Buser, E., Horisberger, M., Lukosz, W., 'Preparation of planar optical SiO_2-TiO_2 and $LiNbO_3$ waveguides with a dip coating method and an embossing technique for fabricating grating couplers and channel waveguides', Proc. SPIE, Vol. 401, Thin Film Technologies (1983).

7. Mattox, D.M., 'Substrate preparation for thin film deposition - a survey', Thin Solid Films, Vol. 124, (1985), pp.3-30.

8. Mukherjee, S.P., Lowdermilk, W.H., 'Gradient Index AR film deposited by the sol-gel proces', Appl. Opt., Vol. 21, No. 2, Jan (1982) pp.293-296.

9. Mogab C.J.,'Ion beam, plasma and reactive ion etching,' Inst. Phys. Conf. Ser. No.53 pp37-54, (1980)

10. Bondur J.A.,'Dry process technology (Reactive Ion Etching),'

J.Vac. Sci. Technol., Vol.13, No.5, pp1023-1029, Sep/Oct(1976)

11. Ephrath L.M.,'Reactive ion etching for VLSI,' IEEE Trans. for Elec. Dev., Vol.28, No.11, pp1315-1319 Nov.(1981)

12. Vossen J.L.,Kern W.,'Thin film processes,' Academic Press, New York, 2nd Edition (1978).

13. Chapman R.E.,'Redeposition: a factor in ion beam etching topography,' J. Mat. Sci., Vol.12, pp1125-1133, (1977).

14. Melliar-Smith C.M.,'Ion etching for pattern delineation,' J. Vac. Sci Technol., Vol.13, No.5, pp1008-1022 Sep/Oct (1976)

Chapter 7. Summary conclusions and future developments.

7.1 Introduction.

The principal achievements of this work have been that an understanding of the coupling behaviour of the TVC has been obtained and that efficient transverse coupling has been demonstrated between a standard single mode fibre and a planar film waveguide.

The importance of the evanescent coupling technique in this case is that it complements rather than competes with the existing technique of butt-coupling. The theoretical development associated with the experimental work of the thesis is described below. The experimental work is then summarised and future work outlined. A new method of performing WDM is proposed which is related to the work of chapter 6 on rib-guidance.

7.2 Development of theory.

7.2.1 Confinement in weakly coupled guides.

The analyses of TVC/film and TVC/prism coupling were based on coupled mode theory[1] (CMT) derived for guides having less complex geometries and which were weakly coupled. CMT was reviewed in chapter 3 and discussed in terms of the degree of confinement inherent in each coupled guide. For weak coupling between lossless, synchronous, parallel guides of equal confinement (e.g. fibre-fibre or film-film) power is periodically coupled between the guides without loss[2]. The modes of the guides in isolation are only weakly perturbed by the coupling.

The situation is more complex for weakly coupled, parallel coupled guides having different degrees of confinement (e.g. fibre-prism, fibre-film). The guide having the lower degree of confinement acts as a mode-sink and in the case of fibre-prism coupling, power coupled from the fibre to the prism is not returned. Radiation from the fibre to the prism occurs at a characteristic angle θ_{ms} such that the components of the fibre and prism fields along the fibre axis are equal. The fibre mode may be considered to be leaky, having a complex propagation constant.

Mode-sinking between a weakly coupled fibre and film guide is again more complex than the fibre-prism case. It has been analysed by Arnaud[3] and Marcatili[4] and is discussed in chapter 3. The coupling

characteristics (fibre to film) are similar to those observed in fibre to prism coupling. Leakage occurs from the fibre into the film at characteristic angles $\pm\theta_{ms}$ such that the components of the fibre and film fields along the fibre axis are equal. However these analyses consider coupling to one plane wave (film-mode) rather than to a beam composed of many plane waves, as discussed in chapters 4 and 5.In addition when the propagation constants of the fibre and film in isolation are equal then the analyses break down giving infinite loss.

In chapter 5, a qualitative description of weak coupling between a weakly coupled fibre and film (which are not necessarily parallel) is given for a range of propagation constants corresponding to different opical wavelengths. Although the questions of beam shape in the film guide and of coupling behaviour at synchronism are considered, it is not possible to calculate the loss from the fibre, or the coupled beam shape, for a particular wavelength. This quantitative analysis does however agree with the experimental results for wavelength dependent coupling. In particular, it is sufficient to explain the sharp cut-off filter, transmission characteristic of figure 5.14.

7.2.2 Strong coupling in branching guides.

The extension of CMT to non-parallel guides is relatively straightforward[5] provided that the local cross-section of the guides changes slowly and smoothly. The weakly coupled theory described above was applicable over the branching guide region of the TVC (region A, figure 3.2) although with increasingly limited accuracy as the guide spacing decreases to zero (region B, figure 3.2). However the prism coupling experiments described in chapter 4 indicated that a significant amount of power was coupled in the tapered core region (region C, figure 3.2). In this region it is not possible to retain the concept of slightly perturbed modes of individual waveguides since the two guides are adjacent and since the fibre core is no longer circularly symmetric. The BPM analysis described in chapter 5, showed that (for one particular fibre film combination) the majority of power transfer occured in the tapered core region. This showed that TVC/film coupling was essentially a three dimensional problem of strong coupling, requiring a computational technique such as the BPM to obtain a qualitative description of coupling.

The essence of the weak-coupling theory was that mode-sinking and on-axis coupling occured at different wavelengths according to the

mismatch in longitudinal propagation constants (figure 5.1). This followed directly from the derivation of Arnaud using the delta-function operator which led to a clearly defined coupling characteristic.

7.2.3 BPM analysis of the TVC.

A BPM analysis of the coupling process in the TVC showed that in the case of strong coupling, both elements, mode-sinking and on-axis coupling were present at a single wavelength. Two solutions were indicated for each wavelength; a perturbation of the fibre mode by the film and similarly a perturbation of the film modes by the fibre. If we consider parallel guides (or a particular local cross-section) then for any particular wavelength, the power coupled to each of these solutions could in principle be calculated. The distribution of power between the two solutions (as well as the mode sinking angle and the mode shape) would alter with wavelength. At a synchronous wavelength the axially propagating solution (of the film modes loaded by the fibre) would dominate whereas at a mode-sinking wavelength the off-axis propagating solution (of the fibre mode loaded by the film) would be more prevalent.

From figure 5.17 it can be seen that the distribution of power between these two solutions also changes with the local cross-section of the TVC. It was clear from figure 5.17 i-iv, and from table 5.1 that although the fibre and film guides were mismatched, (in isolation) power was transferred from the fibre into the film as a mode of the composite rib-waveguide. The exact wavelength at which power was most efficiently transferred from the fibre into the film would in practice be shifted slightly from the synchronous wavelength condition, described in chapter 5 for weak coupling, by the large coupling strength. As the remaining core area diminishes power is coupled from the axial mode into mode sinking beams (figure 5.17 vi-ix). This is in agreement with the conclusions of Marcatili (with the exception that coupling is to a beam rather than to a plane wave).

7.3 Experimental observations of the TVC.

The construction of the TVC, its advantages and problems, and a comparison with other fibre couplers is given in chapter 4. The experimental investigation of the TVC was structured according to the

degree of confinement provided by the elements to which it was coupled. Experimental observations of TVC-prism, TVC-film guide and TVC-rib guide coupling were recorded. The TVC was a useful device in advancing the understanding of transverse fibre film coupling. It was demonstrated to be an efficient fibre-film coupler with potential applications as an in-line fibre filter (figures 5.7, 5.9, 5.14) and as an optical sensor.

7.3.1 TVC-prism coupling.

The objects of the prism coupling experiments were to confirm that the coupler offered access to the evanescent field of the optical fibre and to make use of that field for optical characterisation measurements. The experiments confirmed that evanescent field coupling (region A, figure 3.2) occured as expected but showed in addition that coupling from the tapered core region (region C, figure 3.2) was substantial. The output radiation pattern did not correspond to particular fibre-mode lines as expected but to interference between the radiation from each coupling region. This was shown to correspond closely to the interference pattern arising from plane waves incident on a single-slit and a semi-infinite half space. This comparison led to a figure for the dimensions of the radiation aperture and therefore the fibre core size, which was in good agreement with the core size expected from ESI measurements. Since the radiation pattern was principally a function of the TVC geometry the prism coupling technique was considered unsuitable for fibre characterisation measurements. A TVC and PDC were constructed from single mode fibre (at 633nm) to remove any effects of intermodal interference and to confirm that coupling occured from the tapered core region of the TVC.

7.3.2 TVC-film coupling.

Coupling between the TVC and planar (oil-film) waveguide is discussed in chapter 5. The synchronisation conditions for achieving efficient power transfer in a directional coupler are exacting. Since the coupling characteristics were unknown, 'tuning' was achieved by using a multi-wavelength source and an optical spectrum analyser. This could also have been achieved at a single wavelength by varying the film thickness and therefore the effective index of the film modes, provided that the necessary degree of thickness control could have been

maintained. Any tilting of the (nominally) planar film as the (average) thickness was varied would have affected the accuracy of the results and this method was deemed impractical.

Measurement of the coupler efficiency was considered crucial and an experimental arrangement was devised which minimised the distance which light travelled in the film waveguide. The insertion loss of the device included beam spreading, scattering and material loss as well as the effects of tilt and mechanical misalignments between the fibres. These components were minimised by using the short film waveguide arrangement but were not eliminated. Since they could not be quantified, it was impossible to provide a breakdown of the experimental losses. In principle the theoretical losses could be evaluated using the BPM but the computing time was not available for this.

The coupler insertion loss was found to be a strong function of wavelength and was closely related to the fibre and film dispersion diagram of e.g. figure 5.1, as discussed in section 7.2. The theoretical prediction of mode-sinking was investigated and confirmed in two experiments. The effects of mode-sinking were observed in a multi-wavelength experiment and gave rise to the sharp cut-off, filter transmission characteristic of figure 5.14. Over the 10nm range from λ=1.32μm to λ=1.33μm the fibre to fibre transmission of the device changed by 17dB.

The insertion loss at each wavelength of the device was measured using a cut-back technique. This provided the data for the theoretical analyses described. The minimum insertion loss measured from fibre to film to fibre was 2dB. This was achieved at λ=1.36μm with a film of index n_D=1.470 (figure 5.11) and at λ=1.33μm, λ=1.46μm with a film of index n_D=1.620 (figure 5.14). The fabrication of a coupler operating at such a high efficiency over this range of film thicknesses, indices and signal wavelengths was the principal achievement of this project.

7.3.3 TVC-rib guide coupling.

Coupling between the TVC and a rib or channel waveguide of low mode order was expected to have the characteristics associated with guides of equal confinement. Coupling to relatively high order mode rib-guides was demonstrated but the difficulties of guide fabrication and mask alignment (for polymer ribs) and of flip-chip alignment meant that coupling to guides of low mode order was not demonstrated.

7.4 Future developments.

The investigation of transverse coupling between a single mode fibre and a rib or channel guide and a single mode fibre is necessary before evanescent coupling can be seriously considered, beside end fire coupling, for device production. Such an investigation, especially of a multi-wavelength nature should yield a figure for the coupling coefficient between the guides. The coupling length and the rate of fall-off in power transfer with guide mismatch, could then be calculated. This would allow the tolerances for coupling with a given efficiency at a given wavelength to be evaluated. This would be of less value for planar film coupling (if it could be meaningfully calculated) since planar films are less useful from a device viewpoint.

One possible application of planar film coupling concerns the mode-sinking phenomenon, observed in the sharp cut-off filter (figure 5.14). If the response of an active film in this arrangement was to alter the peak transmission wavelengths (as expected) then this device would perform as an active filter, modulator or switch. A film with an intensity dependent refractive index, incorporated in this device would also have potentially interesting properties.

7.4.1 D-fibre.

The principle vehicle for investigating fibre-rib coupling is expected to be the D-fibre[6]. High index sandwich ribbon (SR) fibres have previously been used to couple to planar waveguides but these required an end-fire connection to standard fibres. D-fibres (figure 7.1) have recently been developed which have an accurately controlled core-flat distance (D), which determines the coupling strength, and would require to be optimised. Since epoxy of lower index than silica is available the fibres could be rigidly aligned by fixing the reference flat of the fibre to the integrated optical waveguide directly. This would eliminate both the need for a precision structure such as the TVC and the use of an optically incompatible epoxy, necessary for polishing purposes.

7.4.2 Wavelength division multiplexing.

Another area of interest arising from this work is the use of mode sinking from a transition in a rib waveguide to perform wavelength

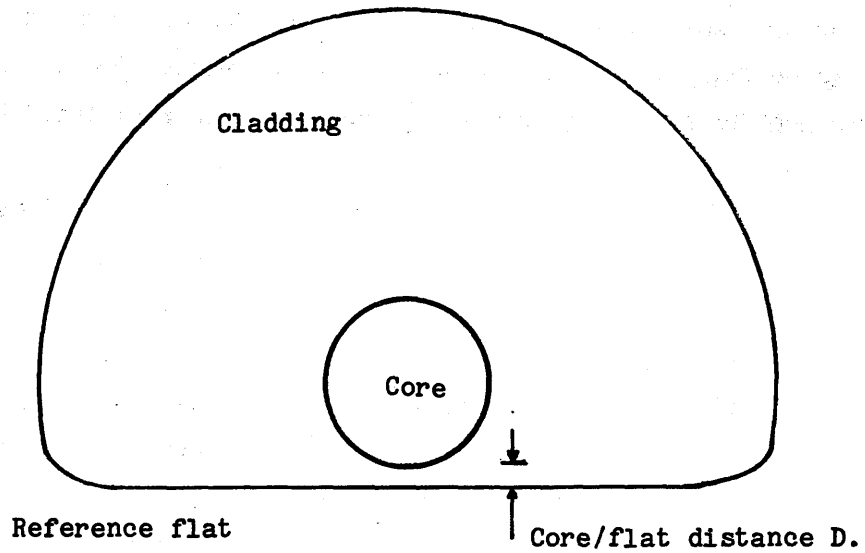

Figure 7.1 D-fibre. This fibre is made by removing part of the preform of a standard fibre before pulling.

division demultiplexing[7,8]. This device could employ D-fibre coupling at the input and/or output stages.

The device has two principal parts integrated on a common substrate figure 7.2. The first part is a thin film rib waveguide, uniform in the direction of propagation (the launch region). Into this region optical power is launched, either by a transverse coupling method or by an end-fire technique) from a second waveguide which may be of the thin-film or fibre types. All wavelengths to be demultiplexed are launched into this rib guide and are guided by it.

The second part of the guide is a transitional waveguide which has one or more tapered sections along its length. These tapers reduce the width of the rib and therefore lower its guiding power. The tapered sections may be separated by uniform sections. As the guiding power of the rib is lowered smoothly the longest wavelength launched and guided in the launch section will become cut-off and will radiate into the thin-film region, in which it will be guided. The transfer of light from the rib to the uniform film occurs through mode-sinking as predicted by Marcatili. This results in two beams of light in the film, at equal angles to the original propagation direction. If the taper is sufficiently smooth and the launch wavelengths are sufficiently well separated then only this wavelength will be cut-off and become guided in the uniform film region. As the rib guide is further tapered, the next longest waveguide is cut-off. The beams of light in the uniform film region have effectively a finite width and have finite divergence as shown in figure 5.17. Each beam is monochromatic and is physically separated from the other beams while it is in the vicinity of the rib-guide. Each beam can therefore be coupled (by transverse or end-fire coupling) to an output guide which can be of the thin-film or optical fibre types. The novelty of the device lies in utilising mode-sinking to selectively remove light of one wavelength from a rib-waveguide and to guide it in a second coupling region where it can be further processed individually.

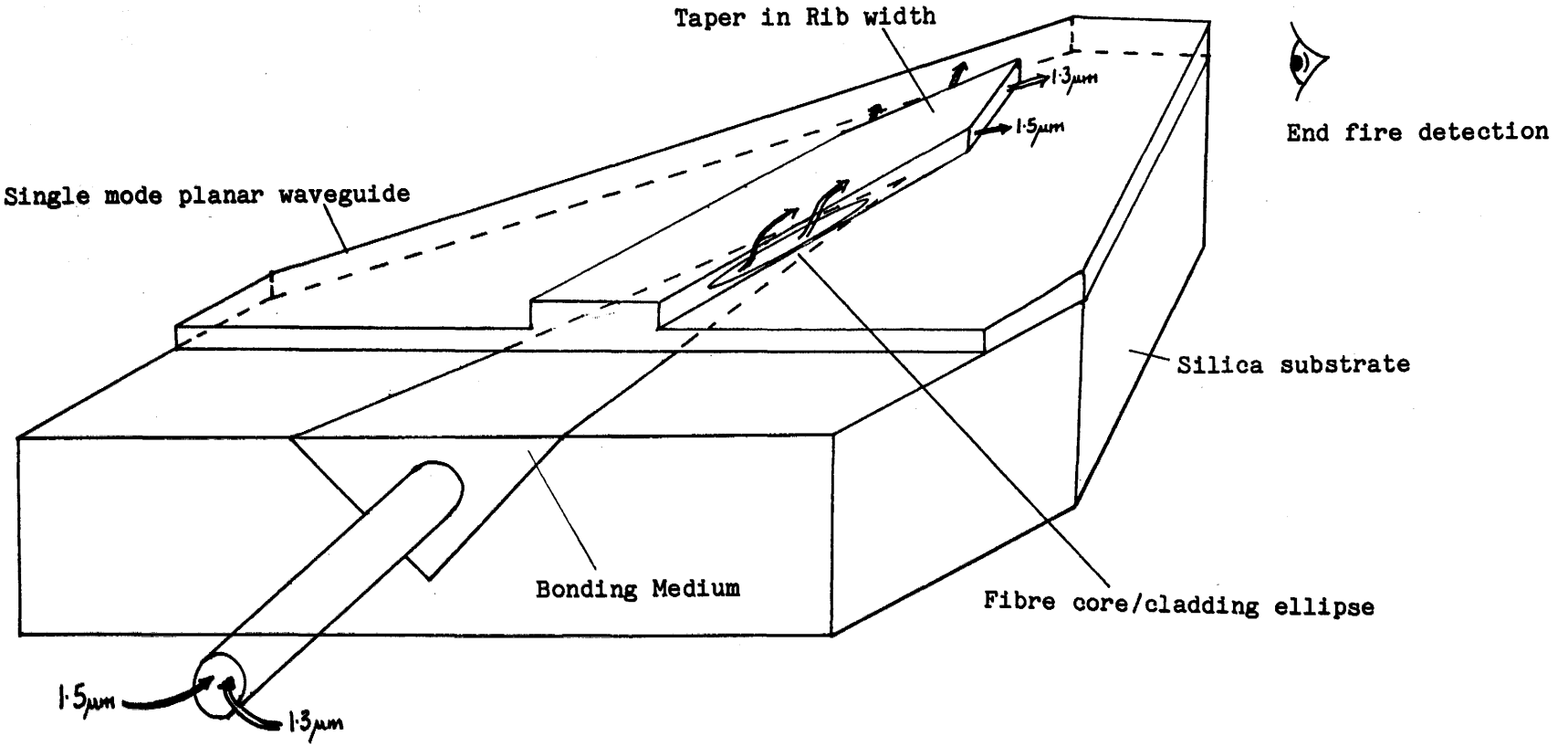

Figure 7.2 Passive WDM at fibre termination using mode-sinking from a transitional waveguide.

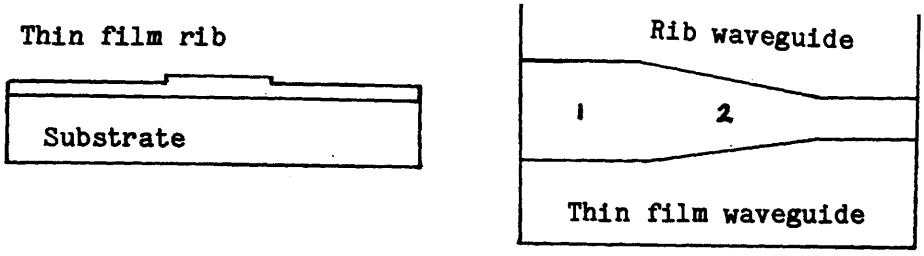

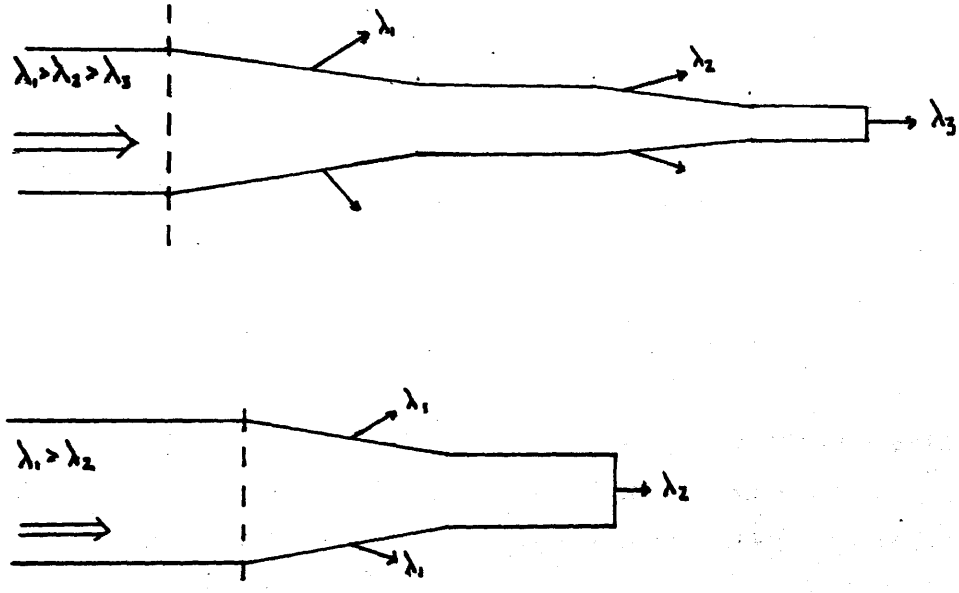

Figure 7.2 b) Details of rib-guide structures.

a) cross-section of integrated optical guide.

b) plan view of rib showing 1, uniform launch region and 2, transitional waveguide.

c) Typical transitional guide structures.

References

1. Miller S.E.,'Coupled wave theory and waveguide applications,' B.S.T.J., Vol.33, No.3, May (1954) pp661-719.

2. Arnaud J.,'Transverse coupling in fibre optics: Part 1: Coupling to trapped modes,' B.S.T.J., Vol.53, No.2, Feb.(1974)pp217-224.

3. Arnaud J.,'Transverse coupling in fibre optics: Part 2: Coupling to mode-sinks,' B.S.T.J., Vol.53, No.4, Apr.(1974)pp675-696.

4. Marcatili E.A.J.,'Slab coupled waveguides,' B.S.T.J. Vol.53 No.4, Apr.(1974) pp645-674.

5. Louisell W.H.,'Analysis of the single tapered mode coupler,' B.S.T.J., Vol.34, No.6, (1955) pp853-866.

6. Millar C.A.,Ainslie B.J.,Brierley M.C.,Craig S.P.,'Fabrication and characterisation of D-fibres with a range of accurately controlled core/flat distances,' Electron Lett. Vol.22, No.6, 13th Mar. (1986) pp322-324.

7. Lawson C.M., Kopera P.M., Hsu T.Y., Tekippe V.J.,'In-line single mode wavelength division multiplexer/demultiplexer,' Electron. Letts. Vol.20, No.23, Nov. (1984) pp963-964

8. Lipson J.,Harvey G.T.,'Low loss WDM devices for single mode systems,' IEEE J.Lightwave.Tech. Vol.1, No.2, June(1983). pp387-389.